



This is to certify that the

dissertation entitled

Catalytic Conversion of Lactic Acid to Commodity and Specialty Chemicals

presented by

Man Sang Tam

has been accepted towards fulfillment of the requirements for

Ph.D. degree in Chemical Engineering

MSU is an Affirmative Action/Equal Opportunity Institution

Date 12/19/97

0-12771

LIBRARY Michigan State University

PLACE IN RETURN BOX to remove this checkout from your record.

TO AVOID FINES return on or before date due.

MAY BE RECALLED with earlier due date if requested.

DATE DUE	DATE DUE	DATE DUE
기취관 확 8 Sub.		
JUL 3 6 5952		
JUL 2 0 2003 JUL 1 1 1 1 1 1 1 1 1 1 1 1 1 1 1 1 1 1 1		
46		

1/98 c/CIRC/DateDue.p65-p.14

CATALYTIC CONVERSION OF LACTIC ACID TO COMMODITY AND SPECIALTY CHEMICALS

Ву

Man Sang Tam

A DISSERTATION

Submitted to
Michigan State University
in partial fulfillment of the requirements
for the degree of

DOCTOR OF PHILOSOPHY

Department of Chemical Engineering

1997

UMI Number: 9822766

UMI Microform 9822766 Copyright 1998, by UMI Company. All rights reserved.

This microform edition is protected against unauthorized copying under Title 17, United States Code.

300 North Zeeb Road Ann Arbor, MI 48103

V

flow react

Formation

and 2-3 se

formation

over these

reaction FT

formation o

thus conclud

condensation

are fully con-

when the salt

ABSTRACT

CATALYTIC CONVERSION OF LACTIC ACID TO COMMODITY AND SPECIALTY CHEMICALS

By

Man Sang Tam

Vapor phase lactic acid conversion has been performed using a fixed-bed, downflow reactor. Lactic acid conversion conducted over sodium salts on low surface area
silica catalysts produces mainly 2,3-pentanedione, acetaldehyde, and acrylic acid.

Formation of acrylic acid from lactic acid is optimum at 23% yield over NaOH at 350°C
and 2-3 second residence time. This yield is relatively low as a result of acetaldehyde
formation which is favored at high temperature. The optimum 2,3-pentanedione yield
over these sodium salts is around 25% of theoretical at 300°C and 3-4 seconds. Postreaction FTIR spectra of catalysts after exposure to lactic acid vapor indicate the
formation of sodium lactate as the dominant species on the surface at 260-320°C. It is
thus concluded that the anions of initial sodium salts used do not participate in the
condensation to 2,3-pentanedione; hence similar yields are obtained for all salts once they
are fully converted to sodium lactate. Conversion of the sodium salt to lactate is favorable
when the salt used has a low melting point and a volatile conjugate acid.

Lewis a loading up to sa support acetalde

and ba

yield obt

80° o sele

proposed

lactic acid

D

significant

amount of

low 2.3-pe

hydroxide a

The results obtained from lactic acid conversion over potassium or cesium salts and bases on silica show that the yield of 2,3-pentanedione increases with decreasing Lewis acidity of the alkali metal. Detailed reaction studies over different alkali metal loadings indicate that the rate of 2,3-pentanedione formation varies linearly with loading up to saturation at 2 mmol of catalyst per gram of support. The acidity of the silica support also reduces the yield to 2,3-pentanedione because of competitive formation of acetaldehyde through acid-catalyzed decarbonylation. As such, the best 2,3-pentanedione yield obtained over a 2 mmol CsOH/g silica catalyst at 280°C is 60% of theoretical with 80% selectivity. A kinetic model of the reaction system is developed along with a proposed mechanism for the formation of 2,3-pentanedione from the condensation of lactic acid catalyzed by alkali lactate.

Deactivation of the catalyst toward the formation of 2,3-pentanedione is not significant over forty hours. Afterward, the selectivity toward 2,3-pentanedione decreases slowly due to coking. A similar effect is also observed with feeds containing a small amount of glucose. However, conversion with feed containing ammonium lactate gives low 2,3-pentanedione yields, primarily as a result of the reaction between ammonium hydroxide and 2,3-pentanedione to form a low volatility product.

To my Lord and Savior, Jesus Christ.

James .

Berglur

Wadley

Varadar

Nagaraja

encourag

Departme

T

Excellenc

support to

ACKNOWLEDGMENTS

I am very grateful for the suggestions and guidance of Dr. Dennis Miller and Dr.

James Jackson throughout the course of this work. Thanks to Dr. Carl Lira, Dr. Kris

Berglund, and Dr. Thomas Pinnavaia for their service as my doctoral committee members.

I would like to thank Radu Craciun, Garry Gunter, Robert Langford, and Doug Wadley for their valuable contributions to this work. Special thanks to Sriraman Varadarajan, Dushyant Shekhawat, Rajesh Baskaran, Shubham Chopade, and Kirthi Nagarajan for making my study at Michigan State University an enjoyable one. The encouragement and support of my family are greatly appreciated.

Thanks to the Department of Chemical Engineering at MSU, United States

Department of Agriculture National Research Initiative, the State of Michigan Research

Excellence Fund, and the Consortium for Plant Biotechnology Research for their financial support to this work.

TABLE OF CONTENTS

List of Tab	les	x
List of Figu	ıres	xii
Introduction	on .	1
List of Figures Introduction Chapter 1. Background 1.1. Literature Review 1.1.1. Lactic Acid 1.1.2. 2,3-Pentanedione 1.1.3. Acrylic Acid 1.1.4. Propionic Acid 1.2. Lactic Acid Reactions 1.2.1. Catalytic and Thermal Decomposition 1.2.2. Self-esterification and Polymerization 1.2.3. Dehydration 1.2.4. Reduction 1.2.5. Condensation to 2.3-Pentanedione	3	
1.1.	Literature Review	3
	1.1.1. Lactic Acid	3
	1.1.2. 2,3-Pentanedione	7
	1.1.3. Acrylic Acid	10
	1.1.4. Propionic Acid	11
1.2.	Lactic Acid Reactions	12
	1.2.1. Catalytic and Thermal Decomposition	12
	1.2.2. Self-esterification and Polymerization	13
	1.2.3. Dehydration	14
	1.2.4. Reduction	15
	1.2.5. Condensation to 2,3-Pentanedione	15

Chapt

2

24

Chapter 3.

3 1.

3 2. F

3.3 Dis

Chapter 2.	Experimental Methods	17
2.1.	Vapor Phase Reaction	17
	2.1.1. Materials	17
	2.1.2. Catalyst Preparation	19
	2.1.3. Vapor Phase Reactor	20
	2.1.4. Reaction Procedure and Product Analyses	22
2.2.	Post-Reaction Transmission FTIR Spectroscopy	25
	2.2.1. FTIR Spectroscopy	25
	2.2.2. Materials and Sample Preparation	27
	2.2.3. Apparatus and Procedure	27
2.3.	Post-Reaction DRIFTS	30
	2.3.1. DRIFTS	30
	2.3.2. Sampling Procedure	30
2.4.	Gas Chromatography - Mass Spectrometry	31
Chapter 3.	Lactic Acid Conversion over Sodium Salts and Base on Silica	32
3.1.	Vapor-Phase Reaction	32
	3.1.1. Results	33
	3.1.2. Effects of Sodium Catalyst Loading	42
3.2.	Post-Reaction FTIR Results	42
	3.2.1. Characteristic Infrared Bands of Sodium Salts and Base	42
	3.2.2. Survey of Sodium Salts and Base	46
3.3.	Discussion	58

Chapter

4.2

4 3

4.5. Sum

	3.3.1. Carbon Balance	58
	3.3.2. Catalyst Activity and Pathways	60
	3.3.3. Mechanism of 2,3-Pentanedione Formation	65
	3.3.4. Decomposition of Sodium Lactate	73
3.4.	Summary	75
Chapter 4.	Lactic Acid Conversion over Alkali Salts and Bases on Silica	77
4.1.	Vapor-Phase Reaction	77
	4.1.1. Results	78
	4.1.2. Catalyst Activity and Pathways	88
	4.1.3. Effect of Loading	89
4.2.	Post-Reaction FTIR	102
4.3.	General Kinetic Model of the Reaction System	110
	4.3.1. Kinetic Analysis of KOH on CPG	114
	4.3.2. Kinetic Analysis of KOH on SiGel	115
	4.3.3. Kinetic Model and Support Effects	116
	4.3.4. Silica Support Sintering by Alkali Metal	121
	4.3.5. Kinetic Analysis of NaOH and CsOH on SiGel	124
4.4.	Methyl Lactate Vapor-Phase Reaction Studies	126
	4.4.1. Reaction Studies	126
	4.4.2. Post -Reaction FTIR	128
4.5.	Summary	128

Chapter 5.	Catalyst Stability and the Effect of Feed Impurities on the Formation of 2,3-Pentanedione from Lactic Acid	132
5.1.	Catalyst Support Regeneration	132
5.2.	Initial Saturation Period	135
5.3.	Stability of Acrylic Acid and 2,3-Pentanedione	136
5.4.	Deactivation of Catalyst with Time	137
5.5.	Effect of Different Lactic Acid Feedstock	141
5.6.	Effect of Ammonium Lactate Concentration in Feed	145
	5.6.1. Materials and Experimental Procedure	145
	5.6.2. Reaction Results and Discussion	146
	5.6.3. Post-Reaction FTIR Results	153
	5.6.4. Reaction of 2,3-Pentanedione in Presence of Ammonium Hydroxide	155
5.7.	Effects of Glucose in Feed	156
5.8.	Summary	158
Chapter 6.	The Production of Propionic Acid from Lactic Acid	159
6.1.	Catalyst Preparation and Reaction Conditions	159
6.2.	Lactic Acid Conversion over Molybdenum and Iron Catalysts	160
Chapter 7.	Summary and Recommendations	165
7.1.	Summary	165
7.2.	Recommendations	166
List of Refe	erences	169

LIST OF TABLES

2.1.	List of Chemicals	18
2.2.	Typical Reaction Conditions	23
2.3.	GC Operating Temperature Program	25
3.1.	Lactic Acid Conversion over CPG and NaC ₃ H ₅ O ₃ /CPG	34
3.2.	Lactic Acid Conversion over NaOH/CPG and Na ₂ SiO ₃ /CPG	35
3.3.	Lactic Acid Conversion over NaNO ₂ /CPG and NaNO ₃ /CPG	36
3.4.	Lactic Acid Conversion over Na ₃ PO ₄ /CPG and Na ₄ P ₂ O ₇ /CPG	37
3.5.	Lactic Acid Conversion over NaCl/CPG and Na ₂ SO ₄ /CPG	38
3.6.	Characteristic Infrared Bands of Sodium Salts	46
3.7.	Properties of Sodium Salts Used as Catalysts	47
4.1.	Lactic Acid Conversion over LiOH/CPG and Ca(OH) ₂ /CPG	80
4.2.	Lactic Acid Conversion over K ₃ PO ₄ /CPG and KCl/CPG	81
4.3.	Lactic Acid Conversion over KOH/CPG and KNO ₃ /CPG	82
4.4.	Lactic Acid Conversion over CsCl/CPG and Cs₂SO₄/CPG	83
4.5.	Lactic Acid Conversion over CsOH/CPG and CsNO ₃ /CPG	84
4.6.	Lactic Acid Conversion over Cs ₃ PO ₄ /CPG and CsNO ₃ /CsOH/CPG	85
4.7.	Melting Points of Alkali Salts and Bases	90

48 La

4.9. Pa

4.10. P

4.11. Se

4.12 Su

4.13 Par

4 14. Par

51 Lacti

52. Lactic

5.3. Lactic Times 5.4. Reaction

5.5. Elemen

5.6. Product Catalyst 61. Lactic A

6.2. Lactic Ac

4.8. Lactic Acid Conversion over SiGel Support Alone	91
4.9. Parameters of Kinetic Model for KOH/CPG	116
4.10. Parameters of Kinetic Model for KOH/SiGel	117
4.11. Sensitivity Analysis of Rate Constants (Percentage Change due to Experimental Uncertainties)	119
4.12. Surface Areas of Used Catalysts	123
4.13. Parameters of Kinetic Model for NaOH/SiGel and CsOH/SiGel	125
4.14. Partial Conversion Results Using Methyl Lactate as Feedstock	127
5.1. Lactic Acid Conversion over Regenerated CPG and KOH/Regenerated CPG	134
5.2. Lactic Acid Conversion - Initial Saturation Period	136
5.3. Lactic Acid Conversion over NaNO ₃ /CPG (Studies at Different Residence Times)	138
5.4. Reaction Conditions of 60 Hour Run	139
5.5. Elemental Analysis of Feed (CHN)	143
5.6. Product Yields (Selectivities) from Different Feeds over CsOH/CPG Catalyst	148
6.1. Lactic Acid Conversion over Na ₂ MoO ₄ /Si-Al and MoCuSn/Si-Al	161
6.2. Lactic Acid Conversion over FeCuSn/Si-Al	163

LIST OF FIGURES

1.1.	Primary Lactic Acid Pathways	4
1.2.	Chemical Synthesis of Lactic Acid	5
1.3.	2,3-Pentanedione Pathways	8
1.4.	Formation of Duroquinone from 2,3-Pentanedione	9
1.5.	Oxidation of Propylene to Acrylic Acid	11
1.6.	Mechanism for Lactic Acid Pyrolysis to Acetaldehyde	13
2.1.	Vapor-Phase Reactor	21
2.2.	Reactor Flow Diagram	24
2.3.	Typical Product Gas Chromatogram	26
2.4.	Preparation Apparatus for Post-Reaction Studies	28
3.1.	2,3-Pentanedione Yields over Various Sodium Salt Catalysts	40
3.2.	Acrylic Acid Yield over Various Sodium Salt Catalysts	41
3.3.	Effect of Sodium Loading on 2,3-Pentanedione Yield	43
3.4.	FTIR Spectra of Standards	44
3.5.	FTIR Spectra of Standards (Continued)	45
3.6.	Post-Reaction FTIR Spectra of NaNO ₃ Exposed to Lactic Acid Vapor	49
3.7.	Post-Reaction FTIR Spectra of Na ₃ PO ₄ Exposed to Lactic Acid Vapor	50

38 Post-l

3.9 Post-I

3 10. Post-

3.11. Post-

3.12 Post-

3 13 Post-I

3.14 Post-F

3.15. Post-R

3 16. Propos

Acid

317 Propose

3.18. Mass Sp

3 19 Mass Sp Convers

320 Mass Spe Conversi

321 Mass Spe Conversion

Mass Spec Conversio

323 Decompos

41 2,3-Pentanec

42 Acrylic Acid

43 Experimental

44 Experimental I

3.8.	Post-Reaction FTIR Spectra of Na ₄ P ₂ O ₇ Exposed to Lactic Acid Vapor	51
3.9.	Post-Reaction FTIR Spectra of Na ₂ SiO ₃ Exposed to Lactic Acid Vapor	52
3.10	Post-Reaction FTIR Spectra of NaOH Exposed to Lactic Acid Vapor	53
3.11	Post-Reaction FTIR Spectra of NaCl Exposed to Lactic Acid Vapor	54
3.12	Post-Reaction FTIR Spectra of Na ₂ SO ₄ Exposed to Lactic Acid Vapor	55
3.13	Post-Reaction FTIR Spectra of NaNO ₃ Exposed to Water Vapor	56
3.14	Post-Reaction FTIR Spectra of Sodium Lactate	59
3.15	Post-Reaction FTIR Spectra of NaNO ₃ Exposed to Propionic Acid Vapor	63
3.16	Proposed Mechanism for the Formation of 2,3-Pentanedione from Lactic Acid	66
3.17	Proposed Mechanism of H/D Exchange for α-hydrogen	67
3.18	. Mass Spectrum of Lactic Acid in Product of Lactic Acid / D ₂ O Conversion	68
3.19	Mass Spectrum of Acrylic Acid in Product of Lactic Acid / D ₂ O Conversion	69
3.20	Mass Spectrum of Propionic Acid in Product of Lactic Acid / D ₂ O Conversion	70
3.21	. Mass Spectrum of 2,3-Pentanedione in Product of Lactic Acid / D_2O Conversion	71
3.22	. Mass Spectrum of Acetaldehyde in Product of Lactic Acid / D ₂ O Conversion	72
3.23	Decomposition of Sodium Lactate at 350°C	74
4.1.	2,3-Pentanedione Yields over Various Alkali Salt Catalysts	79
4.2.	Acrylic Acid Yields over Various Alkali Salt Catalysts	87
4.3.	Experimental Results over KOH/CPG at T = 260°C	92
44	Experimental Results over KOH/CPG at T = 280°C	93

45 E

46 E

47 E

48 E:

49 Ex

410 E

411. E

4 12 E:

413 La

414 Ac

415 2,3

416 Lac

4.17. Acc

418 2.3

419. Pos

4.20 Pos

421. Pos

4.22 P_{OS}

51 Selec

52 FTIR

53 2,3.p

54 Deac 0.51

Ľ

4.5. Experimental Results over KOH/CPG at T = 300°C	94
4.6. Experimental Results over KOH/CPG at T = 320°C	95
4.7. Experimental Results over KOH/CPG at T = 350°C	96
4.8. Experimental Results over KOH/SiGel at T = 260°C	97
4.9. Experimental Results over KOH/SiGel at T = 280°C	98
4.10. Experimental Results over KOH/SiGel at T = 300°C	99
4.11. Experimental Results over KOH/SiGel at T = 320°C	100
4.12. Experimental Results over KOH/SiGel at T = 350°C	101
4.13. Lactic Acid Conversion over NaOH/SiGel	103
4.14. Acetaldehyde Yield over NaOH/SiGel	104
4.15. 2,3-Pentanedione Yield over NaOH/SiGel	105
4.16. Lactic Acid Conversion over CsOH/SiGel	106
4.17. Acetaldehyde Yield over CsOH/SiGel	107
4.18. 2,3-Pentanedione Yield over CsOH/SiGel	108
4.19. Post-Reaction FTIR of CsNO ₃ Exposed to Lactic Acid Vapor	109
4.20. Post-Reaction FTIR of CsCl Exposed to Lactic Acid Vapor	111
4.21. Post-Reaction FTIR of CsNO ₃ Exposed to Methyl Lactate Vapor	129
4.22. Post-Reaction FTIR of CsOH Exposed to Methyl Lactate Vapor	130
5.1. Selectivities of Products over Time	140
5.2. FTIR of Feed I	142
5.3. 2,3-Pentanedione Yields from Different Feed Stocks	144
5.4. Deactivation of 2,3-Pentanedione by Ammonium Lactate (T=280°C and P= 0.5 MPa)	147

55. 2.

56 D

5.7. Ef

5.5.	2,3-Pentanedione Yield vs. Ammonium Lactate Molar Fraction in Feed	150
5.6.	DRIFTS Spectra of Catalyst after Exposure to Ammonium Lactate	154
5.7.	Effect of Glucose on 2,3-Pentanedione Formation (T=280°C and P=0.5 MPa)	157

,

increased which me

biodegrad

and resear

fermentati

Cargnill, P

The availat

lactic acid;

commodity

Pyruvic acic

The

lactic acid by

and propioni

unfavorable c

based feedsto

acid conversion

conditions and

INTRODUCTION

Worldwide production of lactic acid (2-hydroxy-propionic acid) has dramatically increased since the early 1990s and is currently estimated to be over 100 million lb / yr, of which most is produced via fermentation. The viability of making an inexpensive biodegradable polymer - poly (lactic acid) - from lactic acid has sparked extensive interest and research in the area of producing and recovering relatively pure lactic acid from fermentation of starch hydrolysates. Already, major corporations including ADM,

Cargrill, Purac, and A. E. Staley have ventured into the manufacturing of lactic acid (1).

The availability of a high volume of inexpensive lactic acid has also led to research using lactic acid as an alternative feedstock for the production of many specialty and commodity chemicals such as acrylic acid (2-4), propionic acid, 2,3-pentanedione, pyruvic acid (5,6), and propylene glycol (7).

The primary focus of this work is on the formation of 2,3-pentanedione from lactic acid by condensation over simple alkali salt catalysts. The formation of acrylic acid and propionic acid from lactic acid has also been examined but found to be economically unfavorable compared to routes of producing these chemicals starting with petroleum based feedstocks. We have conducted extensive vapor-phase reaction studies of lactic acid conversion over alkali metal catalyst on silica supports to optimize the reaction conditions and the type of catalyst for the formation of 2,3-pentanedione. The

mechanistic aspects of this condensation have been investigated using Nuclear Magnetic Resonance (NMR), Fourier Transform Infrared Spectroscopy (FTIR), Diffuse Reflectance Infrared Fourier Transform Spectroscopy (DRIFTS), isotopic labeling, and molecular modeling. Upon understanding the basic chemistry of lactic acid conversion, a kinetic model of this reaction system has been developed. We have also examined the deactivation of the condensation to 2,3-pentanedione with time and feed impurities.

1.

1.1

read

acı

acry

acid

Whil

lactic

count

cyanic

piqtol

to acqu

ethano]

Lactoba

Chapter 1

BACKGROUND

1.1. Literature Review

1.1.1. Lactic acid

Lactic acid is a simple compound containing both the hydroxyl and carboxylic acid groups which permit it to participate in many interesting and valuable chemical reactions. Among the known reactions of lactic acid (Figure 1.1), the dehydration to acrylic acid, the polymerization to poly (lactic acid) and the newly discovered condensation to 2,3-pentanedione are potentially the most profitable pathways. Lactic acid can be manufactured either by chemical synthesis or carbohydrate fermentation. While it was mostly produced through synthetic routes in the past by the US and Japan, lactic acid is currently produced from fermentation throughout the world (8). The commercially employed synthetic process is via the base-catalyzed addition of hydrogen cyanide to acetaldehyde to produce lactonitrile (Figure 1.2). Lactonitrile is purified and hydrolyzed to lactic acid with concentrated acid. Further purification steps are employed to acquired highly purified lactic acid. Other synthetic routes include direct oxidation of ethanol or propylene glycol and hydrolysis of α-chloropropionic acid (9).

Commercial production of lactic acid via carbohydrate fermentation uses mainly

Lactobacillus delbreuckii (10-12). Many carbohydrates, including whey, corn syrup, and

Figure 1.1. Primary Lactic Acid Pathways

as it reco
to gi
(arou
preve
maini
calciu

can

it m



produ

cane, can be sources for the fermentation. Because lactic acid is an end product inhibitor, it must be converted to lactate salt or extracted from the fermentation broth immediately as it is produced. Traditionally, calcium hydroxide has been used for this purpose. The recovered calcium lactate is then purified by evaporation and acidified with sulfuric acid to give lactic acid (13). However, since calcium lactate has a low solubility in water (around 8 wt%), only low concentration of lactate can be produced from fermentation to prevent formation of a large fraction of solid hydrated calcium lactate in solution and maintain product flow throughout the process. The cost of purifying dilute solution of calcium lactate and disposal of large amount of CaSO₄ has always been a drawback in the production of lactic acid via fermentation.

Figure 1.2. Chemical Synthesis of lactic Acid

use

has

car

١__

Eco

ferm

inste

hence

lactat

and n

broth.

calciu

on its

used in agent, a

tanning

lactic ac

higher co

Recent advances in simultaneous or coupled extractive technology have led to the use of nanofiltration membranes (14-17), anion-exchange resin (18,19) or activated carbon column, or solvent extraction (20,21) for recovering lactic acid. Electrodialysis has also been considered for recovering highly purified lactic acid from its salt form (22,23). These new innovations are currently lowering the production cost of lactic acid. Ecochem, a Du Pont-Conagra partnership which eventually ended, had also developed a fermentation process for lactic acid production in which ammonia is used for pH control instead of calcium hydroxide (24,25). Ammonium lactate is highly soluble in water, hence the concentration of lactate in broth can be as high as 30 wt% before activity of the fermentation organism is impaired. Ammonium lactate can subsequently be converted to lactate esters and ammonia in the presence of gaseous CO₂ and alcohol at around 160°C and moderate pressure (26,27). The ammonia is then recycled back to the fermentation broth. These advantages have made ammonia very attractive as a replacement for calcium hydroxide. The cost of lactic acid ranges between \$0.79/lb to \$0.83/lb depending on its purity (28).

The US consumes over 20 million lbs of lactic acid annually of which 85% is used in food-related applications to improve meat shelf-life and flavors, pH buffering agent, acidulant, and the production of emulsifying agents. Other uses include leather tanning, pharmaceutical and cosmetic application (29). Poly (lactic acid) produced from lactic acid is used as surgical sutures, controlled-release drugs, and prostheses. Currently, the polymer is not used as extensively as non-biodegradable polymers due to the slightly higher cost of production.

1.

ü8

coi

cof

me

nati

synt as m

antic

Vield

לונוני

roaste

in pho

iow sol

liquid-1

method

Many pa

of the rea

1.1.2. 2,3-Pentanedione

With a current market of only around 5000 lb/yr., 2,3-pentanedione has found its use entirely as a flavoring agent due to its strong buttery smell even in dilute concentration. Small amounts of 2,3-pentanedione are also naturally found in beer and coffee (30,31). Chemical synthesis of 2,3-pentanedione is achieved by the oxidation of methyl propyl ketone in excess NaNO₂ and diluted HCl (32). It can also be extracted naturally from the essential oil of Finnish pine and dairy waste. The current price of synthetic 2,3-pentanedione is around \$40/lb; natural 2,3-pentanedione costs around twice as much.

2,3-Pentanedione undergoes self-condensation to form duroquinone (an antioxidant) in basic and heated environment (Figure 1.3) (33). However, because of low yields due to many competitive pathways and the high cost of 2,3-pentanedione, this synthetic route has not been explored intensively. It also reacts with ethylenediamine and propylenediamine to produce, after dehydrogenation, the corresponding pyrazines (nutty, roasted flavoring agents) (34,35). 2,3-Pentanedione can be used as an effective initiator in photopolymerization and as a biodegradable solvent (36,37).

The reaction procedure for the formation of duroquinone from 2,3-pentanedione is relatively simple as the reaction occurs at room temperature. Since duroquinone has a low solubility in water, recovery of duroquinone from reaction mixture can be done by liquid-liquid extraction using an immiscible organic solvent such as toluene. This method can recover around 90% of the duroquinone formed. Figure 1.4 illustrates the many pathways that the condensation of 2,3-pentanedione can take; hence careful control of the reaction environment, especially solution pH and temperature, is necessary to

Fig

obia

This

into a

reactio

duroqu

high ten

accomplis

7

% minute:

optimize the yield to duroquinone. The polymerization of 2,3-pentanedione is favored with increasing temperature.

2,3-pentanedione duroquinone
$$H_2N = R$$

$$H_2N = R$$

$$A,\beta$$
-diamine 2-ethyl-3-methyl alkylpyrazines

Figure 1.3. 2,3-Pentanedione Pathways

After optimization of the reaction parameters, a yield of 29% theoretical was obtained for the formation of duroquinone from 2,3-pentanedione in a batch mode (38). This was achieved by adding 2,3-pentanedione solution (~1 wt%) at around 0.5 ml/min into a 1 M NaOH solution at room temperature. Slow addition of 2,3-pentanedione to reaction mixture reduces polymerization and reaction temperature, since the formation of duroquinone is exothermic. It has also been observed that in the presence of base and high temperature (~80°C), substantial degradation of duroquinone occurs.

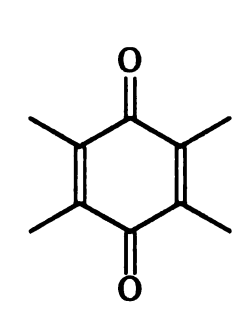
The formation of dihydropyrazine from 2,3-pentanedione and diamine is accomplished by refluxing equimolar quantities of each component in ether at 35°C for 90 minutes. Ether containing the corresponding alkyl group as the diamine is used as the

HC

\

Figure

2,3-Pentanedione



Duroquinone

Figure 1.4. Formation of Duroquinone from 2,3-Pentanedione

desired dihydropy methyl dihydropy can be achieved a pyrazine using a cyfew hours in methal pentanedione and e

1.13. Acrylic Aci

duroquinone and p

The primar solution polymers.

making of polymer

in disposable diape

per year and is exp

Acrylic aci

the development o

been essentially ba

activiene-based R

Popylene to acryl

amlein as an inte

Stateth molybdai

solvent since it is easily removed after the reaction by heating. The selectivity to the desired dihydropyrazine product is usually high. For example, the formation of 2-ethyl-3-methyl dihydropyrazine by reacting 2,3-pentanedione and ethylenediamine in ethyl ether can be achieved at yields on the order of 85%. The dihydropyrazine is then oxidized to pyrazine using a copper II oxide and KOH catalyst. The mixture is allowed to reflux for few hours in methanol. The overall yield to 2-ethyl-3-methyl pyrazine from 2,3-pentanedione and ethylenediamine is 73%. Detailed studies on the formation of duroquinone and pyrazines from 2,3-pentanedione have been performed by Thiel (38).

1.1.3. Acrylic Acid

The primary use of acrylic acid and acrylates is in the preparation of emulsion and solution polymers, which are used in coatings, finishes, polishes, adhesives, and the making of polymer fibers (39). Polymer fibers of acrylic acid are used as superabsorbents in disposable diapers. Worldwide production of acrylic acid is around 2 billion pounds per year and is expected to increase steadily at 3% per year.

Acrylic acid can be produced starting with a variety of petroleum based chemicals including acetylene, ethylene, and propylene. Because of the low cost of propylene and the development of very selective catalysts, commercial production of acrylic acid has been essentially based on propylene oxidation. However, some older plants still use the acetylene-based Reppe process for the production of acrylates. The oxidation of propylene to acrylic acid (Figure 1.5) is a two step process involving the formation of acrolein as an intermediate. Over 80% yield based on propylene can be obtained using a bismuth molybdate catalyst in the first stage and a molybdenum vanadium oxide catalyst

Priced at at

in the second stage. Current price of acrylic acid is about \$0.60/lb, making a lactic acid based process extremely dubious even if the selectivity to acrylic acid is 100%.

propylene
$$+ O_2$$
 $+ H_2O$ $+ H_2O$ OH acrylic acid

Figure 1.5. Oxidation of Propylene to Acrylic Acid

1.1.4. Propionic Acid

Like lactic acid, propionic acid can be manufactured either by chemical synthesis or fermentation of carbohydrates. Commercially, propionic acid is produced exclusively by the oxidation of propionaldehyde which is obtained by the catalytic hydroformylation of ethylene with carbon monoxide and hydrogen under relatively high temperature and pressure (The Oxo process) (40). Propionic acid fermentation of whey or lactose is achieved using *Propionibacterium acidipropionici* (41-43). However, due to its slow fermentation rate and low product concentration and yield, conventional propionic acid fermentation has not been able to compete economically with the synthetic route. Around 400 million pounds of propionic acid is produced annually worldwide, of which 60% is consumed by the US (44). Propionic acid and its salts are used as animal feed and corn preservatives, mold inhibitors, herbicides, cellulosic plastics, and anti-arthritic drugs. Current cost of synthetic propionic acid is around \$0.41/lb, while natural propionic acid is priced at around ten times as much.

1.2. Lactic

Since

can undergo around 190 (

concentrated

molecular we

are considere

1.2.1. Catal

Therr

acetaidehyde elimination c catalyst (45,4

lactone result

decomposes 1

enhanced in a

decarboxylati free-radical n

only \$0.45/1b

Pathway that

One way of d

of the suppor

1.2. Lactic Acid Reactions

Since lactic acid contains both hydroxyl and carboxylic acid functional groups, it can undergo many interesting chemical reactions. The boiling point of lactic acid is around 190°C at atmospheric pressure, but because of the ease of self-esterification, low molecular weight polymers are usually formed at elevated temperature when concentrated. The major pathways of lactic acid are shown in Figure 1.1; these reactions are considered individually in the following sections.

1.2.1. Catalytic and thermal decomposition

Thermal decomposition or pyrolysis of lactic acid results in the formation of acetaldehyde, carbon monoxide, and water. It is reported that this intramolecular elimination can be assisted by the acidic hydrogen of the carboxyl group without any catalyst (45,46). A five-membered cyclic transition state is formed which rearranges to a lactone resulting in the elimination of a water molecule (Figure 1.6). The lactone further decomposes to acetaldehyde and carbon monoxide. The decarbonylation of lactic acid is enhanced in an acidic environment and at high temperature. In the presence of base, decarboxylation of lactic acid to acetaldehyde, carbon dioxide, and hydrogen occurs. A free-radical mechanism is suggested for this reaction. Since the price of acetaldehyde is only \$0.45/lb, the formation of acetaldehyde from lactic acid is a major undesirable pathway that must be suppressed to increase the selectivities to other desirable pathways. One way of doing so is to use a low surface area silica support so as to lower the acidity of the support surface (47).

Н

lac

Figure 1

1.2.2, S

undergo

5

Similar to

dilactide

lactovillac

average n

concentra

Molecular

steps. Aft

catalytic ri

Currently,

Figure 1.6. Mechanism for Lactic Acid Pyrolysis to Acetaldehyde

1.2.2. Self-esterification and polymerization

Since lactic acid contains both the hydroxyl and carboxylic acid groups, it can undergo self-esterification to form either dilactide or lactoyllactic acid (Figure 1.1) (48)

Similar to all esterifications, the latter reaction is acid-catalyzed. The production of dilactide is catalyzed by primarily weak bases (49). Continued esterification of lactoyllactic acid gives poly(lactic acid), but the produced polymer usually has low average molecular weight because of the equilibrium constraint imposed by water concentration. The commercialized route patented by Du-Pont for the production of high molecular weight biodegradable poly(lactic acid) from lactic acid involves two catalytic steps. After the formation of lactide, water is removed by distillation and then a simple catalytic ring-opening polymerization of the purified lactide produces polylactide.

Currently, poly (lactic acid) is estimated to cost in the range of \$1.00-\$1.50. Co-

polymerizatio

of poly (ester-

1.2.3. Dehydi

The de

the past due to Holmen claim

at around 400

phosphate salt explanation ha

sodium bicarbo

159). Recently eactions in su

acrylic acid wi

group and the

lactone as an in

acetaldehyde a

states. Further

catalysts result

acid to acrylic

 G_{chter} and L_{a}

the highest sel

polymerization of lactic acid and diisocyanate has also been examined in the production of poly (ester-urethane) (50-53).

1.2.3. Dehydration

The dehydration of lactic acid to acrylic acid has been the focus of many studies in the past due to the demand for acrylate-based polymers (54-58). In 1958, a patent by Holmen claims the invention of a process in which 68% acrylic acid yields was obtained at around 400°C using sulfate and phosphate catalysts (2). It has been known that phosphate salts are commonly used in catalytic dehydration, but no complete mechanistic explanation has been proposed. Monobasic sodium phosphate catalyst buffered with sodium bicarbonate has also been used to obtain 58% acrylic acid yield from lactic acid (59). Recently, in 1989, Mok, Antal, and Jones published an in-depth study of lactic acid reactions in supercritical water (60). A mechanism for the dehydration of lactic acid to acrylic acid without catalyst was proposed which involved the leaving of the α -hydroxyl group and the carboxyl hydrogen instead of a hydrogen from the methyl group, forming a lactone as an intermediate. They had also identified the decarbonylation of lactic acid to acetaldehyde as the major competing reactions since both go through similar transition states. Further studies on lactic acid conversion in supercritical water using phosphate catalysts resulted in a 58% acrylic acid yield (61). Extensive conversion studies of lactic acid to acrylic acid over various sodium salts and supports have been performed by Gunter and Langford (47,62). It was found that sodium metasilicate and bromate exhibit the highest selectivity toward the formation of acrylic acid.

1.2.4. Red

Lact

fermentation with 50% yi

Velenyi et a

acid to aliph

 $M_aM_b^*O_{x}$, w

M' is at leas

The catalyst

oxides onto

is dried and

of the comp

the silica su

through a d

was able to

and atmosp

125. Con

The catalysts w

exuemely

lactic acid

found that

1.2.4. Reduction

Lactic acid has been reported to undergo direct reduction to propanoic acid during fermentation (63). Catalytic conversion of lactic acid to propionic acid was achieved with 50% yield using platinum and palladium catalysts at 250°C (4). A 1987 patent by Velenyi et al. describes a catalytic process for the conversion of α -hydroxy carboxylic acid to aliphatic carboxylic acid and aldehyde (64). The catalysts used have the formula M_aM'_bO_x, where M is at least one element selected from molybdenum, copper, or tin, and M' is at least one element selected from Group IA, IIA, IVA, VA, VIA, VIIIB, or VB. The catalyst is prepared by water impregnation of approximately 30 wt% of the metal oxides onto 70 wt% of silica or silica-alumina support. After mixing, the aqueous slurry is dried and calcined at 400°C under either oxygen or nitrogen for about 3 hours. Because of the complexity of the catalyst system, the exact structures of these oxide complexes on the silica support are not known. The feed (~26 wt% of lactic acid) is carried by nitrogen through a down flow, fixed bed reactor. Using Mo₅Cu₄SnO₅ on silica-alumina, Velenyi was able to obtain a 64% propionic acid yield with a total conversion of 99% at 350°C and atmospheric pressure.

1.2.5. Condensation to 2,3-pentanedione

The condensation of lactic acid to 2,3-pentanedione over basic sodium salt catalysts was discovered by Gunter et al. in our laboratory (65). This pathway is extremely attractive economically since 2,3-pentanedione is priced so much higher than lactic acid and the catalysts are inexpensive. Studies with various sodium salts have found that the best catalysts for 2,3-pentanedione formation are group IV and V oxides,

with sodium arsenate showing the best 2,3-pentanedione yield of 25% at 300°C and 0.5 MPa (66). Further examinations with sodium phosphates have demonstrated that both conversion and selectivity toward 2,3-pentanedione increase with increasing basicity of the phosphates in the order of Na₃PO₄ > Na₂HPO₄ > NaH₂PO₄. FTIR and ³¹P-NMR spectroscopic studies of the phosphate catalysts before and after lactic acid conversion has reviewed the formations of tetrasodium pyrophosphate and sodium lactate on Na₂HPO₄ and Na₃PO₄ catalyst surfaces after reaction (67). With NaH₂PO₄, sodium polyphosphates and sodium trimetaphosphate were observed with considerably less proton exchange between the phosphates and lactic acid. It was concluded that the presence of sodium lactate and/or pyrophosphate on the supported catalysts had increased the catalytic activity toward the formation of 2,3-pentanedione. Reaction conditions are also optimized for the formation of 2,3-pentanedione from lactic acid at 300°C, 0.5 MPa, and 3 second residence time over sodium salts supported on low surface area silica (68). Using a low surface acidic silica support is recommended to lower the activity toward acetaldehyde formation.

21. Vapor

21.1. Mat

L-(-

solution wa

was the hig

reaction ten

All

form except

purities of a

The

controlled-p

a surface are

support, ma

is also used

Chapter 2

EXPERIMENTAL METHODS

2.1. Vapor Phase Reaction

2.1.1. Materials

L-(-)-lactic acid was obtained from Purac, Inc. at 88 wt% solution and the feed solution was prepared by dilution to 34 wt% with HPLC water. A 34 wt% of lactic acid was the highest lactic acid concentration which can be sufficiently vaporized at typical reaction temperature in the vapor-phase reactor.

All of the alkali salts and bases were obtained from Aldrich in solid crystalline form except for cesium hydroxide, which was obtained at 50 wt% in solution. The purities of all chemicals used in this project are listed in Table 2.1.

The silica catalyst support used in most of the experiments is a low surface area controlled-pore glass (CPG03000D) manufactured by CPG, Inc. This support (CPG) has a surface area of about 7.2 m²/g with a low pore volume of 0.76 cc/g. A silica gel (SiGel) support, manufactured by Davison Chemical Co. with a N₂ BET surface area of 280 m²/g, is also used in some of the loading experiments.

Cesium Su

Copper (II Hemipenta

Deuterated

Heiium

HPLC Wate

Iron (III) Ni

Lactic Acid Lactic Acid

Lithium hyd

Methyl (S)-(

Nitric Acid

23-Pentane

2-Propanol

Phosphoric A

Potassium Bi

Potassium C

Potassium Hy $P_{\text{olassium}} M_{t}$

Table 2.1. List of Chemicals

Chemical Name	Chemical Formula	Purity	Form Obtained
Acetaldehyde	C ₂ H ₄ O	99.5+%	liquid
Acetol	$C_3H_6O_2$	90%	liquid
Acrylic acid	$C_3H_4O_2$	99%	liquid
Ammonium Hydroxide	NH₄OH	99+%	28-30% in water
Calcium Hydroxide	Ca(OH) ₂	95+%	solid
Cesium Chloride	CsCl	99%	solid
Cesium Hydroxide	CsOH	99%	50 wt % in solution
Cesium Nitrate	CsNO ₃	99%	solid
Cesium Sulfate	Cs ₂ SO ₄	99+%	solid
Copper (II) Nitrate	Cu(NO ₃) ₂ • 2.5H ₂ O	98%	solid
Hemipentahydrate			
Deuterated Water	D_2O	99.9%	liquid
Helium	Не	99.7%	gas
HPLC Water	H ₂ O	99.9997%	liquid
Iron (III) Nitrate Nonahydrate	Fe(NO ₃) ₃ • 9H ₂ O	98+%	solid
Lactic Acid (Aldrich)	C ₃ H ₆ O ₃	85%	solution
Lactic Acid (Purac, Inc.)	$C_3H_6O_3$	88%	solution
Lithium hydroxide monohydrate	LiOH•H ₂ O	98%	solid
Methyl (S)-(-)-Lactate	C ₃ H ₅ O ₃ CH ₃	98%	liquid
Nitric Acid	HNO ₃	70%	solution
2,3-Pentanedione	$C_5H_8O_2$	98%	liquid
2-Propanol	C ₃ H ₈ O	100%	liquid
Phosphoric Acid	H ₃ PO ₄	85+%	solution
Potassium Bromide	KBr	99.99%	solid
Potassium Chloride	KCl	99+%	solid
Potassium Hydroxide	КОН	85%	pellet
Potassium Methoxide	KOCH ₃	95%	powder

Potassium Phe

Propionic Acid

Sodium Chlor:

Sodium Hydro

Sodium Lactata

Sodium Metas:

Sodium Molyb

Sodium Nitrate

Sodium Nitrite

Sodium Phosph

tribasic dodecat

Sodium Pyroph

decahydrate

Sodium Sulfate

Tin (II) Oxide

2.1.2. Catalyst I

The catal

water before the

The CPG suppor

grinding. The m

of the water was

SiGel support wa

Table 2.1. List of Chemicals (Continued)

Chemical Name	Chemical Formula	Purity	Form Obtained
Potassium Nitrate	KNO ₃	99%	solid
Potassium Phosphate, tribasic	K_3PO_4	97%	solid
Propionic Acid	$C_3H_6O_2$	99.5%	liquid
Sodium Chloride	NaCl	99+%	solid
Sodium Hydroxide	NaOH	98.7%	pellet
Sodium Lactate	NaC ₃ H ₅ O ₃	99%	solid
Sodium Metasilicate	Na ₂ SiO ₃	89%	solid
Sodium Molybdate (VI)	Na ₂ MoO ₄	98+%	powder
Sodium Nitrate	NaNO ₃	99%	solid
Sodium Nitrite	NaNO ₂	97+%	solid
Sodium Phosphate,	Na ₃ PO ₄ •12 H ₂ O	98+%	solid
tribasic dodecahydrate			
Sodium Pyrophosphate,	Na ₄ P ₂ O ₇	99%	solid
decahydrate			
Sodium Sulfate	Na ₂ SO ₄	99+%	solid
Tin (II) Oxide	SnO	99+%	powder

2.1.2. Catalyst Preparation

The catalyst was prepared by completely dissolving the salt or base in HPLC water before the silica support was added at the amount specified by the desired loading. The CPG support was purchased as 60-70 mesh particles and was used with no further grinding. The mixture was then dried over a hot plate with constant stirring. After most of the water was removed, the mixture was dried in a furnace at 100°C overnight. The SiGel support was finely ground (<230 mesh) and calcined in air at 500°C for 24 hours

prior to pore \\
120°C and ag.

21.3. Vapor

(Figure 2.1) with

All reac

long. 1.25" OD

0.5" thick copp

section. The se

tube with a six

19" long and 0

top. The cataly

through. A V1

the Helicoflex

The liquid feec

in at the side.

tube by lactic a

lactic acid with

The rea

sink portion of

controller whice

thermocouple,

temperature is

prior to pore volume impregnation of the alkali salt. The resulting catalyst was dried at 120°C and again calcined in air at 500°C.

2.1.3. Vapor Phase Reactor

All reactions were performed in a downflow fixed-bed vapor-phase reactor (Figure 2.1) with an inner quartz liner. The reactor body is a stainless steel tube 19.5" long, 1.25" OD, and 0.55" ID. The heated portion of the reactor contains a 6.5" long and 0.5" thick copper heat sink to give better temperature control and distribution over that section. The second part (bottom piece) of the reactor is attached to this stainless steel tube with a six screw flange, and can be removed to allow insertion of a quartz liner. The 19" long and 0.5" OD quartz liner contains a fused medium fine quartz frit 10" from the top. The catalyst is supported on the frit, which allows the vaporized product to flow through. A Viton O-ring and a spring-loaded metal-to-metal seal ring manufactured by the Helicoflex Company are used to seal the two pieces of the reactor from gas leakage. The liquid feed is fed into the reactor at the top through a glass tube, while helium is fed in at the side. Glass and quartz are used to prevent any corrosion of the stainless steel tube by lactic acid at high temperature. They also suppress any unwanted side reaction of lactic acid with the metal.

The reactor is heated by a clamshell electric heater surrounding the copper heat sink portion of the reactor. The heater is controlled by an Omega PID temperature controller which receives feedback information from a thermocouple inside a thermocouple well between the heating element and the copper heat sink. The reaction temperature is measured inside the reactor using the thermocouple well located below the

Catalyst Bed

Figure 2.1. Val

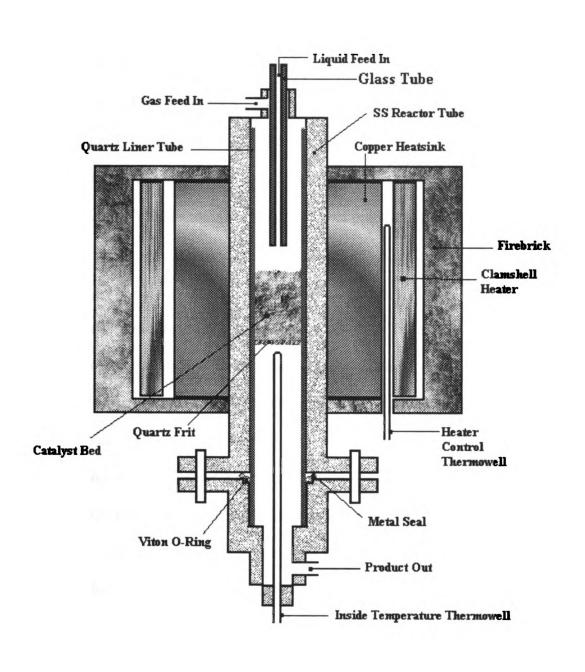


Figure 2.1. Vapor-Phase Reactor

supporting free heating element temperature is portions above another Omeganother Omeganother provides removable piece reaction.

2.1.4. Reaction

reactor. The reactor. The reactor. The reactor into the pumped into the lactic acid satural allowed to equilibriat samples collicious the carbon

discussed further

Table 2.2.

The reacto

Periods before and

through a meterin

supporting frit. The reaction temperature is controlled by adjusting the temperature of the heating element until the desired inside temperature is achieved. The heating element temperature is usually 30°C higher than the inside reaction temperature. The reactor portions above and below the copper heat sink are heated by heating tape controlled by another Omega PID temperature controller. Preheating the feed at the top portion of the reactor provides better temperature control throughout the catalyst bed. The bottom removable piece of the reactor is not heated to avoid product decomposition and further reaction.

2.1.4. Reaction Procedure and Product Analyses

The catalyst is weighed and loaded into the quartz liner which goes into the reactor. The reactor is heated to 260°C under helium flow before lactic acid feed is pumped into the reactor at a high flowrate (~0.5 ml/min) for 20 minutes. After the initial lactic acid saturation period, the flowrate is lowered to the desired value and the reactor is allowed to equilibrate for 30 minutes before product samples are collected. It is found that samples collected during the saturation period do not contain sufficient lactic acid to close the carbon balance. The reactions occurring during the initial saturation period is discussed further in Section 5.2. Typical steady-state reaction conditions are listed in Table 2.2.

The reactor effluent passes through a stainless steel trap immersed in ice water to condense out the liquid products. A separate bypass trap is used during equilibration periods before and in between sample collection. The gases leaving the ice trap flow through a metering valve, a filter, two infrared analyzers and a bubble meter before

venting into

flowrate is m

Riken infrare.

are used to ma

These reading

reached. The

(GC), and only

Table 2.2. Typ Temperature (

Pressure (MPa)

Liquid flow rate

Helium flow rat

Vaporized Feed

(mole fractio

Catalyst weight

Catalyst bed hei

Residence time

Once stea

products are coll

filter. The liquid

containing 10 g/l

acolumn conditio

glass 2 mm x 2 m

venting into the hood. A schematic of the reactor system is shown on Figure 2.2. Gas flowrate is measured by the bubble meter and controlled by the metering valve. Two Riken infrared gas analyzers (model no. RI-550A) obtained from CEA Instruments, Inc. are used to measure the amounts of CO and CO₂ in volume percentage continuously. These readings are useful to confirm that steady state reaction conditions have been reached. The gases were collected in gas bags and analyzed by gas chromatography (GC), and only CO and CO₂ were detected.

Table 2.2. Typical Reaction Conditions

Temperature (°C)	260 - 370		
Pressure (MPa)	0.5		
Liquid flow rate (ml/min)	0.1		
Helium flow rate (ml/min)	20		
Vaporized Feed Composition	Lactic acid: 0.08		
(mole fraction)	Water : 0.75		
	Helium: 0.17		
Catalyst weight (g)	2.0-3.0		
Catalyst bed height (cm)	5.0-6.0		
Residence time (sec)	3.0-4.0		

Once steady state has been reached at the specified reaction conditions, the liquid products are collected for 25 minutes and if necessary filtered using a disposable syringe filter. The liquid product is then mixed in an equal amount with a standard solution containing 10 g/l of 2-propanol as internal calibration standard and 0.06 M oxalic acid as a column conditioner. The resulting mixture is analyzed in a Varian 3700 GC with a glass 2 mm x 2 m 4% Carbowax 20M, 80/120 Carbopack B-DA column from Supelco,

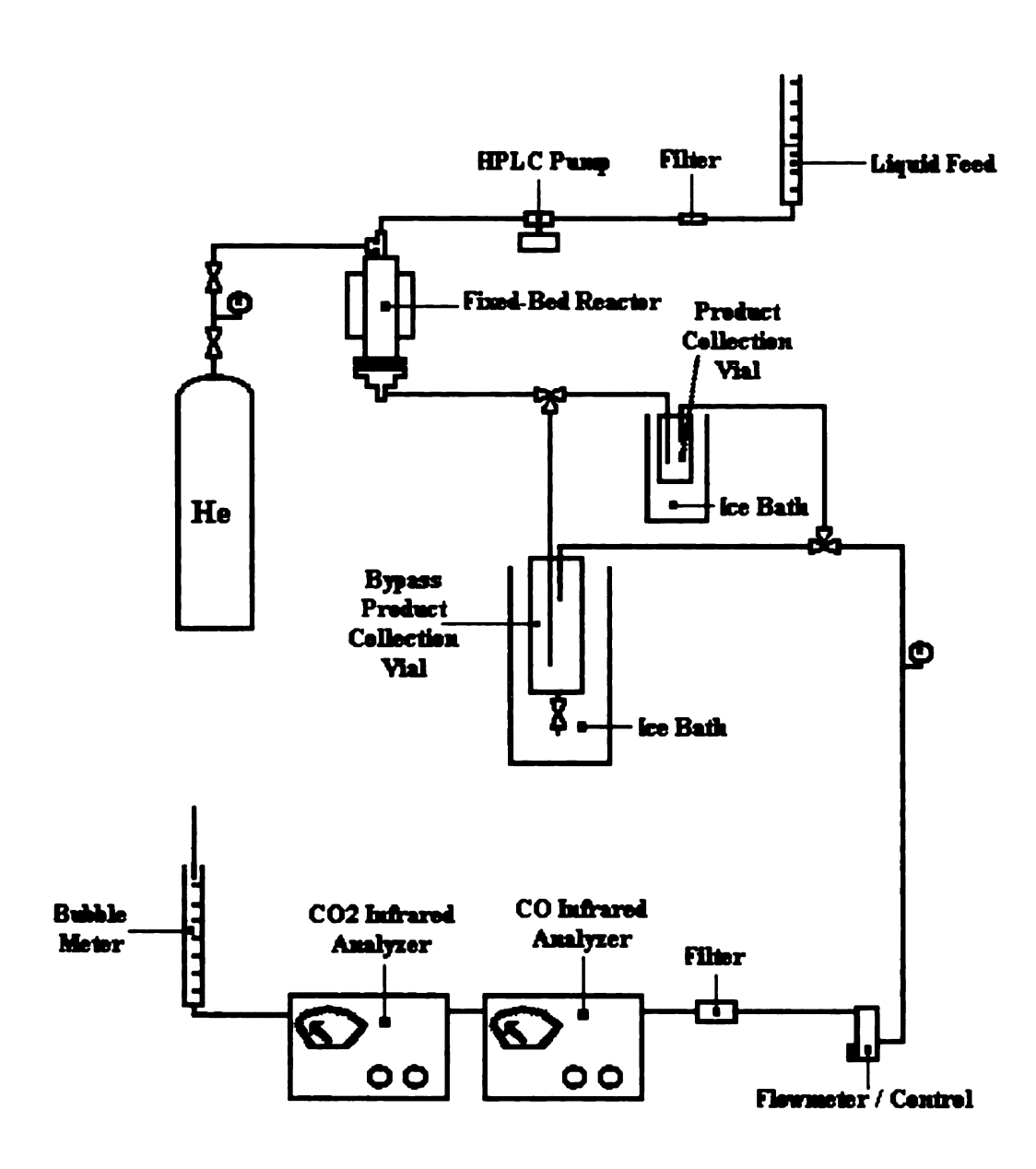


Figure 2.2. Reactor Flow Diagram

Inc. using a

Packard HP.

Table 2.3, an

are of concer

pentanedione

Table 2.3. G(

Column

Injector Tempe Initial Column

Ramp Rate

Final Column

Detector Temp

22. Post-Read

22.1. FTIR S₁

Transm

used in studying

information unc

for acquiring IR

obtained at mod

information on t

system can be at

species, either ac

Inc. using a flame ionization detector. Chromatograms were recorded on a Hewlett Packard HP3394 Integrator. The temperature program used for GC analysis is given in Table 2.3, and a typical product chromatogram is shown on Figure 2.3. Products which are of concern in this project include acetaldehyde, ethanol, acetic acid, acetol, 2,3-pentanedione, propionic acid, acrylic acid, and lactic acid.

Table 2.3. GC Operating Temperature Program

Column	Supelco 4% Carbowax 20M 80/120
	Carbopack B-DA in glass
Injector Temperature	200 °C
Initial Column Temperature	100 °C / 0 min.
Ramp Rate	5 °C / min.
Final Column Temperature	200 °C / 6 mins.
Detector Temperature	200 °C

2.2. Post-Reaction Transmission FTIR Spectroscopy

2.2.1. FTIR Spectroscopy

Transmission Fourier Transform Infrared (FTIR) spectroscopy has been widely used in studying heterogeneous catalytic reaction because of the ability to provide surface information under extreme reaction conditions (68-71). Standard equipment necessary for acquiring IR spectra and even doing *in situ* studies has been manufactured and can be obtained at moderate cost. Depending on the types of catalyst and reaction conditions, information on the structures of the adsorbed species and the kinetics of the reaction system can be attained from the infrared spectra. Quantitative information on the reaction species, either adsorbed or free, is usually obtained using the Beer-Lambert law.

Typical

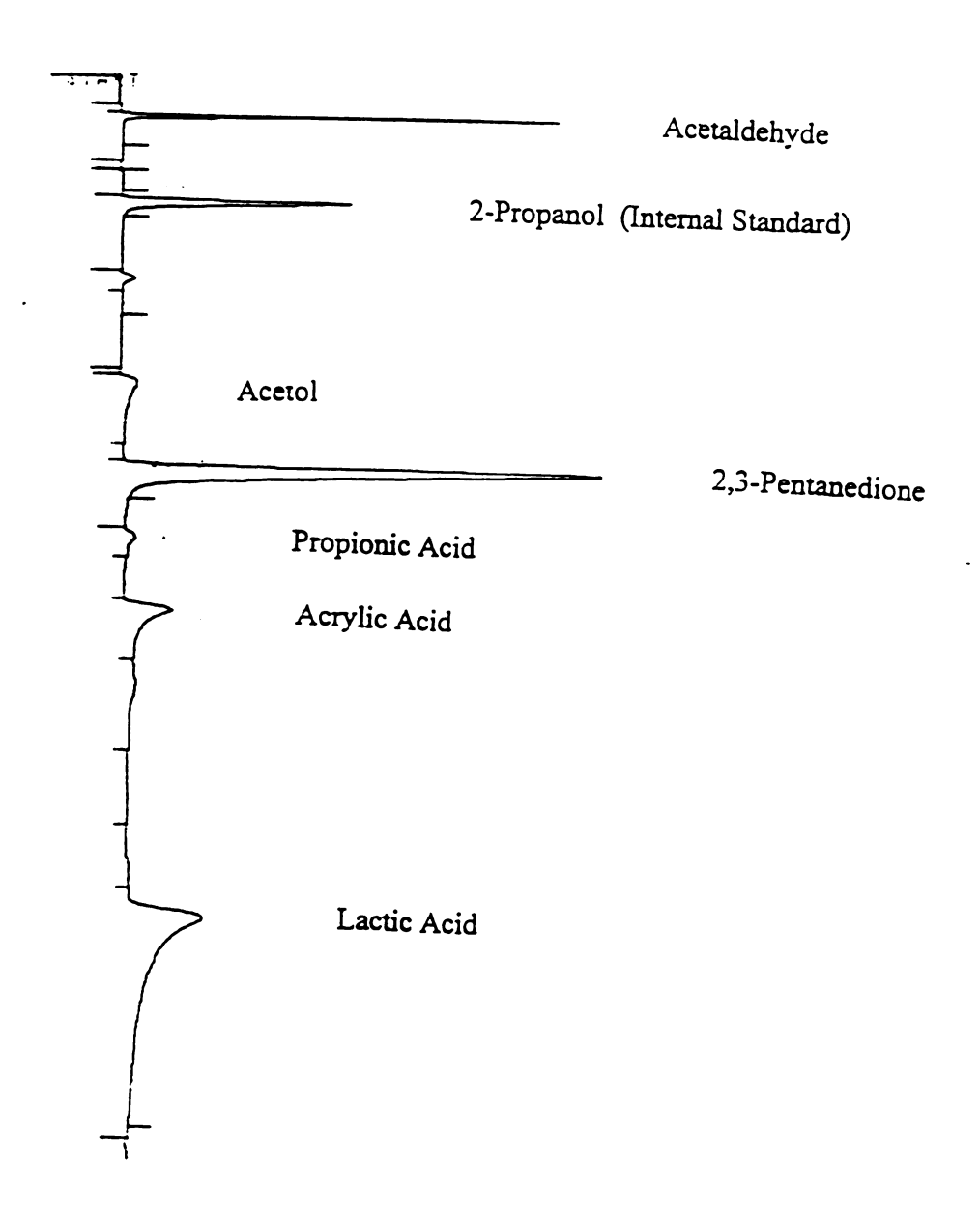


Figure 2.3. Typical Product Gas Chromatogram

In the silicon disk spectrum w. treatment. The low surface of the spectrum characterize the silicon disk.

222 Materi

The ch

2.1.1. The 9 r window from of the alkali sa solutions were spectra. Twen

223. Appara

silicon disk ins

3.7.

The appropriate the street of the street of

is controlled by

In the current project, alkali salts were vacuum dried onto an IR-transparent silicon disk and then exposed to lactic acid vapor at reaction temperature. An infrared spectrum was then taken to determine the chemical species present on the disk after the treatment. The silicon disk was chosen to imitate the actual catalyst support which has low surface area and pore volume. This technique provides us with a clear and accurate IR spectrum of the surface species without support interference and a rapid method to characterize the surface chemistry of our reaction system.

2.2.2. Materials and Sample Preparation

The chemicals used in the post-reaction FTIR studies are discussed in Section 2.1.1. The 9 mm diameter and 2 mm thick silicon disks with an infrared transparent window from 8300-660 cm⁻¹ were obtained from Spectra Tech Inc.. Aqueous solutions of the alkali salts were prepared using HPLC water. The molar concentrations of these solutions were chosen by trial and error to give appropriate transmittances and thus clear spectra. Twenty-five µl of the solution were then vacuum dried onto both sides of the silicon disk inside a glass desiccator. Concentrations of these solutions are listed in Table 3.7.

2.2.3. Apparatus and Procedure

The apparatus employed to expose the sample silicon disk to lactic acid vapor developed by Gunter (62) and is shown in Figure 2.4. It contains a 200 ml three-neck round bottom flask where lactic acid solution is vaporized using a heating mantle which is controlled by a variable autotransformer. The lactic acid solution temperature is

Figure 2 4

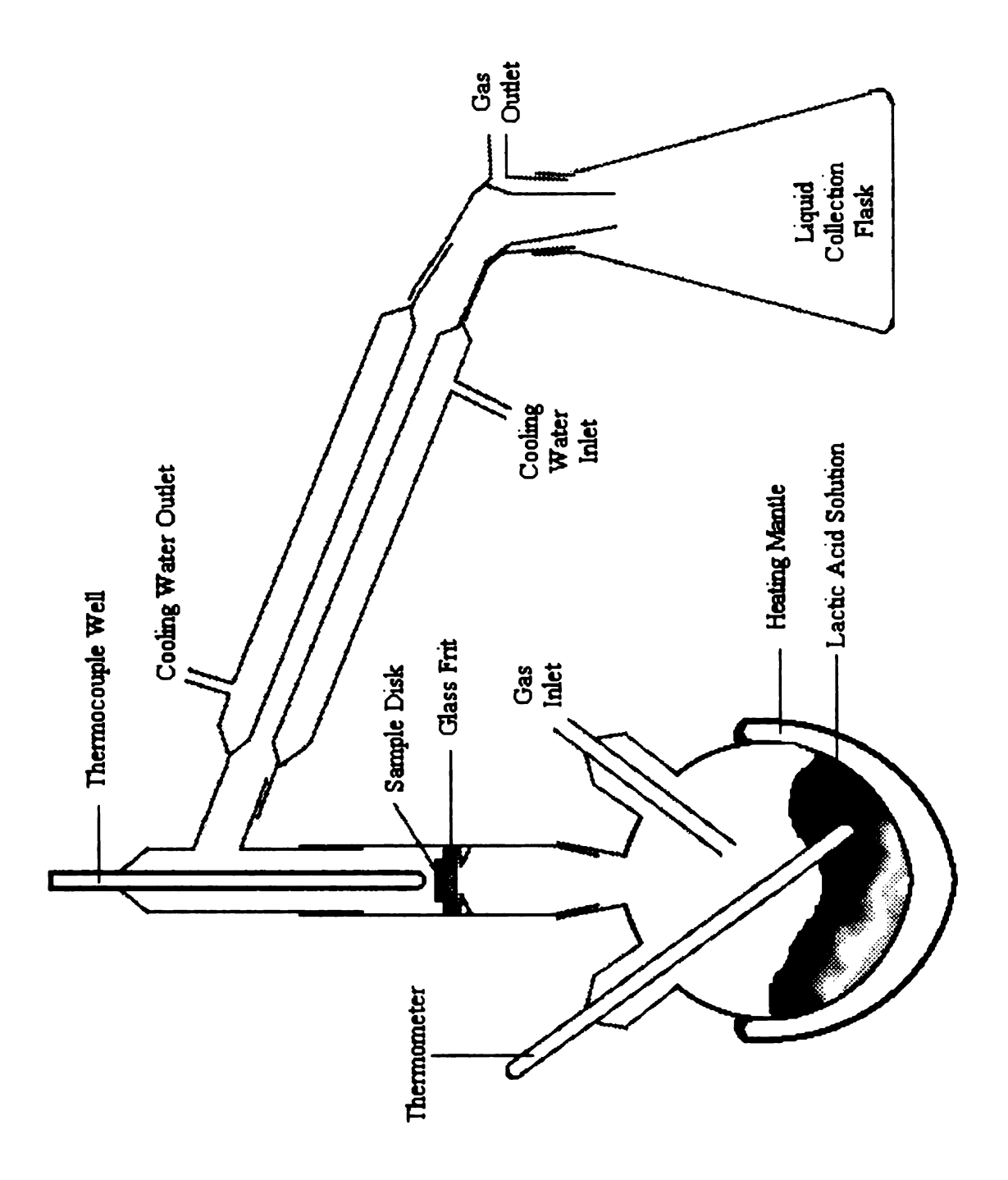


Figure 2.4. Preparation Apparatus for Post-Reaction Studies

through the water conde measured at heated to the PI controller slightly above The 85 most of the wa preheated to th above was ther temperature wi 10 minutes befo The disk was th magnetic sampl was transferred disk was collect of 1 cm-1 at amb helicoil globar s with a KBr wind

using Nicolet PC

subtraction of the

the chemical spec

monitored t

monitored by a thermometer and is usually kept at 170°C. Lactic acid vapor is carried through the glass frit and sample disk by helium gas before being condensed out by a water condenser and finally collected in an Erlenmeyer flask. The gas flowrate is measured at the end by a bubble meter. The column which contains the sample disk is heated to the desire reaction temperature with heating tape that is controlled by an Omega PI controller which receives its feedback from a thermocouple in a thermocouple well slightly above the sample disk.

The 85% lactic acid solution was dried at 170°C for around one hour to remove most of the water before the experiments. After water removal, the column was preheated to the desired temperature. A sample disk prepared by the procedure described above was then placed in the column on the glass frit. After returning to the desired temperature with reversed gas flow, the disk was exposed to lactic acid vapor for about 10 minutes before gas flow was reversed again and the column heating tape is turned off. The disk was then cooled to below 100°C, taken out of the column and inserted into a magnetic sample holder (Spectra Tech) which fits into the FTIR spectrometer. The disk was transferred immediately to a Nicolet IR/42 spectrometer where an IR spectrum of the disk was collected in the mid-IR region of 400-4800 cm⁻¹ with 32 scans and a resolution of 1 cm⁻¹ at ambient temperature under nitrogen. The spectrometer contains a broadband helicoil globar source and a deuterated triglycine sulfate (DTGS) pyroelectric detector with a KBr window. The spectrum is obtained with a Dell system 200 personal computer using Nicolet PC/IR version 3.00. After the spectrum of the sample disk was collected, subtraction of the background clean silicon disk spectra was done to obtain a spectrum of the chemical species on the disk surface after exposure to lactic acid vapor. The baseline

of the spect presentable

temperature

23. Post-Re

23.1. Diffus

DRIF including cata

pressed into so

are used to op:

the complexity

transmission F1

commercialized

Another drawba

band intensities

23.2 Sampling

The powd

before being loade

a.Mattson Galaxy

atachment. For hi

which needs to be a

of the spectrum was usually corrected with a second or third order method to give a more presentable spectrum. This procedure was repeated using different sample disks for temperatures from 150-350°C.

2.3. Post-Reaction DRIFTS

2.3.1. Diffuse Reflectance Infrared Fourier Transform Spectroscopy (DRIFTS)

DRIFTS is an extremely promising technique for the study of powder samples including catalysts (72-75). Unlike transmission FTIR, powder samples do not have to be pressed into self-supporting wafers. In DRIFTS, semi-ellipsoidal or ellipsoidal mirrors are used to optimize IR beam collection from the irradiated sample surface. Because of the complexity in building sampling cells, DRIFTS has not been as widely used as transmission FTIR. However, this will soon change due to the availability of commercialized DRIFTS cells which can be attached to ordinary FTIR spectrometers. Another drawback of DRIFTS is that a dilute sample has to be used to get reproducible band intensities for quantitative analysis.

2.3.2. Sampling Procedure

The powder catalyst samples are mixed with KBr in a 1:10 sample to KBr ratio before being loaded into a microsample cup. The sample cup is then placed directly into a Mattson Galaxy 3000 FTIR spectrometer equipped with a SpectraTech DRIFTS attachment. For high sensitivity, a mercury-cadmium-telluride (MTC) detector is used which needs to be cooled to liquid N₂ temperature before spectrum collection. The IR

spectru

Backgr

24. G

product

provide

This is a to the sta

Vanan V

·

chromate Lab-Base

'emperati

1-1

analysis.

spectrum is collected at 4 cm⁻¹ resolution for 50-100 scans in the range of 600-4000 cm⁻¹.

Background subtraction is done to obtain the spectrum of the sample itself.

2.4. Gas Chromatography - Mass Spectrometry (GC-MS)

GC-MS is used in addition to NMR and FTIR spectroscopies to identify unknown products which elute out of our standard GC analysis. It is also useful in this project to provide locations of isotopes for isotopic labeling experiments with deuterated water. This is accomplished by comparing the fragments in the mass spectra of labeled products to the standard mass spectra of these products (76). GC-MS analyses are carried out on a Varian VG-TRIO1 8288 mass spectrometer coupled to a Hewlett Packard 5890J gas chromatograph via a heated interface. The data are processed and recorded using the Lab-Base software running on a personal computer. A similar GC column and temperature program as the ones described in the Section 2.1.4 were used for GC-MS analysis. Direct (splitless) injection of around 0.5 µl of sample was used.

LAC

over se

mechar

interme

reaction

observe.

identific

pentaned

3.1. Va₁

system w

Ŋ

1/21/O_{2, 1}

Aldrich ir

chosen to

results fro

Chapter 3

LACTIC ACID CONVERSION OVER SODIUM SALTS AND BASE ON SILICA

This chapter focuses on vapor-phase reaction studies of lactic acid conversion over selected sodium salts supported on low surface area silica, and the development of a mechanism for the condensation of lactic acid to 2,3-pentanedione. Information on the intermediate species and steps of 2,3-pentanedione formation are provided by post-reaction FTIR spectroscopy of model catalysts and explanations are given regarding the observed activity differences between the studied sodium salts. These results aid in the identification of the ideal catalysts and reaction conditions for the production of 2,3-pentanedione.

3.1. Vapor-phase reaction

Materials used in these studies were discussed in Section 2.1.1. and the reactor system was described in Section 2.1.3. The selected sodium salts (NaOH, NaCl, NaNO₃, NaNO₂, Na₂SiO₃, Na₂SO₄, NaC₃H₅O₃, Na₄P₂O₇, and Na₃PO₄·12H₂O) were obtained from Aldrich in solid form and impregnated onto CPG (Section 2.1.2). This support was chosen to minimize the formation of acetaldehyde from lactic acid in accordance with results from previous work (66).

ۀ'

3.1.1. Results

All reported results are obtained at reaction conditions listed in Table 2.2 and usually at a loading of 1 mmol of salt per gram of CPG. Product yields and selectivities of lactic acid conversion over CPG alone and over NaC₃H₅O₃, NaOH, Na₂SiO₃, NaNO₂, NaNO₃, Na₄P₂O₇, Na₃PO₄, NaCl, and Na₂SO₄ supported on CPG are presented in Tables 3.1-3.5. Product yield is defined as percentage of the theoretical yield except for CO and CO₂, which are reported as moles of gas formed per 100 moles of lactic acid fed into the reactor. Selectivities are reported as the percentage of lactic acid converted to the specific products. Minor products such as ethanol, acetic acid, and methyl ethyl ketone are included as "Other" in these tables. The row labeled "Unknown" include all unidentified compounds on the chromatogram; "unknown" yield is calculated with an assumed response factor of 1 with respect to the internal standard (2-propanol).

Over the support alone, production of acetaldehyde and carbon monoxide from decarbonylation of lactic acid is dominant. This is especially apparent at 350°C, where 77% of the converted lactic acid goes to acetaldehyde through decarbonylation.

Selectivities toward the other conversion pathways increase dramatically when sodium salt or base, except for Na₂SO₄, is added as catalysts. Although addition of Na₂SO₄ does not enhance the production of the desirable products, it does lower the extent of decarbonylation of lactic acid to acetaldehyde at high temperature, presumably by blocking or neutralizing some of the acid sites on the surface of the silica support. Lactic acid conversion over NaNO₂ is performed since it is a decomposition product of NaNO₃ at high temperature.

CPG alone

Table 3.1. Lactic Acid Conversion over CPG and NaC₃H₅O₃/CPG

Catalyst			CPG alone				1 mmol 1	NaC3H5O3		
Temperature (°C)	260	280	300	320	320	260	280	300	320	350
Contact Time(s)	4.7	4.1	4.1	3.8	3.9	3.2	3.0	2.9	2.8	2.7
Error (% Carbon)	19.7	10.7	17.3	2.9	-14.4	9.8	4.4	12.6	-5.0	-23.4
Conversion (BOF)	-18.4	-8. 8.	-13.3	10.5	54.6	4.2	16.1	36.1	85.3	95.3
Yield (% Theoretical)										
Acrylic acid	0.0	0.4	0.2	1.1	2.0	1.5	3.3	9.4	20.5	16.7
Propionic acid	0.0	0.1	0.5	0.4	0.1	0.4	0.0	0.4	6.0	2.4
2,3-Pentanedione	0.1	0.2	0.2	0.3	9.0	6.3	12.9	23.6	26.0	18.5
Acetaldehyde	6.0	6.0	2.5	11.2	33.6	4.5	3.9	7.9	15.4	20.0
Acetol	0.0	0.0	0.0	0.0	0.0	0.0	0.0	6.3	6.9	6.1
Other	0.0	0.0	0.0	0.0	0.0	0.0	0.0	0.0	0.0	2.0
Unknown	0.7	0.5	1.0	1.6	4.8	0.3	0.0	0.0	10.7	5.3
*00	0.5	0.5	1.4	6.4	28.1	2.2	1.4	1.9	5.6	0.9
C02*	8.0	6.0	1:1	1.3	2.0	4.8	8.6	20.8	25.6	29.8
Selectivity (%)	.,=									
Acrylic acid	0	27	9	6	S	12	91	20	29	25
Propionic acid	0	9	9	3	3	33	0	_	_	4
2,3-Pentanedione	12	10	7	7	7	49	8	20	37	28
Acetaldehyde	88	99	80	98	8	36	61	17	22	30
Acetol	0	0	0	0	0	0	0	13	10	6
Other	0	0	0	0	0	0	0	0	0	33
-										

*Yields reported as mole per 100 moles of lactic acid fed.

: Ja. J. HOr.N. Journ

Catalyst

Table 3.2. Lactic Acid Conversion over NaOH/CPG and Na₂SiO₃/CPG

Catalyst		l mmo	I NaOH / s	g CPG		=	nmol Na ₂ S	SiO3 / g CPG	2
Temperature (°C)	260	280	280 300	320	350		300 320	320	350
Contact Time(s)	3.9	4.0	3.8	3.6	3.4		3.6	3.3	3.1
Error (% Carbon)	-20.7	-16.1	-11.5	9.6-	-18.5		-14.8	-26.6	-22.9
Conversion (BOF)	31.3	39.2	62.5	85.0	95.4		80.5	9.96	96.4
Yield (% Theoretical)									
Acrylic acid	1.5	3.7	12.8	25.6	32.8	6.5	15.2	12.8	15.8
Propionic acid	0.0	0.0	1.1	1.5	4.1	0.0	2.0	3.6	5.6
2,3-Pentanedione	8.2	15.3	23.1	21.9	13.3	24.8	29.6	21.3	11.9
Acetaldehyde	8.0	2.5	6.2	11.9	14.7	4.6	10.2	14.8	14.0
Acetol	0.0	1.9	7.4	12.5	6.5	1.7	7.4	7.6	5.1
Other	0.0	0.4	9.0	1.6	1.9	0.0	1.0	2.0	8.1
Unknown	1.5	8.0	1.6	3.8	5.5	8.0	1.6	4.8	14.7
*00	0.0	9.0	1.4	3.0	5.6	2.0	1.9	4.0	8.9
C02*	6.0	5.7	11.9	12.2	12.6	13.7	21.1	34.1	29.6
Selectivity (%)									
Acrylic acid	14	91	25	34	45	17	23	21	53
Propionic acid	0	0	7	7	9	0	3	9	01
2,3-Pentanedione	78	65	45	29	<u>8</u>	99	45	34	22
Acetaldehyde	∞	10	12	91	70	12	91	24	5 6
Acetol	0	∞	14	17	6	S	=	12	6
Other	0	7	_	7	3	0		33	3
W. 11.	2	1-1-61	1.21.						

Yields reported as mole per 100 moles of lactic acid fed.

Table 3.3. Lactic Acid Conversion over NaNO2/CPG and NaNO3/CPG

Catalyst		1 mmol	I NaNO2/	g CPG			1 mmo	I NaNO3/	g CPG	
Temperature (°C)	260	280		320	350		280		320	350
Contact Time(s)	3.8	3.6	3.6	3.5	3.3		3.1		2.8	2.7
Error (% Carbon)	6.0	0.4	-21.5	-29.6	-29.0		-13.0	-9.3	-26.1	-26.0
Conversion (BOF)	16.2	39.2	79.5	9.96	96.2		41.6		98.5	8.86
Yield (% Theoretical)										
Acrylic acid	9.1	7.9	13.9	13.3	14.4	1.9	4.9	11.6	16.8	15.7
Propionic acid	0.0	0.7	0.0	3.9	7.8	0.3	6.0	5.6	5.9	9.6
2,3-Pentanedione	8.4	21.1	25.8	18.5	9.01	7.8	17.2	23.5	18.8	11.9
Acetaldehyde	2.0	5.1	10.7	17.7	19.9	4.2	4.6	12.3	18.2	28.2
Acetol	0.0	2.8	5.7	6.3	3.7	0.0	0.0	4.0	6.2	3.2
Other	0.0	0.0	8.0	1.8	8.1	0.3	0.2	8.0	1.2	2.5
Unknown	1.3	2.1	1.6	5.2	0.9	8.0	1.2	1.7	3.8	3.2
CO	4.5	1.6	2.8	5.9	14.5	8.0	8.0	<u>8.</u>	3.3	6.7
CO2*	7.3	14.6	20.5	25.2	22.4	5.8	11.9	24.9	31.4	27.5
Selectivity (%)										
Acrylic acid	=	21	24	22	25	13	81	21	25	22
Propionic acid	0	7	0	9	13	7	3	2	6	13
2,3-Pentanedione	26	26	45	30	18	24	62	43	28	17
Acetaldehyde	33	14	61	29	34	56	17	22	27	40
Acetol	0	7	01	01	9	0	0	7	6	5
Other	0	0		3	3	7	_	_	7	က

*Yields reported as mole per 100 moles of lactic acid fed.

- 1
1
•
,
•
The state A said Change and a second
•
-
-
- 7
•
•
_
7
,
•
•
٠,
•
•
-
- 7
_
•
-
ž
12
1111
1111
Link
J. die
Link
Lille
Tille
Talle
Little
Little
Table
Table
Table
Table
J. O. L.
J. O. L.

Table 3.4. Lactic Acid Conversion over Na₃PO₄/CPG and Na₄P₂O₇/CPG

Cotoling		1	A DO ON I				10000	No D O	Say	
Temperature (OC)	260	780	1 14d31 O4 / 200		350	260	780	200	330	350
l'emperature (C)	207	780	36	220	320	007	780	3	220	320
Contact Time(s)	4.0	3.7	3.6	3.5	3.4	2.5	2.8	2.7	2.3	2.5
Error (% Carbon)	<u>~</u>	-9.1	-10.4	-27.7	-30.6	1.4	8.1	-12.4	5.9	6.0
Conversion (BOF)	11.3	37.3	9.89	89.4	95.4	18.6	19.1	0.09	55.6	80.0
Yield (% Theoretical)	<u> </u>									
Acrylic acid	1.9	4.8	13.7	17.2	20.0	2.1	5.4	7.8	14.7	17.2
Propionic acid	0.8	0.5	2.3	3.2	6.7	0.0	9.0	0.7	2.2	3.0
2,3-Pentanedione	8.4	15.4	24.9	16.9	12.5	7.1	16.5	22.3	20.9	16.5
Acetaldehyde	=	3.0	7.4	11.1	11.5		4.1	9.1	14.6	18.3
Acetol	0.5	2.4	7.4	9.5	9.9	0.0	1.0	2.4	0.0	0.0
Other	0.0	0.3	9.0	1.3	1.6	0.0	0.0	0.5	6.3	5.5
Unknown	6.0	5.9	4 .8	4.6	6.4	9.5	0.2	5.7	1.0	17.9
*00	0.0	0.5	1.3	2.2	3.0	8.0	1.2	1.7	4.9	8.1
C02*	3.9	7.4	10.6	12.9	15.5	.5 4.3 9.6 17.2 33	9.6	17.2	33.3	32.8
Selectivity (%)										
Acrylic acid	15	18	24	56	34	61	19	16	25	28
Propionic acid	9	7	4	2	11	0	7	2	4	2
2,3-Pentanedione	99	28	4	56	21	65	9	53	36	27
Acetaldehyde	6	11	13	19	70	91	15	21	25	30
Acetol	4	6	13	16	=	0	4	9	0	0
Other	0	_		7	3	0	0	_	=	6

*Yields reported as mole per 100 moles of lactic acid fed.

Catalyst Temperature (°C)	092	lomm 1	I mmol NaC1/g CPG	; CPG	150	096	lomm 1	1 mmol Na.SO ₄ / g CPG	g CPG
		251				207	CCV		
/ conference (C)	007	CXT	005	075	3.50	200	CXCI	ÇÇ.	320

350

Table 3.5. Lactic Acid Conversion over NaCl/CPG and Na₂SO₄/CPG

Catalyst		1 mmol NaCl /	ol NaCl / g	CPG		l mmo	Na2SO4/	g CPG	
Temperature (°C)	260	280	300	320	350	280	300	320	350
Contact Time(s)	3.5	3.3	3.3	3.2	3.0	4.1		3.7	3.5
Error (% Carbon)	9.3	-0.7	-10.0	-11.7	-3.2	8. 8.		-2.5	-17.0
Conversion (BOF)	0.4	11.9	28.1	44.1	2.99	-5.7	•	13.3	46.9
Yield (% Theoretical)									
Acrylic acid	0.5	8.0	2.1	5.7	10.6	0.3		1.4	4.0
Propionic acid	0.5	0.4	6.0	2.2	5.0	0.3		1.2	3.1
2,3-Pentanedione	1.6	3.9	8.2	11.8	12.5	0.4		=	2.4
Acetaldehyde	9.0	1:1	3.0	7.4	16.7	1.7		6.7	20.0
Acetol	0.0	0.0	0.0	2.2	3.1	0.0		0.0	0.0
Other	0.3	0.1	0.0	0.0	1.2	0.0		0.0	0.1
Unknown	8.9	5.7	5.8	6.4	19.3	0.5		1.3	2.5
*00	0.0	0.0	0.1	0.3	2.3	1.0		2.7	10.9
C02*	0.2	9.0	1.7	3.3	9.1	1.0		1.9	4.5
Selectivity (%)									
Acrylic acid	14	12	15	19	22	13		13	13
Propionic acid	13	7	9	7	10	01		=	01
2,3-Pentanedione	47	19	28	40	25	13		=	∞
Acetaldehyde	18	8	21	25	34	2		2	89
Acetol	0	0	0	∞	9	0		0	0
Other	7	7	0	0	7	0		0	0
	00.								

Yields reported as mole per 100 moles of lactic acid fed.

Among the desired products, acrylic acid and propionic acid are favored at higher temperature, while the formation of 2,3-pentanedione is preferred at lower temperature. Yields of 2,3-pentanedione and acrylic acid from 260°C to 370°C over the selected sodium salts and base are displayed in Figures 3-1 and 3-2. Only a small amount of propionic acid is generally produced over these catalysts, and attempts are made to increase propionic acid yield by using metal catalysts. Detailed discussions of these experiments are presented in Chapter 6.

For the active sodium salts and base (NaOH, NaNO₃, NaNO₂, Na₂SiO₃, NaC₃H₅O₃, Na₄P₂O₇, and Na₃PO₄), the yield of 2,3-pentanedione is a maximum at 300°C, and is the same for all salts within experimental uncertainty, except silicate. These results are similar to yields obtained with Na₂HAsO₄ in previous studies completed in our group (66). Yields for sodium metasilicate are slightly higher at 300°C, because twice as much sodium is present (i.e. twice the base equivalence) per mole of loading. Further discussion on catalyst loading effects are presented below and Chapter 4. Unsupported sodium silicate was also used as catalyst, however, there were a lot of coking and the highest 2,3-pentanedione yield obtained was only 15% of theoretical.

The decline in 2,3-pentanedione as temperature is increased above 300°C is attributable to competition with acrylic acid and acetaldehyde formation pathways. Acrylic acid yield reaches a maximum at around 350°C for most of the sodium salts studied. Both 2,3-pentanedione and acrylic acid yields from NaCl and Na₂SO₄ are significantly lower at all temperatures, indicating that NaCl and Na₂SO₄ behave differently than the other sodium salts.

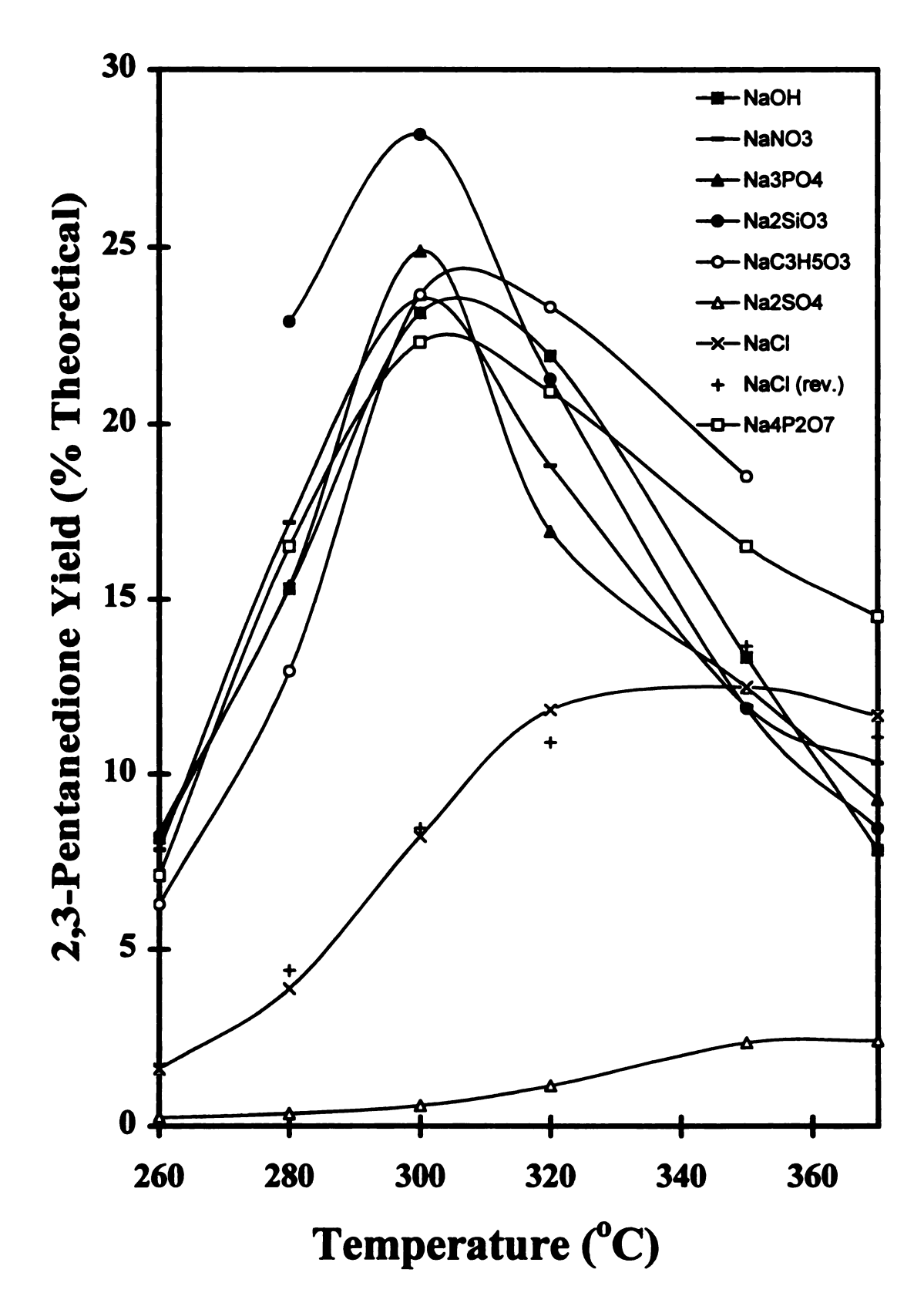


Figure 3.1. 2,3-Pentanedione Yields over Various Sodium Salt Catalysts

 F_{ig}

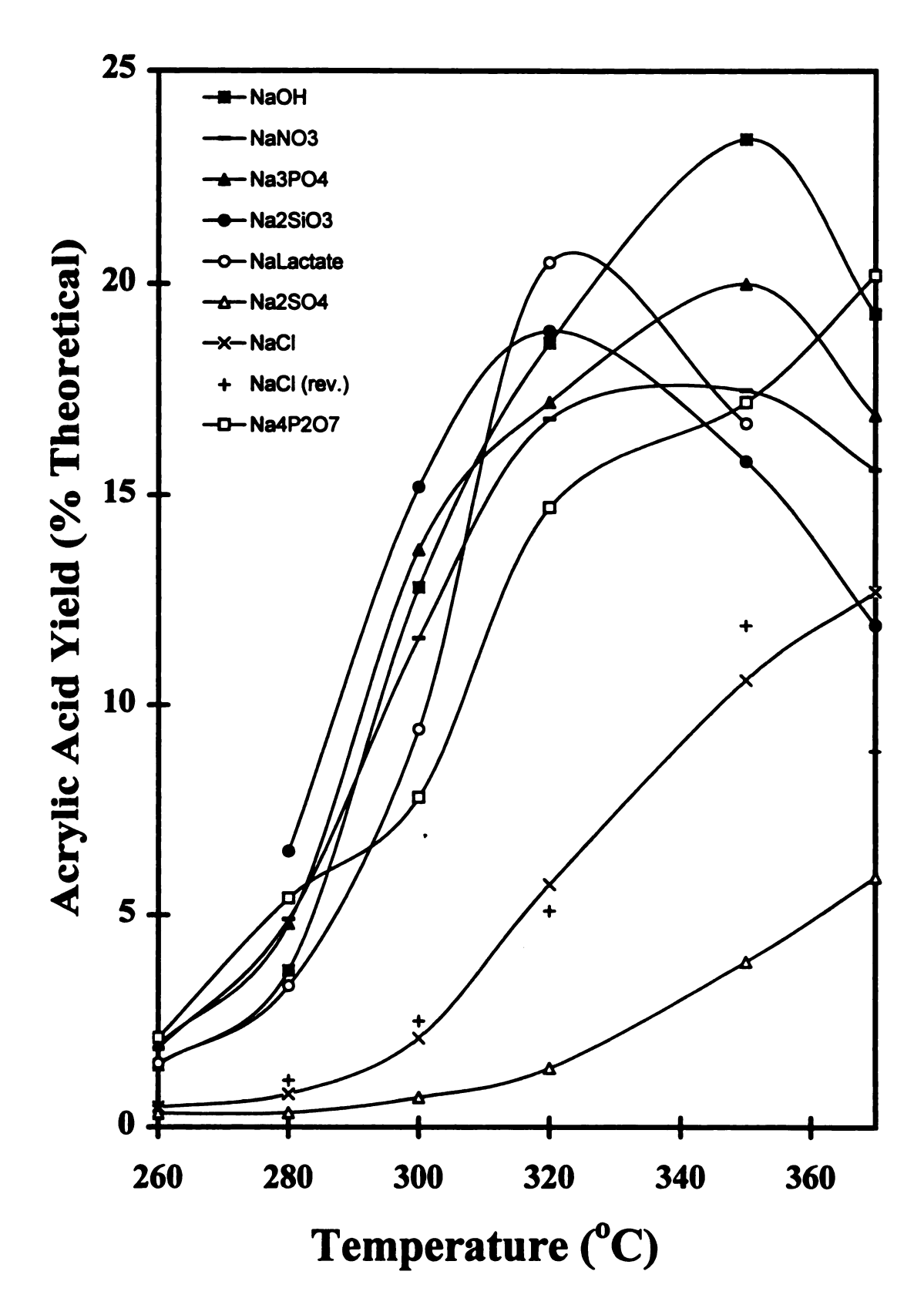


Figure 3.2. Acrylic Acid Yield over Various Sodium Salt Catalysts

3.1.2. Effects of sodium catalyst loading

The effect of loading on lactic acid conversion over sodium catalysts was investigated using NaOH and NaNO₃ with loading ranging from 1.0 to 4.0 mmol/g of CPG (Figure 3.3). It was found that sodium loading of 2 mmol/g of support gives the highest yield of 2,3-pentanedione at the optimum temperature of 300°C. The slightly higher 2,3-pentanedione yield obtained over Na₂SiO₃ in Figure 3.1 was a consequence of higher loading (2 mmol Na / g support). However, higher loadings did increase the yield slightly at lower temperatures. Further examination of the effect of loading is discussed in Section 4.1.2, where a kinetic model of the reaction system for sodium catalysts is developed.

3.2. Post-reaction FTIR results

The apparatus and procedure used for exposing sodium salts to lactic acid vapor have been described in Section 2.2.2. The FTIR spectra of the samples on silicon disks are taken at room temperature after the samples were exposed to lactic acid vapor at 150-350°C. This model catalyst system provides important information about the species on the catalyst after the reaction.

3.2.1. Characteristic infrared bands of sodium salts and base

Standard infrared spectra of lactic acid, sodium lactate, NaOH, NaNO₃, Na₂SiO₃, Na₂SO₄, Na₃PO₄, and Na₄P₂O₇ are given in Figure 3.4-3.5 in the region between 2000-700 cm⁻¹, where most of the significant spectral information is provided in the

Figi

ŗ

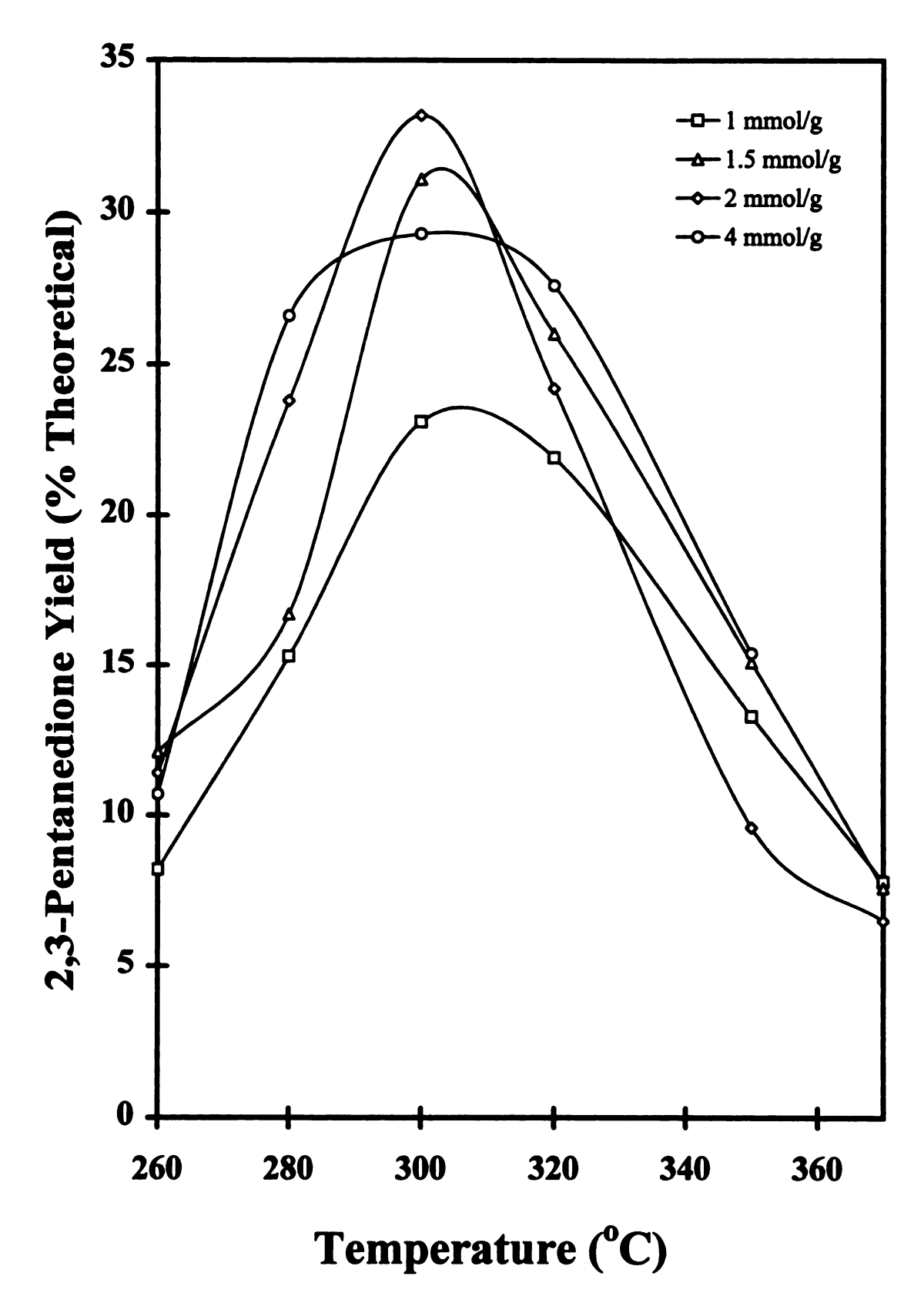


Figure 3.3. Effect of Sodium Loading on 2,3-Pentanedione Yield

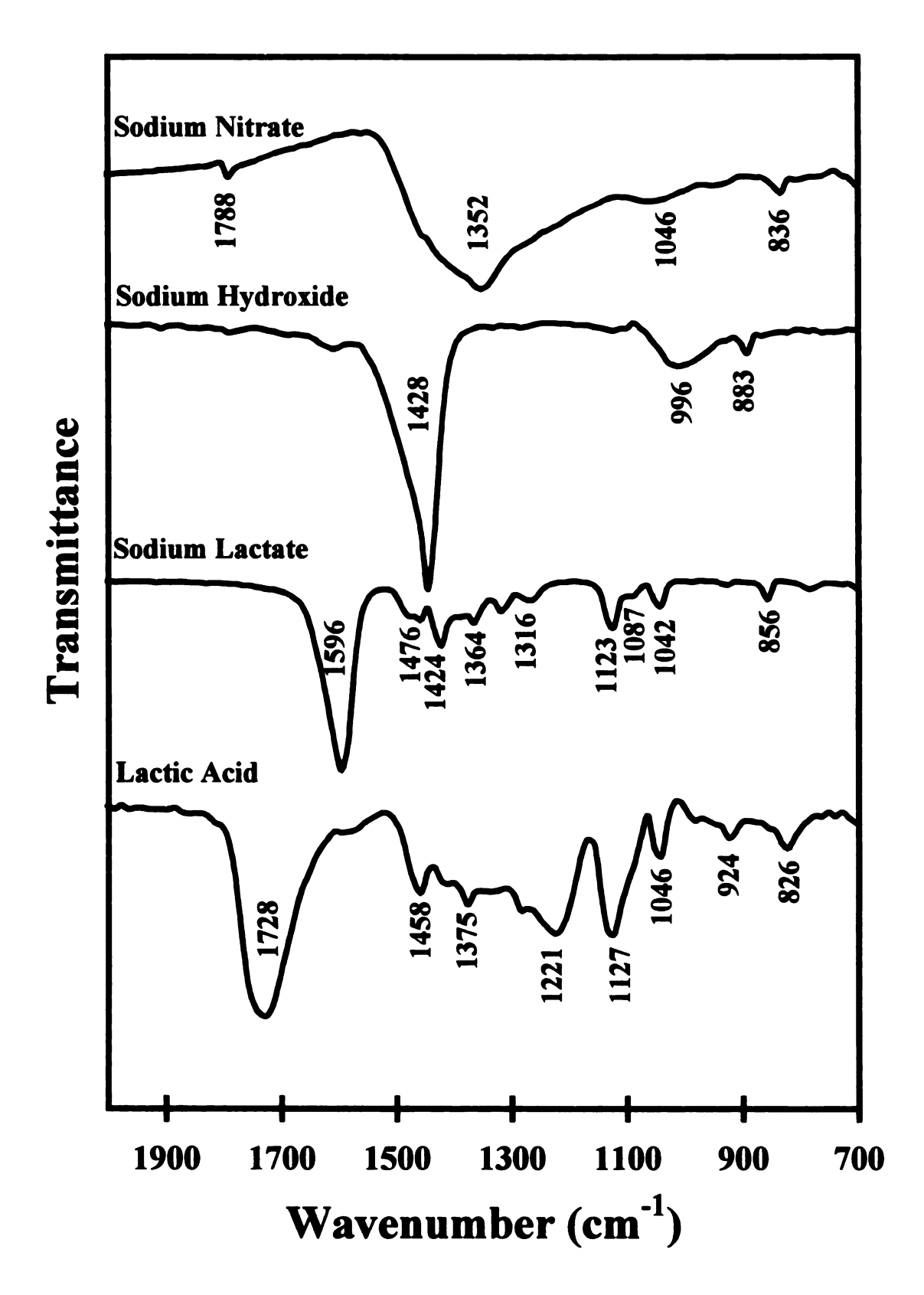


Figure 3.4. FTIR Spectra of Standards

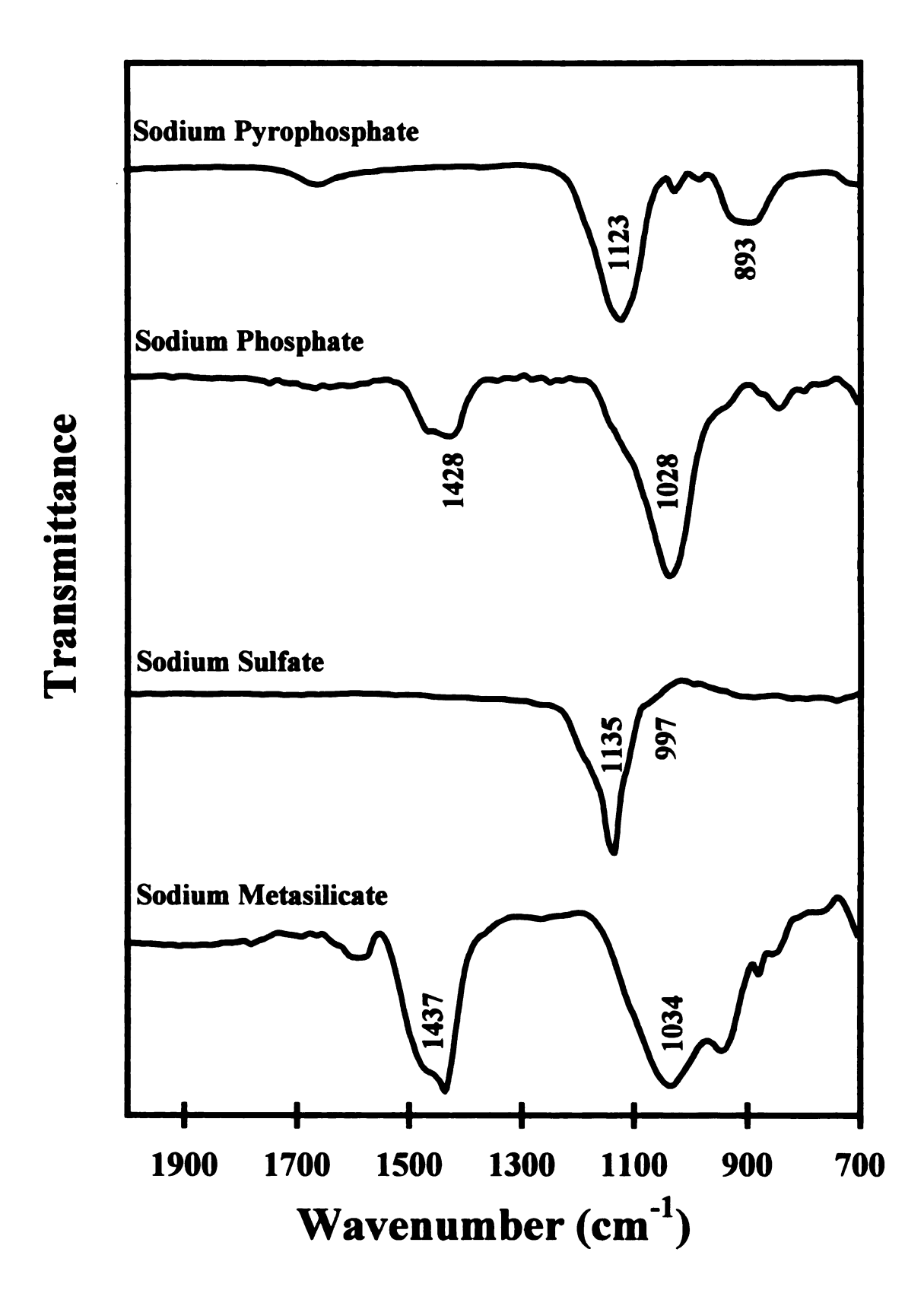


Figure 3.5. FTIR Spectra of Standards (Continued)

identifi

saits ar

Table 3

The salt

infrared these sai

infrared

FTIR stu

noubors

350°C (8

322. St

S_IOH, N

ideratification of the species. Frequencies of strong absorption bands for these sodium salts are listed in Table 3.6 (79).

Table 3.6. Characteristic Infrared Bands of Sodium Salts (79)

Sodium Salt	Characteristic IR Bands (cm ⁻¹)
NaNO ₃	2427, 1789 (v _{N-O}), 1354, 837
Na ₃ PO ₄	1028 (v _{P-O})
$Na_4P_2O_7$	1123, 893, 552
Na_2SiO_3	1437, 1034 (v _{Si-O})
NaOH	1428, 996, 883
$NaC_3H_5O_3$	1599 ($v_{C=O}$), 1460, 1422, 1361, 1123, 1087, 1042
NaCl	
Na ₂ SO ₄	1135 (v _{s-o}), 997
CPG	1396, 1103 (v _{Si-O}), 919, 800

infrared spectrum is taken. Concentrations of the sodium salt solutions used to prepare these samples on silicon disks are listed in Table 3.7. Sodium chloride does not have an infrared spectrum itself, hence no standard infrared spectrum is given. A post-reaction study was not done with NaNO₂ because it is of interest only as the decomposition Product of NaNO₃. This decomposition does not occur until temperature reaches above 350°C (80).

3_2_2. Survey of sodium salts and base

Spectra from post-reaction FTIR studies on NaNO₃, Na₃PO₄, Na₄P₂O₇, Na₂SiO₃, Na₄P₂O₇, Na₂SiO₃, Na₅PO₄, NaCl, and Na₂SO₄ at temperatures from 25-350°C are presented in Figures 3.6-

Table 3.7. Properties of Sodium Salts Used as Catalyst

Sodium Salt	Solution Concentration	Melting Point		Conjugate Acid Conjugate Acid Conjugate Acid	Conjugate Acid
	on IR Disk	၁		Boiling Point	pKa (25°C)
	(Momm)			ာ့	
NaNO ₃	1.04 x 10 ⁻¹	306	HNO ₃	83	~-1.3
Na ₃ PO ₄ • 12 H ₂ O	3.70×10^{-3}	d ~73	Na ₂ HPO ₄	ı	12.67
			NaH ₂ PO ₄		7.21
			H ₃ PO ₄		2.16
Na ₄ P ₂ O ₇ • 10 H ₂ O	3.7×10^{-3}	-H ₂ O, 94	$Na_3HP_2O_7$	•	8.22
Na ₂ SiO ₃ •9 H ₂ O	5.64×10^{-2}	40 - 48	H_2SiO_3	d 25	12
NaOH	1.50×10^{-2}	318	H_2O	100	14
NaC3H5O3	1.50×10^{-2}	164	$C_3H_6O_3$	122	3.08
NaCl	1.14×10^{-1}	801	HCI	-85	~-7.0
Na ₂ SO ₄	1.50×10^{-2}	884	NaHSO,	330	1.98
			H ₂ SO ₄		2

have been g
acid vapor a
metric acid. I
bands at 15
bands at 24
FTIR spects
to water val
clearly shor

3.12. respec

reak. In the sodium lact condenses the reaction

lemperature

At:

3.81. The b

complicate

alti sodiui

guperatur

Titled, it c

ave 2.3-pe

3.12, respectively. Detailed discussions of the spectra for NaNO₃, Na₃PO₄, and Na₄P₂O₇ have been given in earlier publications (67,68). In short, upon exposing NaNO₃ to lactic acid vapor at temperature above 200°C, sodium lactate is formed and the conjugate acid, nitric acid, is vaporized (Figure 3.6). This interpretation is supported by sodium lactate bands at 1599, 1415, 1123, 1042, 855, and 778 cm⁻¹ and the disappearance of NaNO₃ bands at 2427, 1789, 1354, and 837 cm⁻¹ as temperature is increased. As a reference, FTIR spectra were collected after sodium nitrate deposited on a silicon disk was exposed to water vapor at temperatures between 150°C and 350°C (Figure 3.13). These spectra clearly show that sodium nitrate is thermally stable over the entire range of reaction temperature.

Peak. In the case of Na₃PO₄, proton exchange with lactic acid results in the formation of sodium lactate and Na₂HPO₄ (Figure 3.7). At temperatures above 200°C, Na₂HPO₄ condenses to Na₄P₂O₇ (1123 cm⁻¹), which stays on the silicon disk. To further understand the reactions of phosphates, post-reaction FTIR spectra of Na₄P₂O₇ was obtained (Figure 3.8). The high concentration of lactic acid condensed on the silicon disk at 150°C complicates the interpretation of the spectrum, but at higher temperature, sodium lactate is clearly observed (peaks at 1600, 1421, and 1416 cm⁻¹) in significant amounts. Along with sodium lactate, Na₄P₂O₇ / Na₃HP₂O₇ are the dominant species present at reaction temperatures. Although proton transfer to pyrophosphate from lactic acid is equilibrium limited. it does proceed to a significant extent and enough sodium lactate is formed to give 2.3-pentanedione yield similar to those from other monosodium salts.

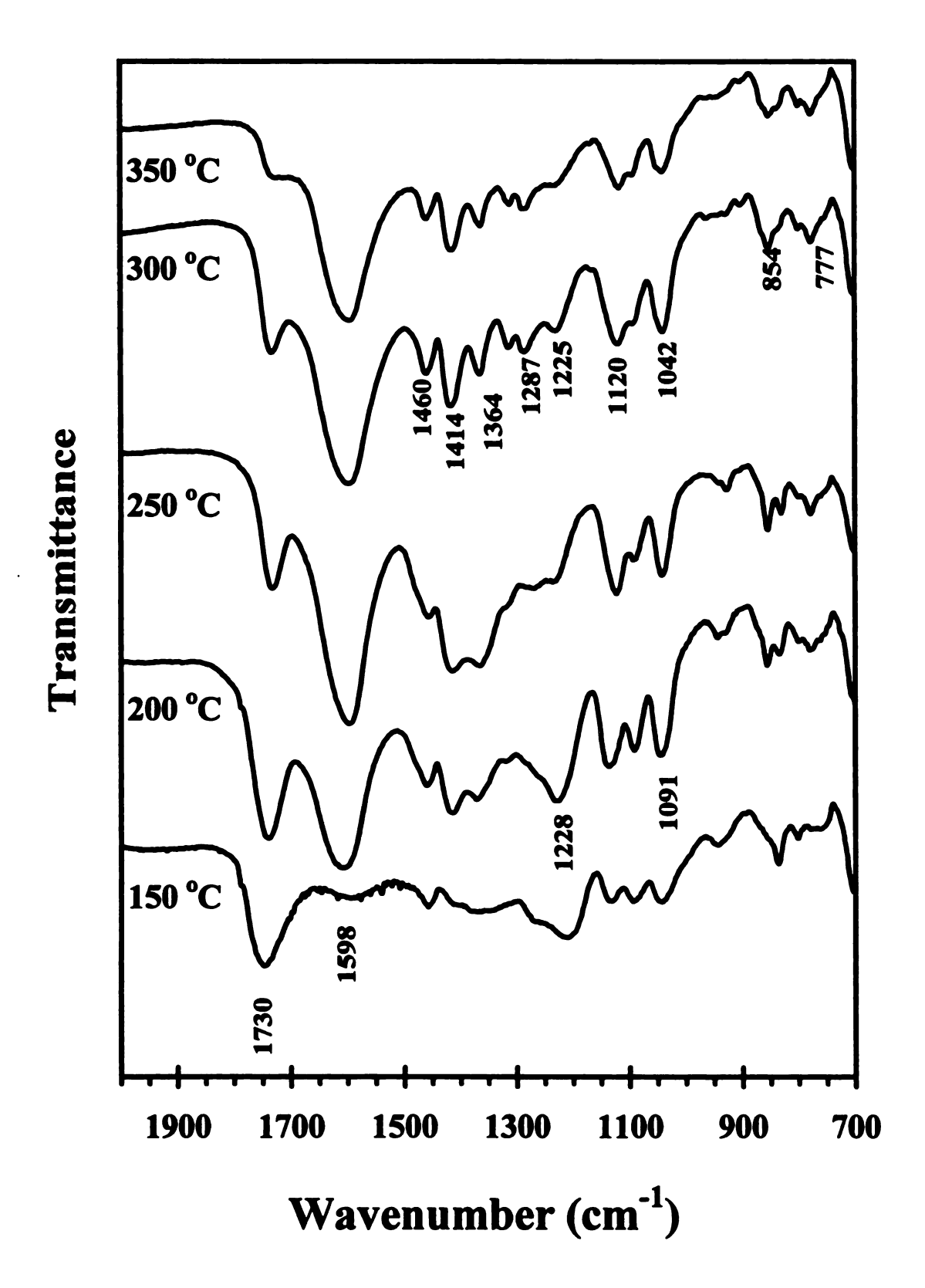


Figure 3.6. Post-Reaction FTIR Spectra of NaNO₃ Exposed to Lactic Acid Vapor

Figure 3

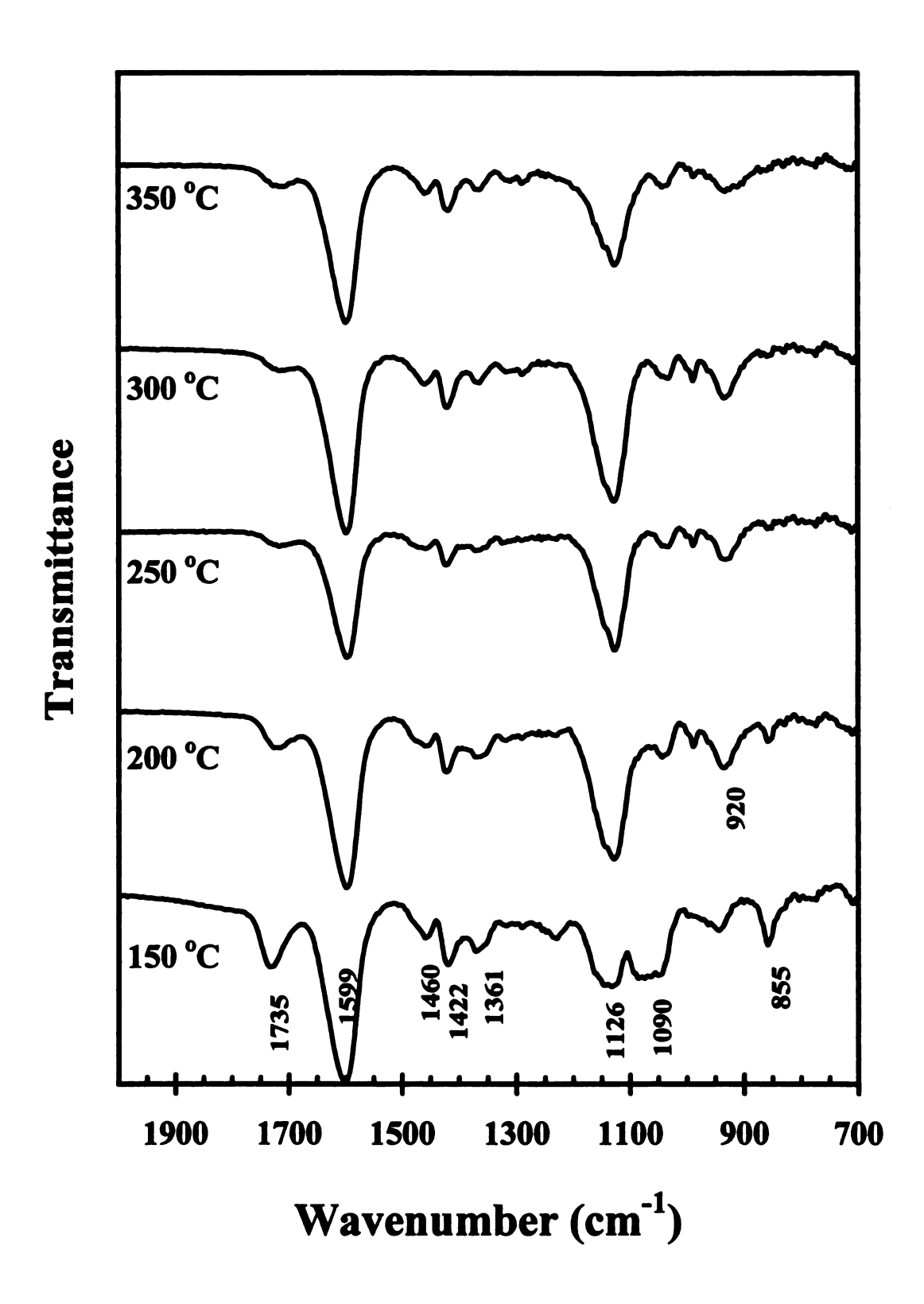


Figure 3.7. Post-Reaction FTIR Spectra of Na₃PO₄ Exposed to Lactic Acid Vapor

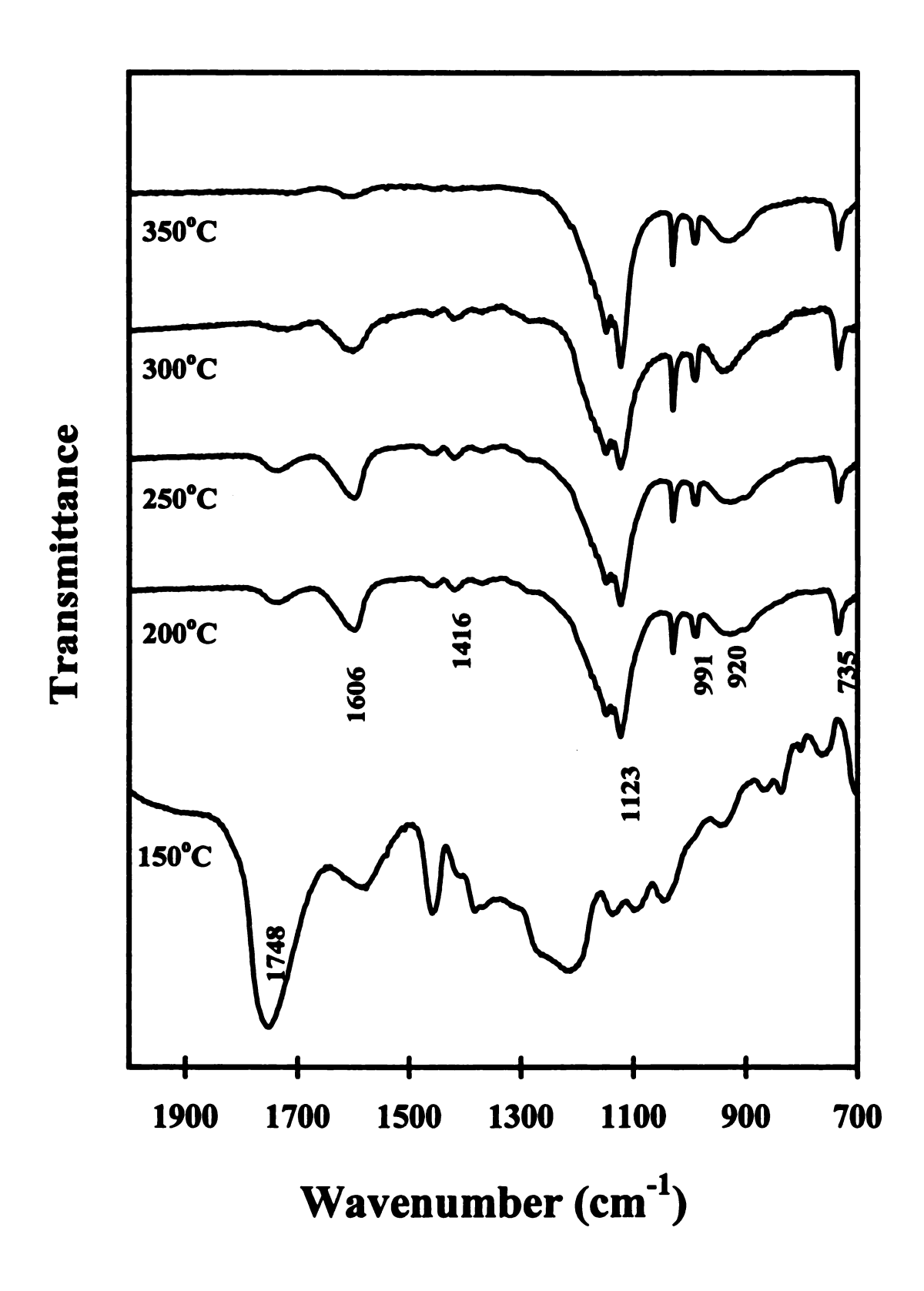


Figure 3.8. Post-Reaction FTIR Spectra of Na₄P₂O₇ Exposed to Lactic Acid Vapor

Figure

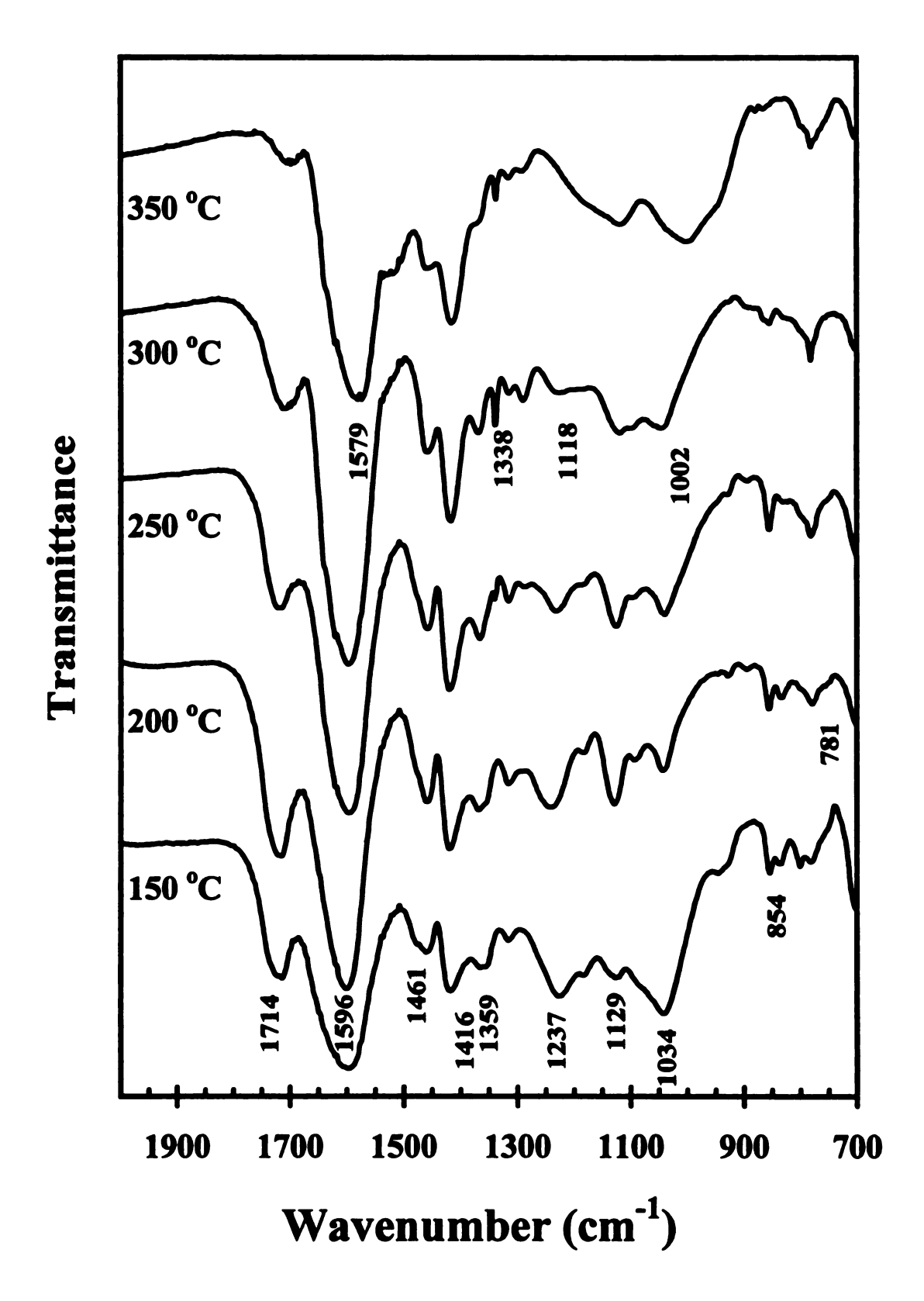


Figure 3.9. Post-Reaction FTIR Spectra of Na₂SiO₃ Exposed to Lactic Acid Vapor

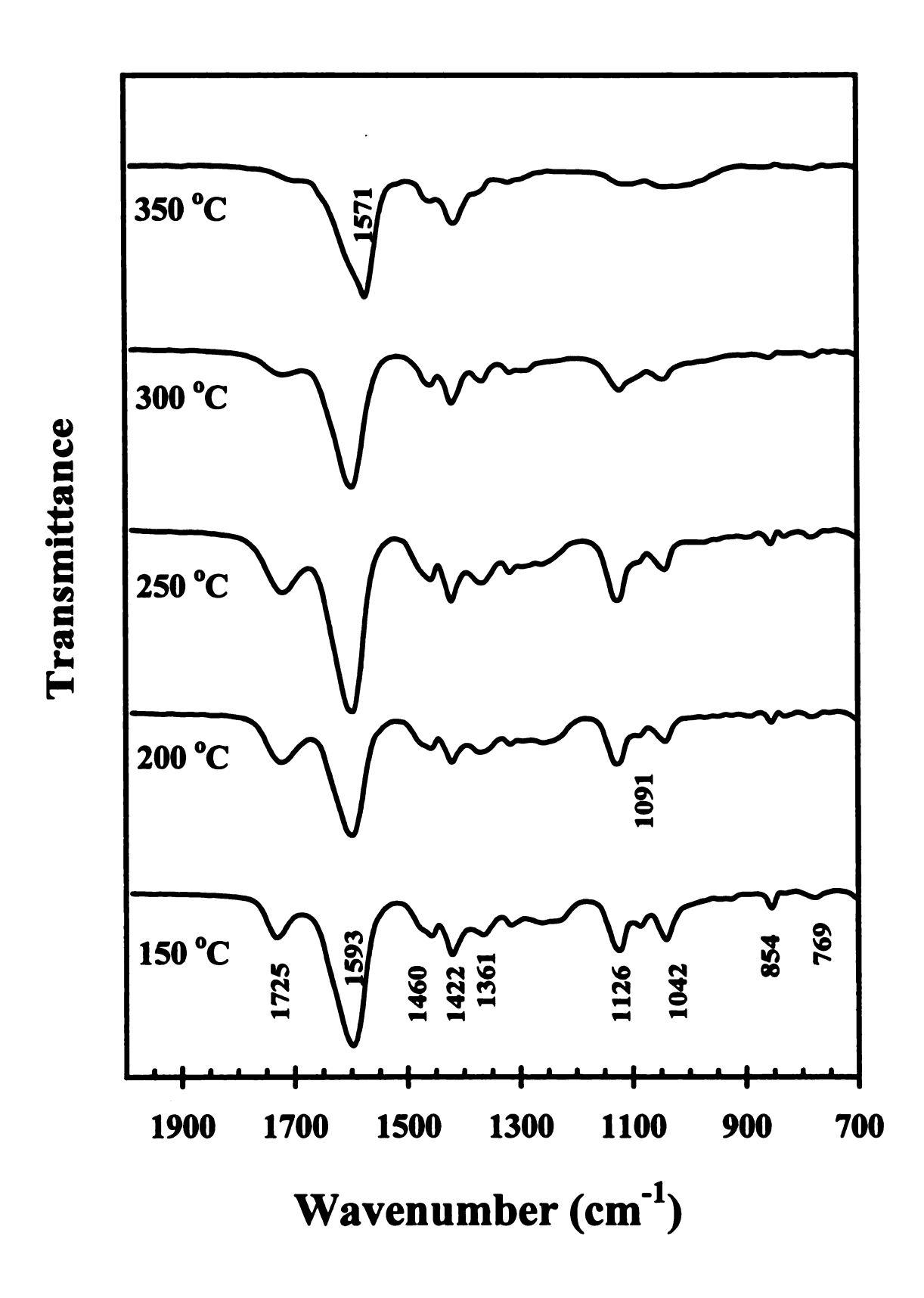


Figure 3.10. Post-Reaction FTIR Spectra of NaOH Exposed to Lactic Acid Vapor

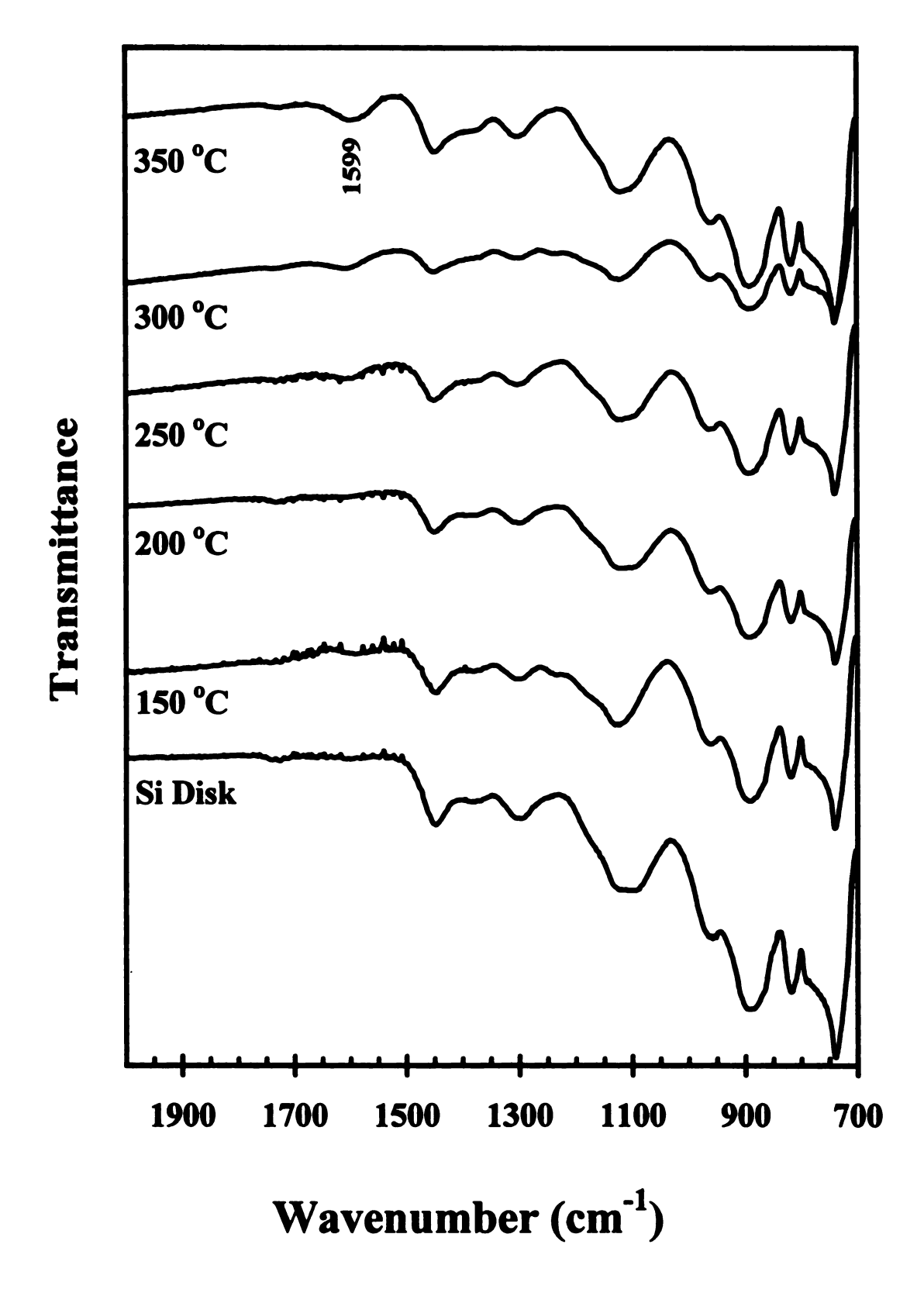


Figure 3.11. Post-Reaction FTIR Spectra of NaCl Exposed to Lactic Acid Vapor

Figure 3.12.

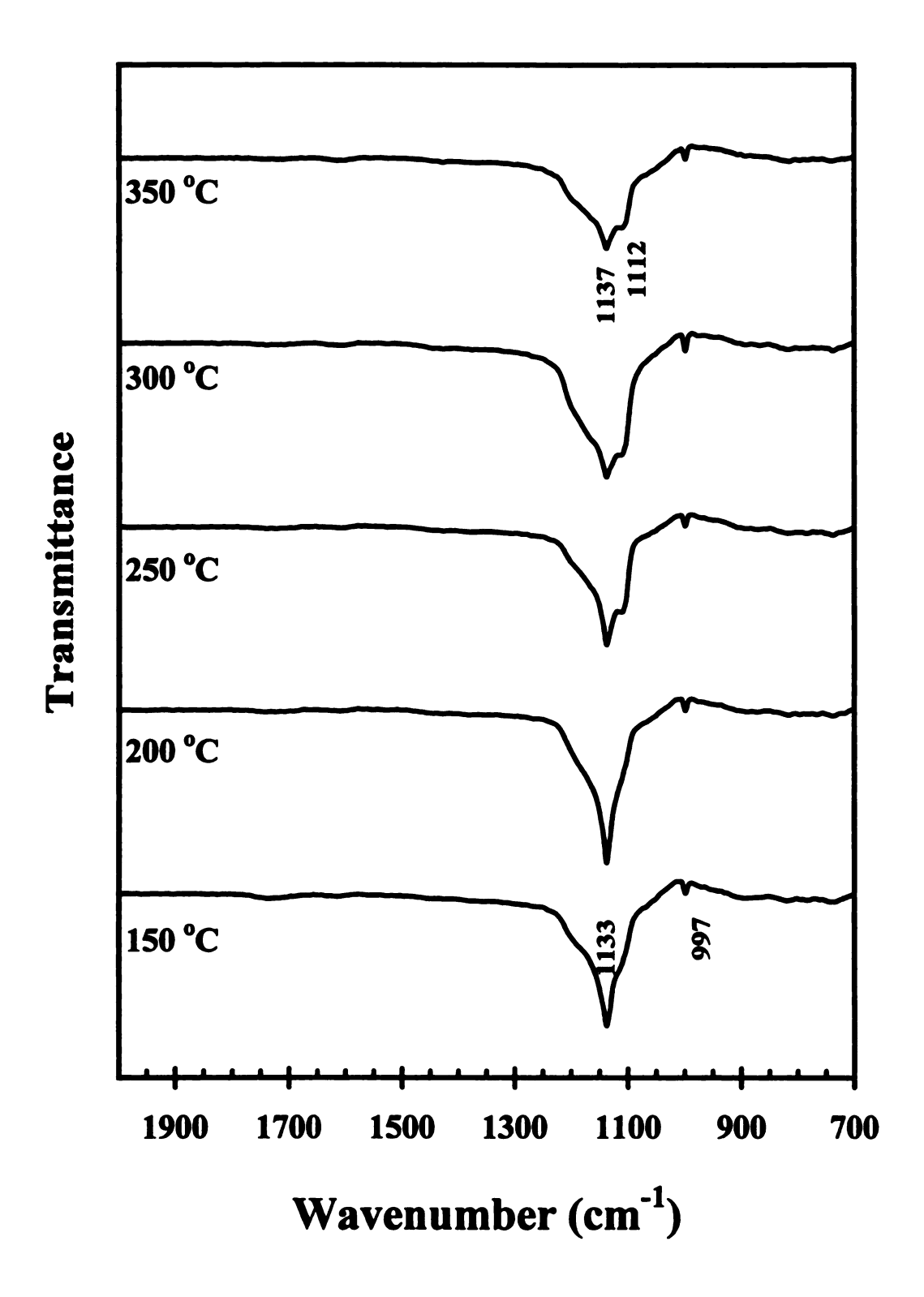


Figure 3.12. Post-Reaction FTIR Spectra of Na₂SO₄ Exposed to Lactic Acid Vapor

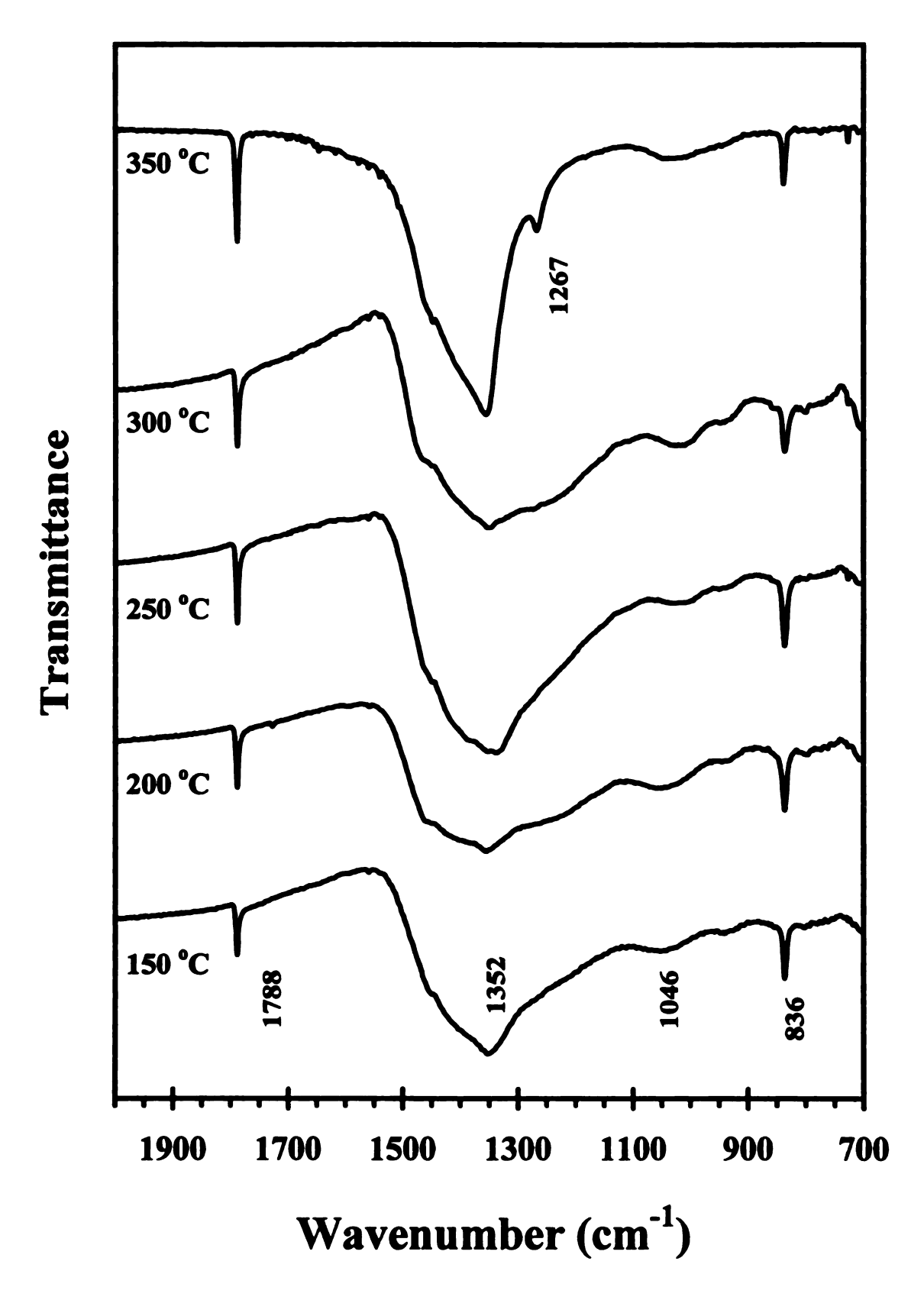


Figure 3.13. Post-Reaction FTIR Spectra of NaNO₃ Exposed to Water Vapor

sodium upon exposure i the disk (1596 c decomposes. It metasilicate and

formation of sodi results of post-resistance of the clean silicon the signal from the performed. For the temperature reach presence of sodius spectra of the FT even lactic acid is

There are
Na;SiO3 or NaO4
Observed in spect

small peak at 111

temperature.

cerbonyl stretchin

Sodium metasilicate (Na₂SiO₃) exhibits behavior similar to that of sodium nitrate upon exposure to lactic acid vapor (Figure 3.9). Sodium lactate forms on the surface of the disk (1596 cm⁻¹) while silicic acid (characterized by the band of SiO₃⁻² at 1034 cm⁻¹) decomposes. It was also observed that chemical reaction occurs between the sodium metasilicate and the silicon disk, which distorts the FTIR spectra at 300°C and 350°C.

Figure 3.10 displays the spectra for NaOH following exposure to lactic acid. The formation of sodium lactate is inevitable and the water produced is evaporated. The results of post-reaction FTIR studies on NaCl (Figure 3.11) and Na₂SO₄ (Figure 3.12) show that these salts behave differently than the other studied sodium salts. Subtraction of the clean silicon disk spectrum was not done for NaCl post-reaction spectra because the signal from the sample was quite weak and the spectra are distorted if subtraction was performed. For NaCl, no noticeable change in the disk spectrum is encountered until the temperature reaches 250°C, where a small peak is observed at 1599 cm⁻¹ indicative of the presence of sodium lactate. This band becomes more apparent as temperature rises.

Spectra of the FTIR studies with Na₂SO₄ are shown on Figure 3.12. No sodium lactate or even lactic acid is observed on the disk from 150-350°C. However, the intensity of a small peak at 1112 cm⁻¹, which we attribute to a K₂SO₄ impurity, increases slightly with temperature.

There are several noticeable changes in the sodium lactate absorption bands when Na₂SiO₃ or NaOH are exposed to lactic acid vapor at 350°C. These changes were also observed in spectra of used NaNO₃ or Na₃PO₄ catalysts collected with DRIFTS. The carbonyl stretching band of sodium lactate, which usually absorbs at 1599 cm⁻¹, shifts to about 1579 cm⁻¹. Accompanying this shift, the bands at 1129, 1040, and 3360 cm⁻¹

3.3. Discussion

vanish. In orde

sodium lactate

dned onto the s

350°C for 10 m

decomposition l

observed with N

changes are disc

33.1. Carbon b

carbon be results. The carbon catalyst coking, it carbon. These date degree of conversion and te 100% conversion resulting from coking the coki

usually not comple

molecular weight 1

opon prolonged hea

vanish. In order to examine these changes, reaction experiments were conducted with sodium lactate deposited on the silicon disk (Figure 3.14). Sodium lactate was vacuum dried onto the silicon disk and then exposed to helium gas at temperatures between 150-350°C for 10 minutes. The FTIR spectrum was taken afterward to see if any decomposition had occurred without exposure to lactic acid. At 250°C, the same shifts observed with Na₂SiO₃ or NaOH are detected for sodium lactate. The reasons for these changes are discussed in Section 3.3.4.

3.3. Discussion

3.3.1. Carbon balance

Carbon balance closure is an important measure of the quality of the experimental results. The carbon recovery for each experiment, which does not take into account catalyst coking, is given with the results in Tables 3.1-3.5 as error in percentage of carbon. These data clearly establish a relationship between carbon recovery and the degree of conversion. While almost complete carbon recovery is achieved at lower conversion and temperature (T < 300°C), the carbon balance is as much as 30% off at 95-100% conversion and higher temperature. This can be explained by the weight gain resulting from coking on the catalyst bed which can amount to 50% of the initial bed weight (68). Most of the coke deposits are observed on top of the catalyst bed and on the walls of the glass liner above the bed. Vaporization of lactic acid under pressure is usually not complete due to self-polymerization at reaction temperature. These low molecular weight lactic acid polymers are essentially nonvolatile and will decompose upon prolonged heating which leads to coke formation on top of the catalyst bed.

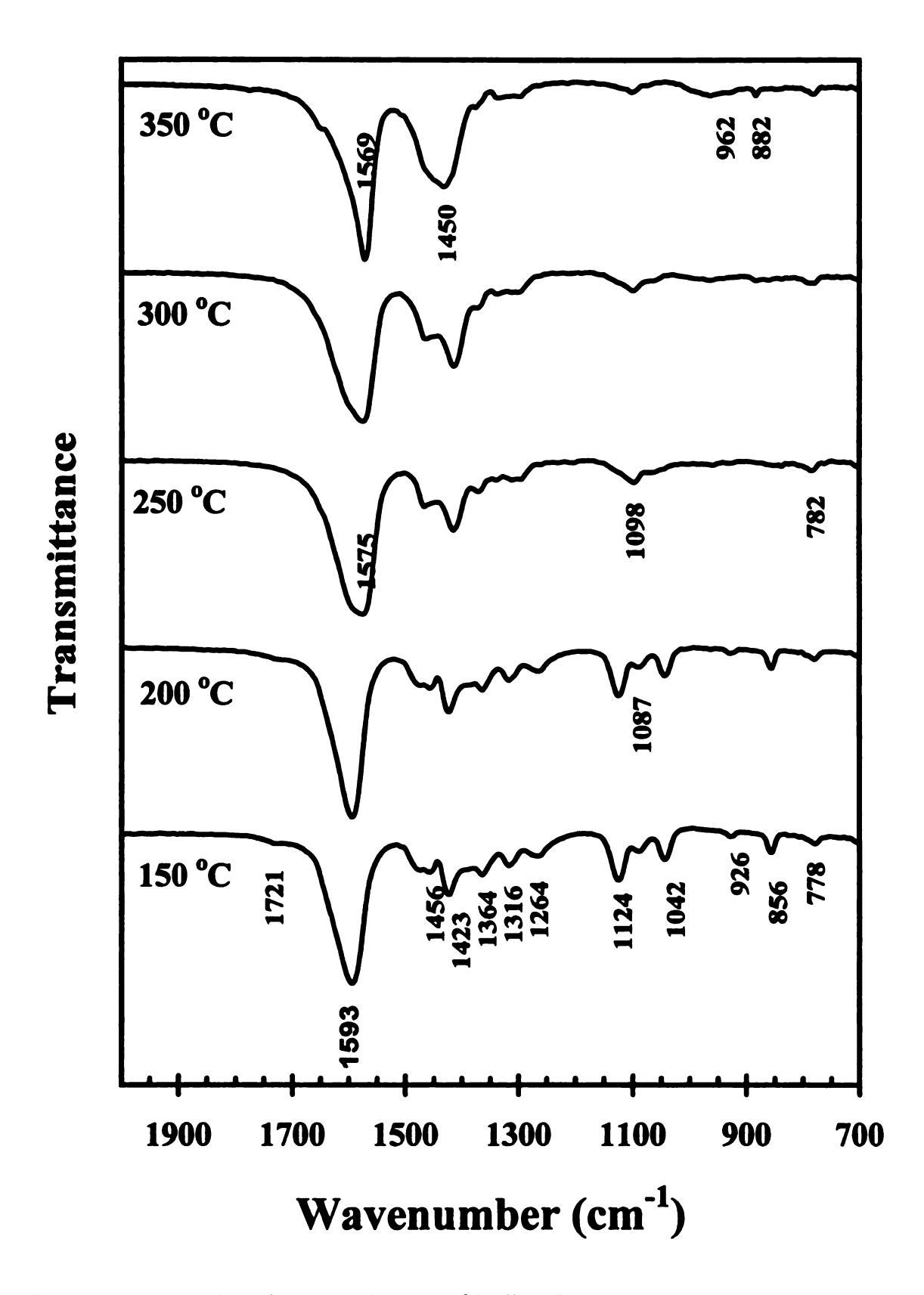


Figure 3.14. Post-Reaction FTIR Spectra of Sodium Lactate

decarboxylation

CO to CO₂ prod

the case of sodiu

obtained by decar

aione.

Post-react

the formation of 2

form sodium lacta

therefore conclude

formation of 2.3-p

supported by the fa

lactate on the suppo

evidence that all ac

the examined range

anions do not partic

Indeed, in most case

Although the

all active sodium sal

emperatures where a

3.3.2. Catalyst activity and pathways

As mentioned previously, decarbonylation of lactic acid to acetaldehyde and carbon monoxide is activated by the acid sites on the silica support. Following impregnation of the sodium salts, most of the acetaldehyde is produced by decarboxylation of lactic acid on the basic catalyst, as revealed by the dramatic shift from CO to CO₂ production in the presence of catalyst at high temperatures. For example, in the case of sodium lactate catalyst at 350°C, 75% of the acetaldehyde formed was obtained by decarboxylation of lactic acid as compared to only 23% on the CPG support alone.

Post-reaction FTIR results indicate a clear connection between activities toward the formation of 2,3-pentanedione and acrylic acid and the ability of the sodium salt to form sodium lactate on the support surface upon exposure to lactic acid vapor. It is therefore concluded that sodium lactate is an important stable intermediate in the formation of 2,3-pentanedione and acrylic acid in the reaction system. This idea is supported by the fact that similar product yields are obtained when starting with sodium lactate on the support at the same loading and reaction conditions. Together with the evidence that all active sodium salts and base give similar 2,3-pentanedione yields across the examined range of temperatures, these results lead to the additional conclusion that anions do not participate in the condensation process once sodium lactate is formed. Indeed, in most cases the anions have been protonated and departed as volatile acids.

Although the yields of acrylic acid were similar at temperatures below 300°C for all active sodium salts studied, there were differences between them at higher temperatures where acrylic acid production is maximum. Since acrylic acid yields over

NaCl and Na2S lactate must be acid yield occur observed by pos NMR spectrosc Na₂P₂O₇ catalys experimental ter and different cor extremely difficu competitive path

> The result the catalytic conv Step I - Initial so

> Step II - Sodium

 $2C_3H_6$

where NaX represe

Because the acid (Step I) appear

consider both the th

the ease of lactate for

thermodynamically,

from lactic acid via s

NaCl and Na₂SO₄ were substantially lower than over active salts, the presence of sodium lactate must be considered a factor in formation of acrylic acid. The maximum acrylic acid yield occurred at around 350°C, where sodium lactate decomposition was also observed by post-reaction FTIR. Investigation of the decomposition products via IR and NMR spectroscopies is discussed further in Section 3.3.4. Acrylic acid yield over Na₄P₂O₇ catalyst seems to still be increasing beyond 370°C, which is the highest experimental temperature investigated. However, lactic acid conversion studies at 390°C and different contact time revealed no further increase in acrylic acid yield. It is extremely difficult to optimize the selectivity toward acrylic acid because of the competitive pathways to acetaldehyde, which increase dramatically with temperature.

The results discussed so far lead to the following two-step reaction pathway for the catalytic conversion of lactic acid to 2,3-pentanedione with simple sodium salts:

(Step I - Initial sodium lactate formation)

$$C_3H_6O_3 + NaX \rightarrow Na^{\dagger}C_3H_5O_3^{} + HX \uparrow$$

(Step II - Sodium lactate catalyzed 2,3-Pentanedione production)

$$2 C_3H_6O_3 + Na^{\dagger}C_3H_5O_3^{-} \rightarrow C_5H_8O_2 + 2 H_2O + CO_2 + Na^{\dagger}C_3H_5O_3^{-}$$
where NaX represents any sodium salt.

Because the formation of surface sodium lactate from the sodium salt and lactic acid (Step I) appears critical in the condensation to 2,3-pentanedione, it is important to consider both the thermodynamics and kinetics of this proton transfer in order to explain the ease of lactate formation and observed activities of the sodium salts. It is thermodynamically unfavorable to form strong acids such as HNO₃, H₂SO₄, and HCl from lactic acid via Step I, so the only way proton transfer can proceed to any extent is by

the continuou

occur, the term

acid and high

points and pK

are reported or

except H₂SO₄,

somewhat diffe

The val
sodium nitrate of
4.9). The FTIR
sodium propion

understandable

propionate as co

The rate

accessibility of t

for sodium salts

conditions. This

spreading of the s

decompose at or I

hidrates) melt uni

discussed above. a

catalytic activity o

the continuous removal of these acids from the surface as they form. In order for this to occur, the temperature of the reaction has to be above the boiling point of the conjugate acid and high enough to compensate for the unfavorable difference in pK_a. The boiling points and pK_a of the conjugate acids formed by protonation of the studied sodium salts are reported on Table 3.7. Of the acids formed, all decompose or vaporize below 260°C except H₂SO₄, which vaporizes at 330°C. The reaction of Na₃PO₄ with lactic acid is somewhat different from other sodium salts studied, as the conjugate acid phosphate is consumed via reaction to pyrophosphate (Gunter, 1996).

The validity of this proton transfer reaction was further confirmed by exposing sodium nitrate on a disk to propionic acid (a weaker acid then lactic acid with a pK_a of 4.9). The FTIR spectra of the resulting sample (Figure 3.15) shows the formation of sodium propionate at temperatures above 300°C. Because of the lower pK_a value, it is understandable that higher temperature is necessary in the formation of sodium propionate as compared to sodium lactate.

The rate of formation of sodium lactate must also depend strongly on the accessibility of the salt to lactic acid. We propose that maximum accessibility is expected for sodium salts that form a molten or liquid film on the support surface at reaction conditions. This film provides a medium for rapid proton exchange as well as enhanced spreading of the salt over the support. While the active salt hydrates either melt or decompose at or below 300°C (Table 3.7), neither Na₂SO₄ nor NaCl (which do not form hydrates) melt until 800°C. This factor, together with the thermodynamic considerations discussed above, account for the slow formation of sodium lactate and the resulting low catalytic activity of NaCl and Na₂SO₄ relative to other salts. The relatively large quantity

Figure 3.15. Vapor

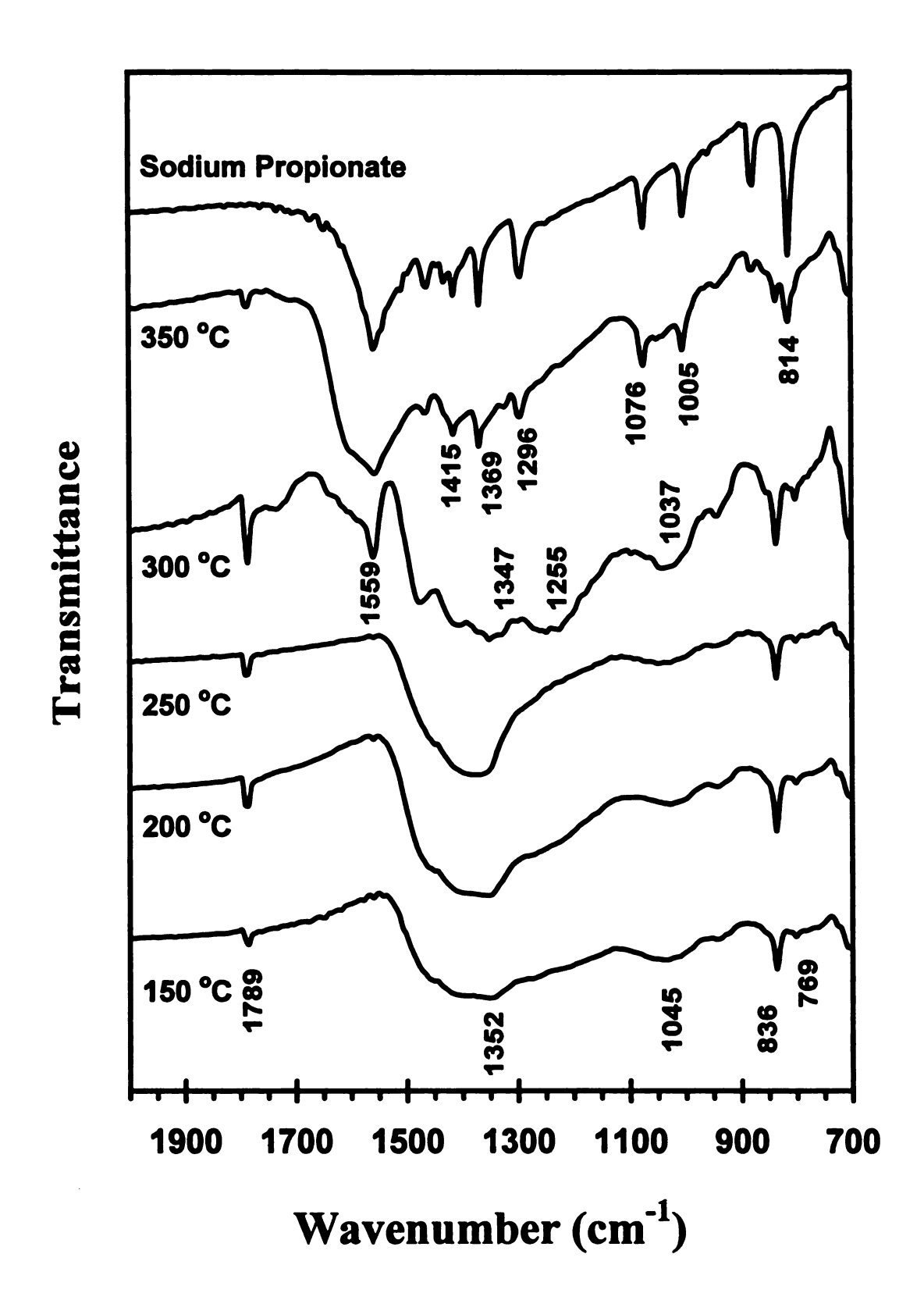


Figure 3.15. Post-Reaction FTIR Spectra of NaNO₃ Exposed to Propionic Acid Vapor

of carbon mo: Na:SO₄ and St support surfact of the conjugat sodium lactate results suggest acid could be en

because sodium With act that all of the sal product collectio initial period are

lactate is formed. experimental term

no change in 2,3-p

that 2,3-pentanedi surface, this sugge

with reaction time

were collected from

pentanedione yield

experiments. Incre

lactate concentratio used NaCl catalyst i

of carbon monoxide produced with Na₂SO₄ at 350°C indicates little interaction between Na₂SO₄ and support acid sites on the surface; Na₂SO₄ is therefore not dispersing on the support surface as active salts do. The effect of these two factors- the vapor temperature of the conjugate acid and the melting temperature of the salt- on the formation rate of sodium lactate is clearly observed in the post-reaction spectra on Figures 3.6-3.12; these results suggest that any low melting point sodium salt with a low boiling point conjugate acid could be employed for the catalytic formation of 2,3-pentanedione from lactic acid because sodium lactate is the ultimate catalyst.

With active sodium salts, the formation rate of sodium lactate is relatively fast, so that all of the salt is converted to sodium lactate in the initial saturation period before product collection begins. This is why carbon balances of samples collected during the initial period are substantially off. However, NaCl FTIR results show that little sodium lactate is formed, and the 2,3-pentanedione yield stays relatively low throughout the experimental temperature range. An eight hour reaction study of NaCl at 300°C showed no change in 2,3-pentanedione yield within experimental uncertainty. Since we believe that 2,3-pentanedione formation rate is related to the quantity of sodium lactate on the surface, this suggests that the surface concentration of sodium lactate does not increase with reaction time. A reverse temperature experiment for NaCl, where product samples were collected from 370°C down to 260°C, was also conducted. The resulting 2,3pentanedione yields, given in Figure 3., are mostly the same for the forward and reverse experiments. Increasing the temperature does not seem to affect the surface sodium lactate concentration neither. Finally, a simple AgNO₃ titration of the wash solution of a used NaCl catalyst indicates that at least 65% of the Cl impregnated on the catalyst

remains after range of the st lactic acid. Be pentanedione. of the sodium salts to sodium dependence of a surface lactic ac

33.3. Mechani

A propositivolving only late the enolization at an enolate form of attacks another mondensation, follows:

According to the proportionate the α -pentanedione. How

The deprote examined with hydre proposed mechanis;

and lactic acid will

remains after 6 hour of reaction. The above results indicate that within the temperature range of the studies, most of the NaCl present is not accessible for proton exchange with lactic acid. Because sodium lactate is not consumed in the formation of 2,3-pentanedione, the concentration of surface sodium lactate, depends only on the properties of the sodium salt - its melting point and anion. Also, since conversion of active sodium salts to sodium lactate is complete at all temperatures studied, the temperature dependence of 2,3-pentanedione yield results from kinetic effects and the concentration of surface lactic acid.

3.3.3. Mechanism of 2,3-pentanedione formation

A proposed mechanism for Step II of the reaction pathway to 2,3-pentanedione involving only lactic acid and sodium lactate is shown in Figure 3.16. The initial step is the enolization at the α-carbon of lactic acid by surface sodium lactate, which produces an enolate form of pyruvaldehyde hydrate. After deprotonation, the compound then attacks another molecule of lactic acid at the carbonyl carbon and undergoes a Claisen condensation, followed by decarboxylation and ketonization with loss of water. According to the proposed mechanism, any strong base can be used as a catalyst to deprotonate the α-hydrogen of lactic acid, and initiate the condensation toward 2,3-pentanedione. However, if a base stronger than lactate is used, reaction between this base and lactic acid will occur readily and lactate will ultimately be the catalyst.

The deprotonation of the α -hydrogen of lactic acid in a basic environment can be examined with hydrogen-deuterium (H-D) exchange by using D_2O as the feed solvent. A proposed mechanism for base catalyzed H-D exchange in the α carbon of lactic acid is

E -

(

+ eN.O O

110 0

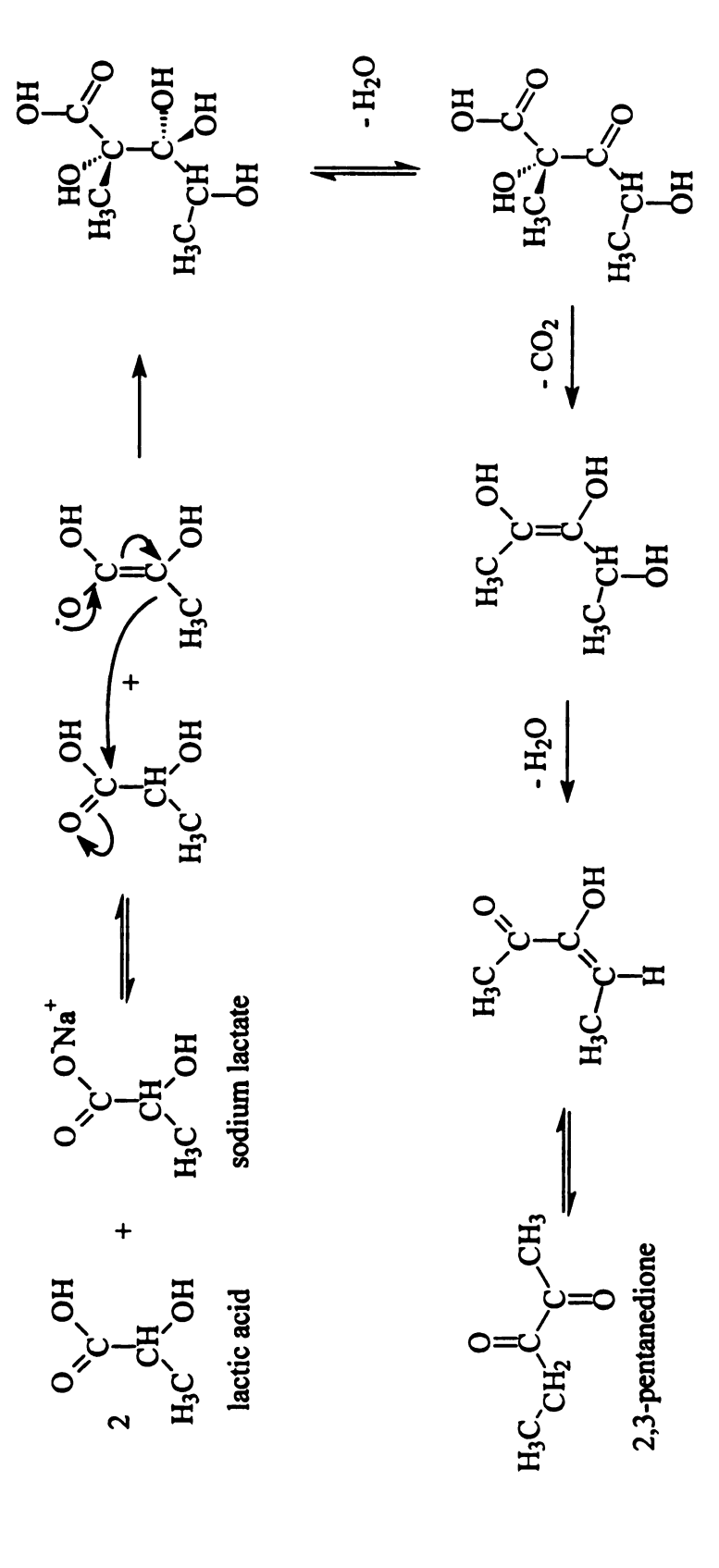


Figure 3.16. Proposed Mechanism for the Formation of 2,3-Pentanedione from Lactic Acid

shown in Figure 3.17. Lactic acid conversion over sodium nitrate catalyst was done at 260°C and 300°C using lactic acid feedstock that was diluted from 88 wt% to 34 wt% with D₂O. Samples of feed and products were analyzed by gas chromatography-mass spectroscopy (GC-MS) and the mass spectra of products collected at 260°C are presented in Figures 3.18-3.22 for lactic acid, propionic acid, acrylic acid, 2,3-pentanedione, and acetaldehyde, respectively. Standard mass spectra of the compounds are reproduced on the upper-right corner of the product mass spectra for comparison. Fragment ions of the major peaks are also included on these spectra to specify where H-D exchanges had occurred.

Figure 3.17. Proposed Mechanisum of H/D Exchange for α-hydrogen

The mass spectrum of the lactic acid in feed (not shown) only displays H-D exchanges in the carboxyl and hydroxyl hydrogen, which are expected. However, the peak at m/z = 47 amu in Figure 3.18 clearly demonstrates that H-D exchange in the α position of lactic acid occurs under reaction conditions. This is further confirmed by the H-D exchanges observed in the α carbons of acrylic acid and propionic acid and the carbons adjacent to the carbonyl group of 2,3-pentanedione and acetaldehyde in the product (Figures 3.19-3.22). The H-D exchanges of these products can be a consequence of H-D exchanges in the lactic acid or direct exchanges on the products after they are

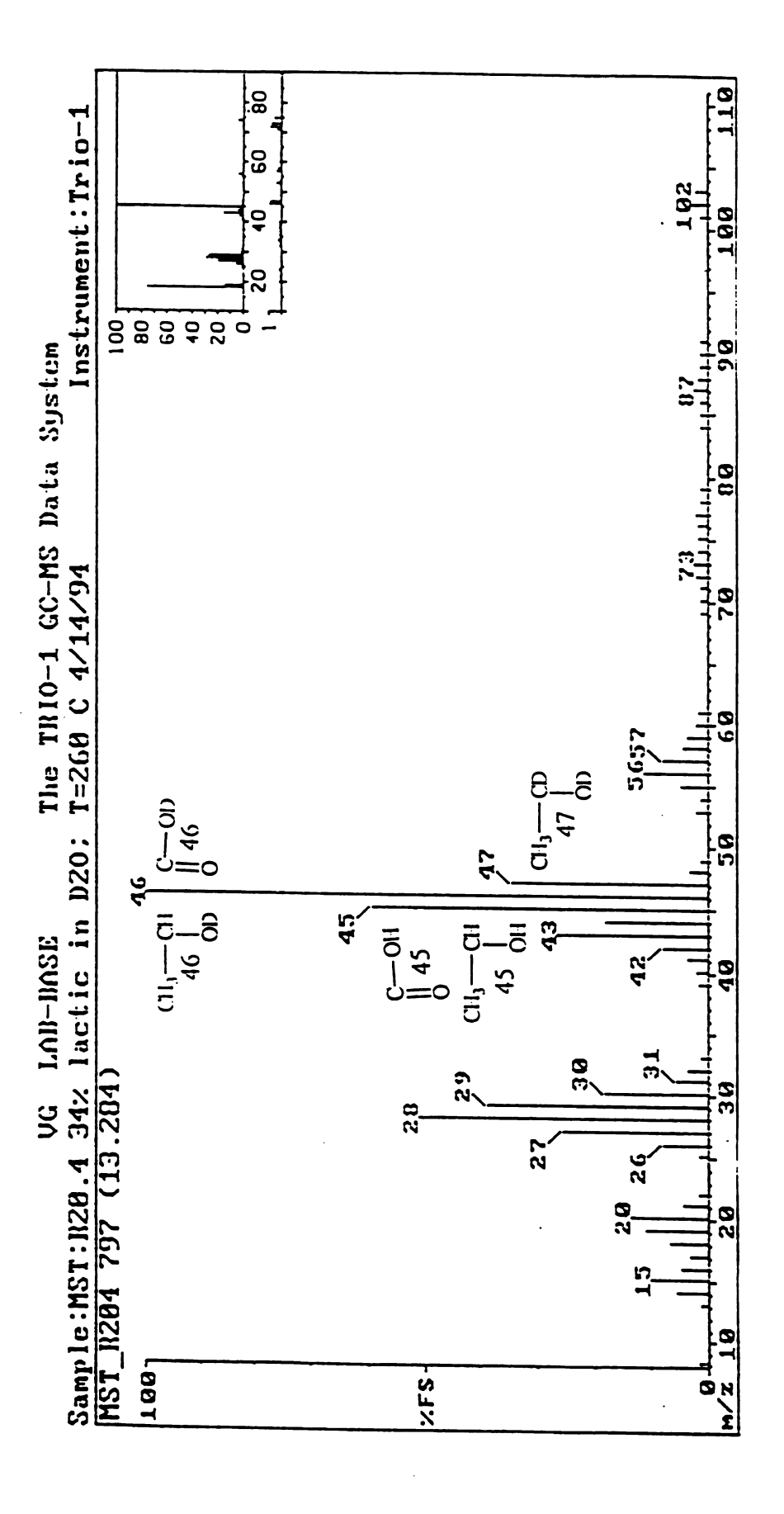


Figure 3.18. Mass Spectrum of Lactic Acid in Product of Lactic Acid / D₂O Conversion

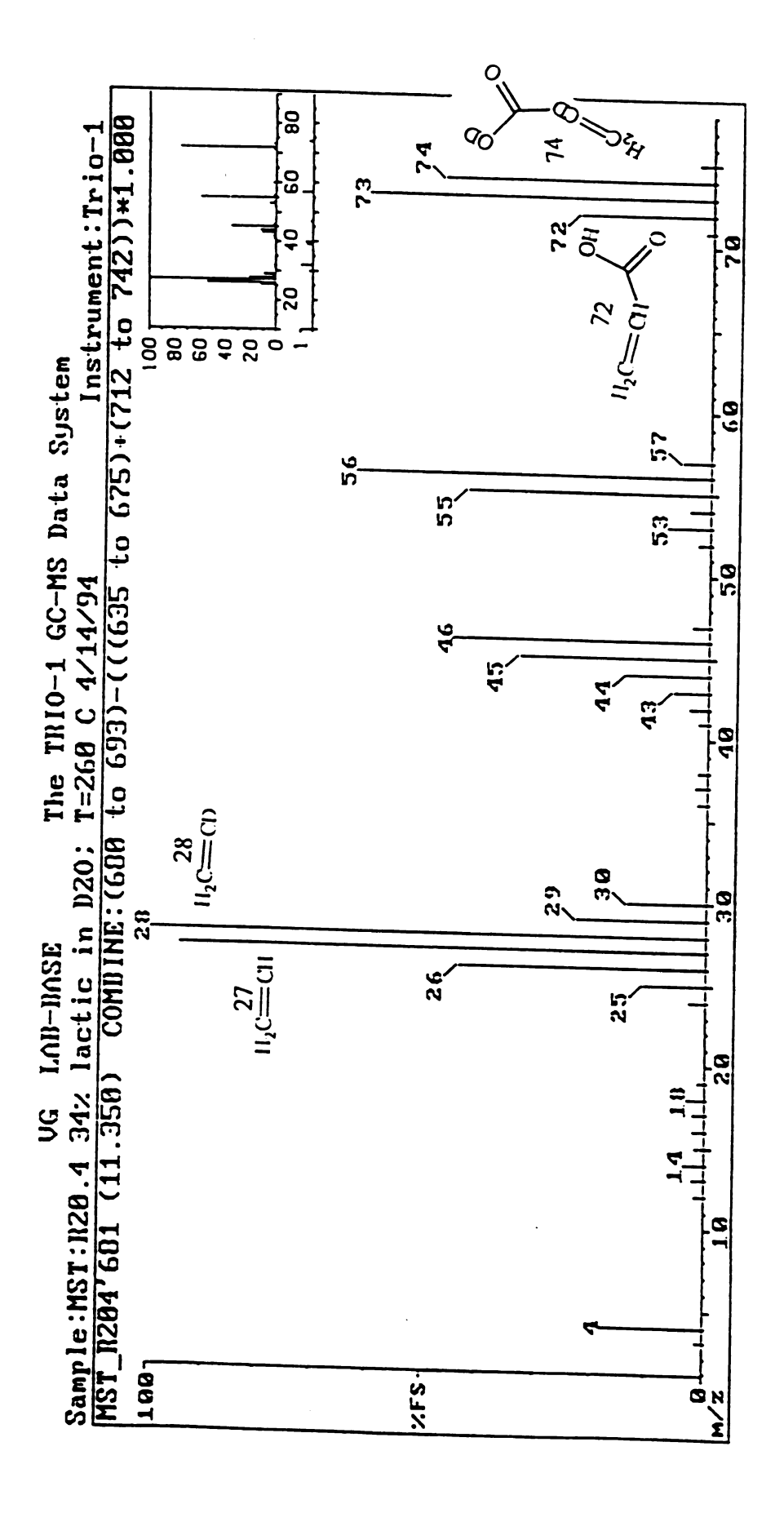


Figure 3.19. Mass Spectrum of Acrylic Acid in Product of Lactic Acid / D₂O Conversion

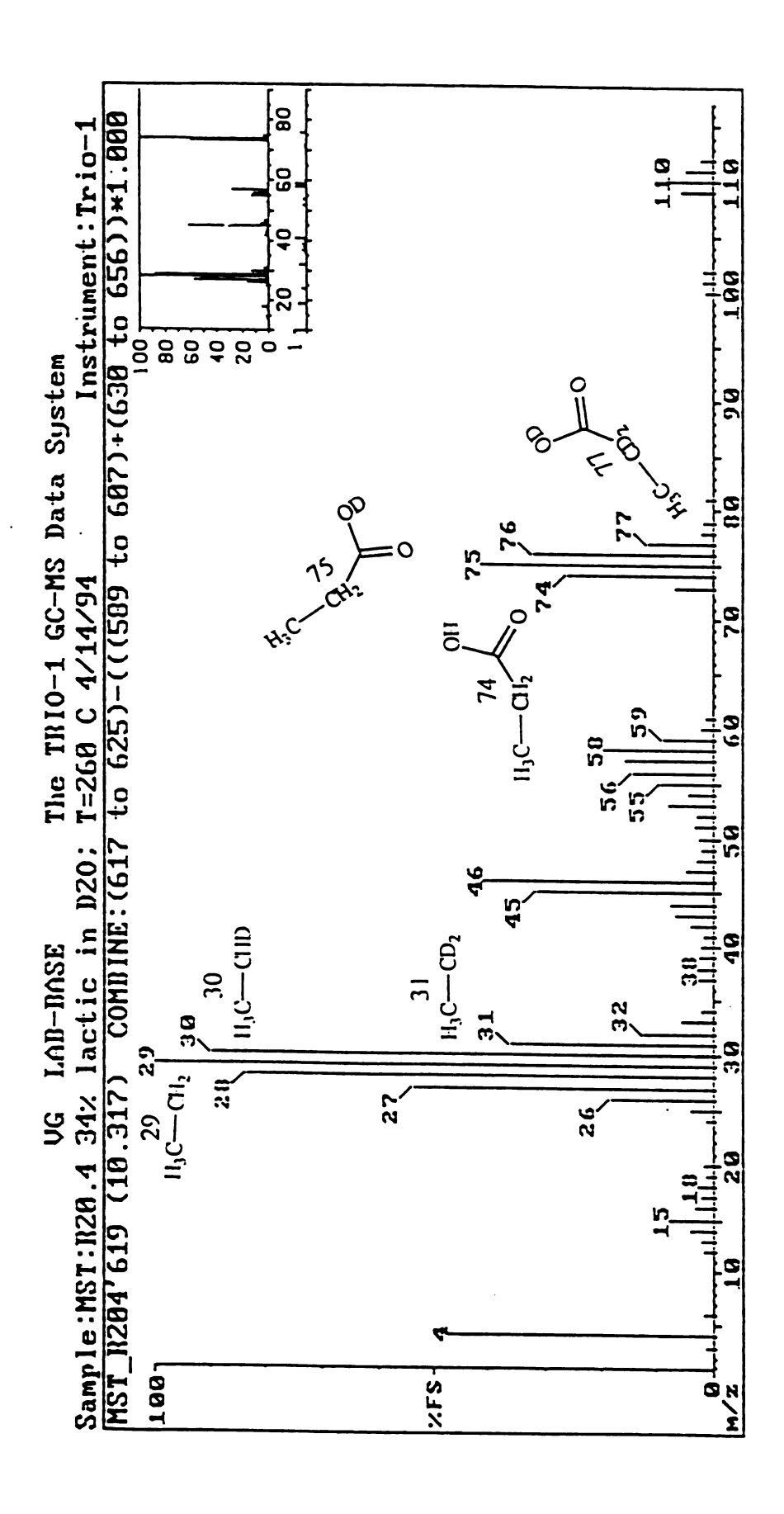


Figure 3.20. Mass Spectrum of Propionic Acid in Product of Lactic Acid / D₂O Conversion

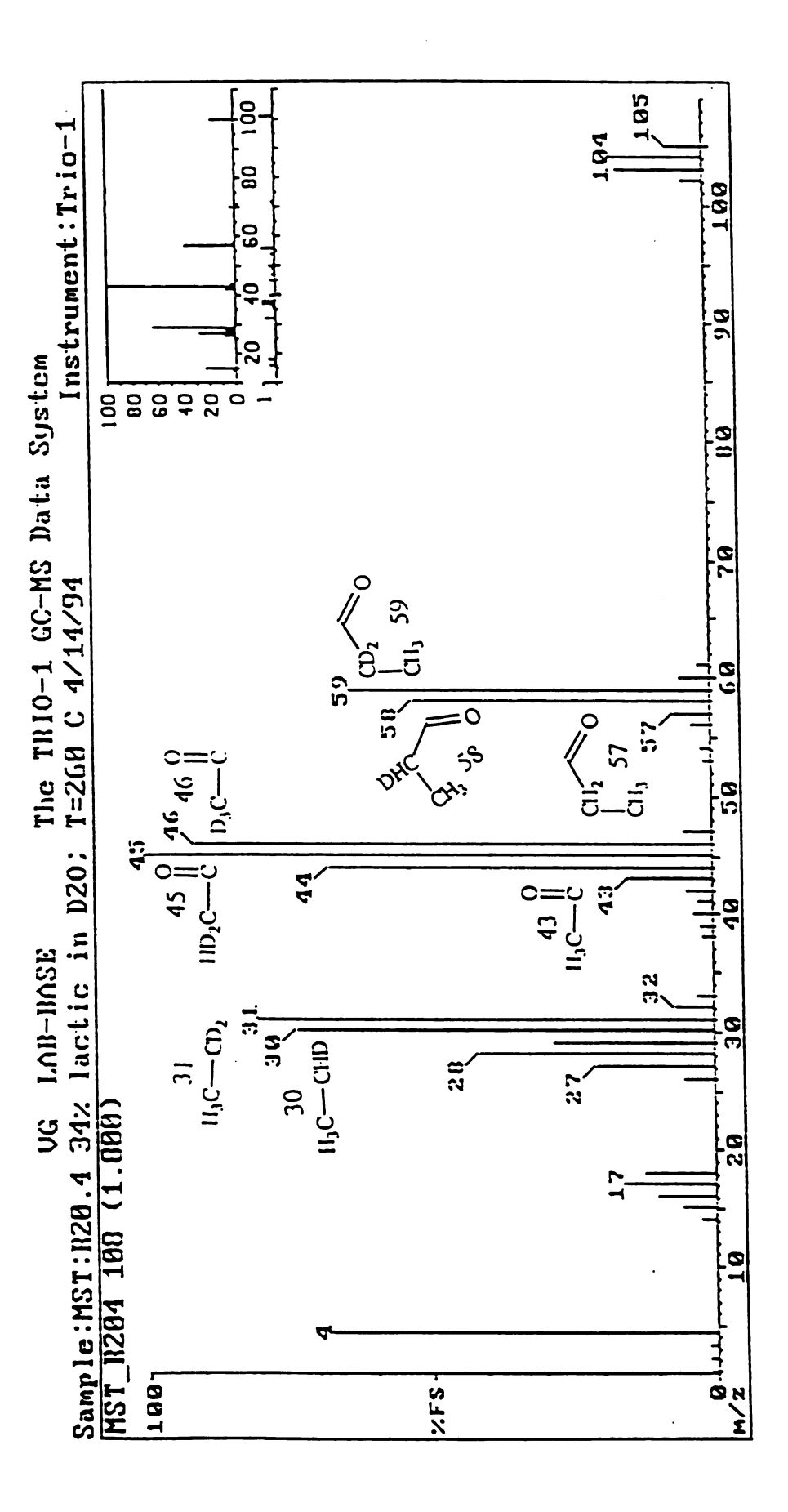


Figure 3.21. Mass Spectrum of 2,3-Pentanedione in Product of Lactic Acid / D₂O Conversion

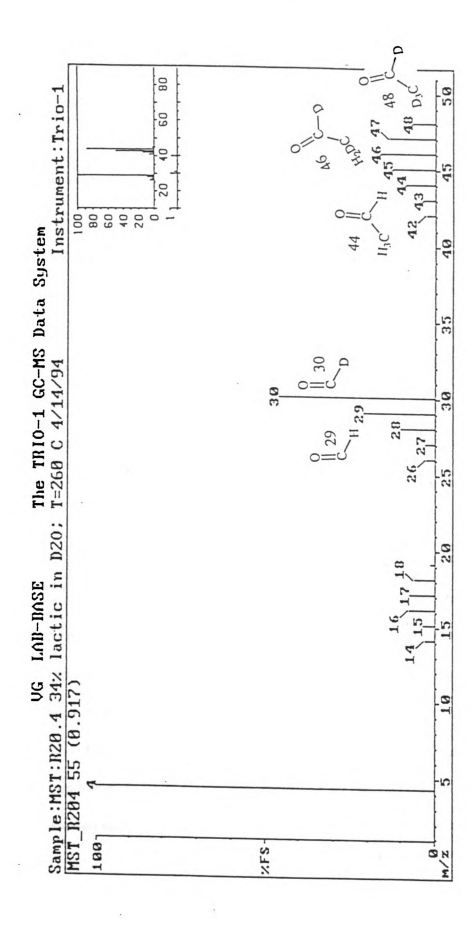


Figure 3.22. Mass Spectrum of Acetaldehyde in Product of Lactic Acid / D2O Conversion

formed in the reactor. Further examination and development of this mechanistic scheme has been done by Craciun (81) using molecular modeling, isotopic labeling, DRIFTS, NMR and variable temperature-mass spectroscopies.

3.3.4. Decomposition of sodium lactate

The DRIFTS spectrum of a NaOH on CPG catalyst (Figure 3.23a) after vaporphase lactic acid conversion at 350°C displays features similar to those obtained from sodium lactate on silicon disk experiments (Figure 3.14). This further assures us that our post-reaction IR spectra accurately reflect the actual species on the catalysts after experiments. Strong peaks at 1103, 919, and 800 cm⁻¹ are attributed to the support. The absence of absorption bands at 1124 and 1043 cm⁻¹ and the lower frequencies of the observed methyl stretching ($v_{as} = 2955 \text{ cm}^{-1}$ and $v_{s} = 2875 \text{ cm}^{-1}$) and carbonyl stretching (1569 cm⁻¹) in Figure 3.12 (350°C) are consistent with the loss of the α -hydroxyl group on sodium lactate.

To identify the species present on the support following reaction at 350°C, the used catalyst was treated with water or D₂O to dissolve the sodium species on the support surface. Approximately two-thirds of the material present on the support dissolved in water. The aqueous solution containing the dissolved portion of the residue was acidified with HNO₃ and analyzed via gas chromatography/mass spectroscopy (GC/MS). Propionic acid and acetic acid were identified as the main compounds in the solution. The sodium forms of these species were confirmed via ¹H NMR as the dominant species in the dissolved residue. Further, the carbonyl and methyl stretching frequencies of pure

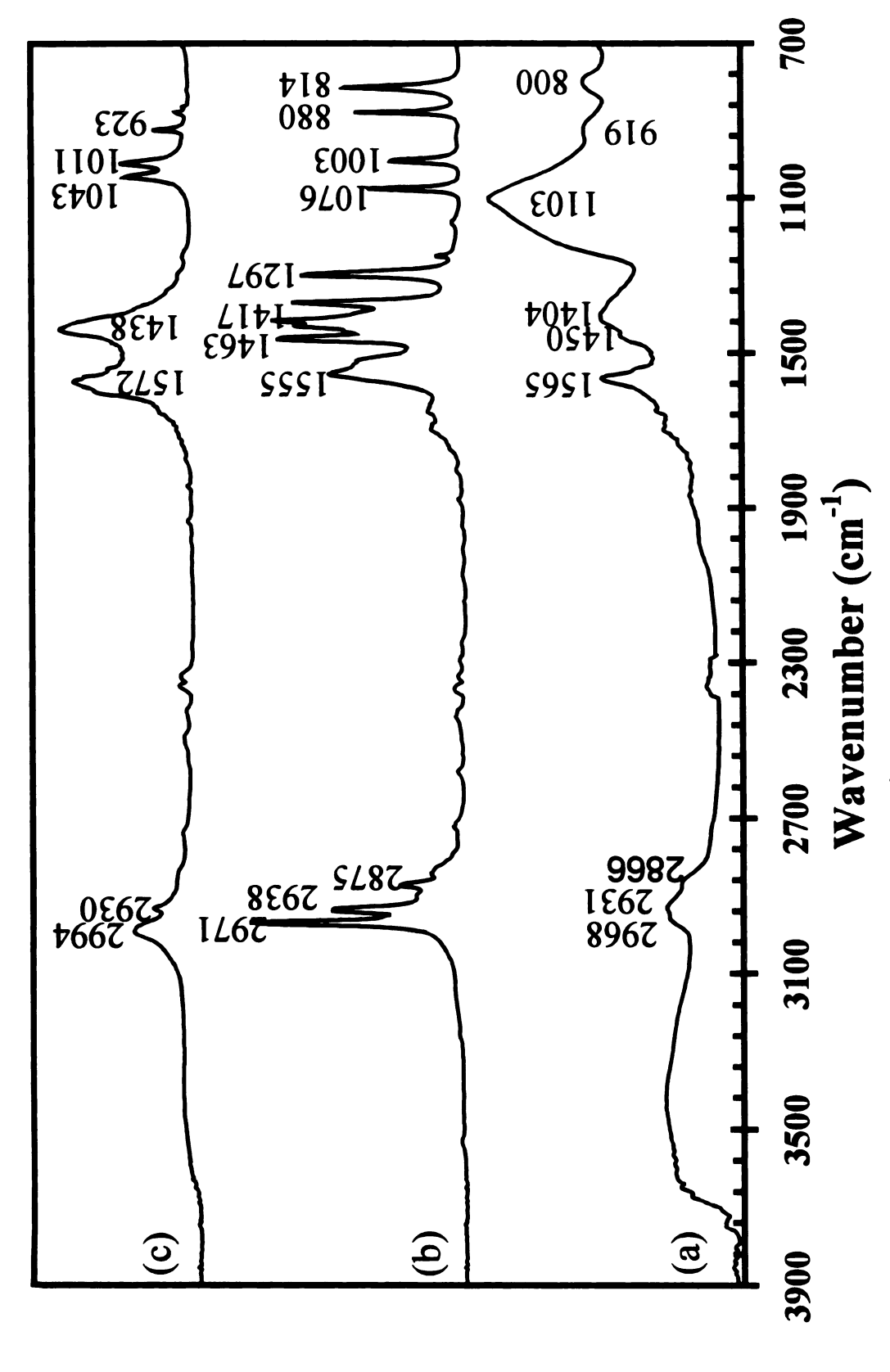


Figure 3.23. Decomposition of Sodium Lactate at 350°C

sodium propionate and sodium acetate (IR spectra shown on Figures 3.23b and 3.23c, respectively) match those of the species on the support following reaction at 350°C.

Finally, an x-ray photoelectron spectroscopy (XPS) survey of the used catalyst indicates the presence of carboxylate carbon (288.1 eV), oxygen (531.0 eV), and sodium (1075.0), consistent with the presence of sodium acetate and sodium propionate. The survey also shows no (C-OH) carbon in accordance with lactate decomposition at 350°C. Finally, a large non-oxygen bonded carbon (285.0 eV) peak was observed, which is believed to be from coke on the catalyst formed by decomposition of sodium lactate. lactic acid, and products. The surface sodium acetate and sodium propionate will convert back to sodium lactate in the presence of lactic acid similar to the protonation observed with the other salts. However, if the rate of sodium lactate decomposition (loss of the α hydroxyl group) at 350°C is more rapid than the deprotonation of the α -hydrogen of another lactic acid, which initiates the condensation toward 2,3-pentanedione, then the production of 2,3-pentanedione will be lowered at these temperatures due to the thermal decomposition of sodium lactate. Nevertheless, the consumption of lactic acid by other pathways, especially the formation of acetaldehyde, are the major cause of low 2,3pentanedione yield at high temperatures.

3.4. Summary

On low surface area silica support has been studied. Yield and selectivity toward 2,3pentanedione are optimal at around 300°C, 3-4 seconds residence time, and 0.5 MPa total

pressure. Anions of initial salt catalysts used do not participate in lactic acid

instead, sodium lactate has been identified by post-reaction FTIR spectroscopy as the primary, stable species on the support during reaction. Sodium lactate is believed to be an intermediate and ultimately the actual catalyst in 2,3-pentanedione formation and a mechanism for the condensation of sodium lactate and lactic acid is proposed. Such acid-base chemistry may be significant in a wide range of catalysis systems. Conversion of a sodium salt to sodium lactate is greatest when the salt has a low melting point and a volatile conjugate acid is used; the extent of conversion depends weakly on reaction time and temperature within experimental conditions. The requirement for a low-melting salt supports the notion that a fluid film is needed to achieve the NaX + HC₃H₅O₃ — NaC₃H₅O₃ + HX metathesis. At high temperature (~350°C), sodium lactate decomposes to sodium propionate and sodium acetate, which may be responsible for the reduced 2,3-pentanedione yields at higher temperatures.

Chapter 4

LACTIC ACID CONVERSION OVER ALKALI SALTS AND BASES ON SILICA

This chapter details the investigation of using alkali metal salts other than sodium salts as potential catalysts for the condensation of lactic acid to 2,3-pentanedione at various loadings. The identification of sodium lactate as the actual catalyst in all sodium salt catalysts has led to the conclusion that activity toward 2,3-pentanedione formation does not depend strongly on the anion of the salt. However, the anion does play a major role in determining the extent of sodium lactate formation. Alkali metal hydroxides are the principal catalysts used in these studies, even though conversions were done on other salts of the alkali metals for comparison. Potassium hydroxide was loaded at different catalyst loadings on a high surface area silica support (SiGel) and on CPG to further examine support and loading effects. A detailed kinetic model of lactic acid conversion over KOH on silica was developed from these experimental results. The model was further applied to obtain rate constants for NaOH/SiGel and CsOH/SiGel, and provides a reasonably accurate description of the system.

4.1. Vapor-phase reaction

Feedstock and catalyst supports used in the following studies were discussed in Section 2.1.1. and the reactor system was described in Section 2.1.3. All salts and bases

(KOH, KNO₃, K₃PO₄, KCl, CsNO₃, CsCl, Cs₂SO₄, LiOH, and Ca(OH)₂) were obtained in solid form from Aldrich except for CsOH, which was purchased as a 50 wt% aqueous solution. These salts were wet impregnated onto CPG with the procedure described in Section 2.1.1. Experiments were conducted with Cs₃PO₄ which was made by reacting 3 moles of CsOH per mole of H₃PO₄ before impregnation.

4.1.1. Results

All lactic acid conversion studies reported in this Section were conducted at similar reaction conditions as listed in Table 2.2 at a loading of 1 mmole per gram of **CPG.** Figure 4.1 summarizes the 2,3-pentanedione yields obtained over various alkali salts as catalysts for the conversion of lactic acid. Substantial effects are seen with increased 2,3-pentanedione yield corresponding to increasing the atomic weight of the metal cation. The optimum temperature also declined from 320°C for lithium to 280°C for cesium; both sodium and potassium have their optimum yields at 300°C. Complete product yield and conversion data for the different catalysts (LiOH, Ca(OH)₂, KOH, KNO₃, K₃PO₄, KCl, CsOH, CsNO₃, CsCl, Cs₂SO₄, and Cs₃PO₄) from 260-350°C are tabulated in Tables 4.1-4.6. Results over the support alone are given in Table 3.1. Cesium hydroxide gave a 49% 2,3-pentanedione yield with 64% selectivity at 280°C when dispersed on CPG at 1 mmol/g. Higher selectivity (>80%) was achieved at 260°C but with lower yield. Similar product yields were found with cesium nitrate and Phosphate (Figure 4.1), suggesting that the anions of the active catalysts do not participate in the formation of 2,3-pentanedione. This is consistent with the results observed with sodium and potassium catalysts. KCl and CsCl gave significantly lower yields as

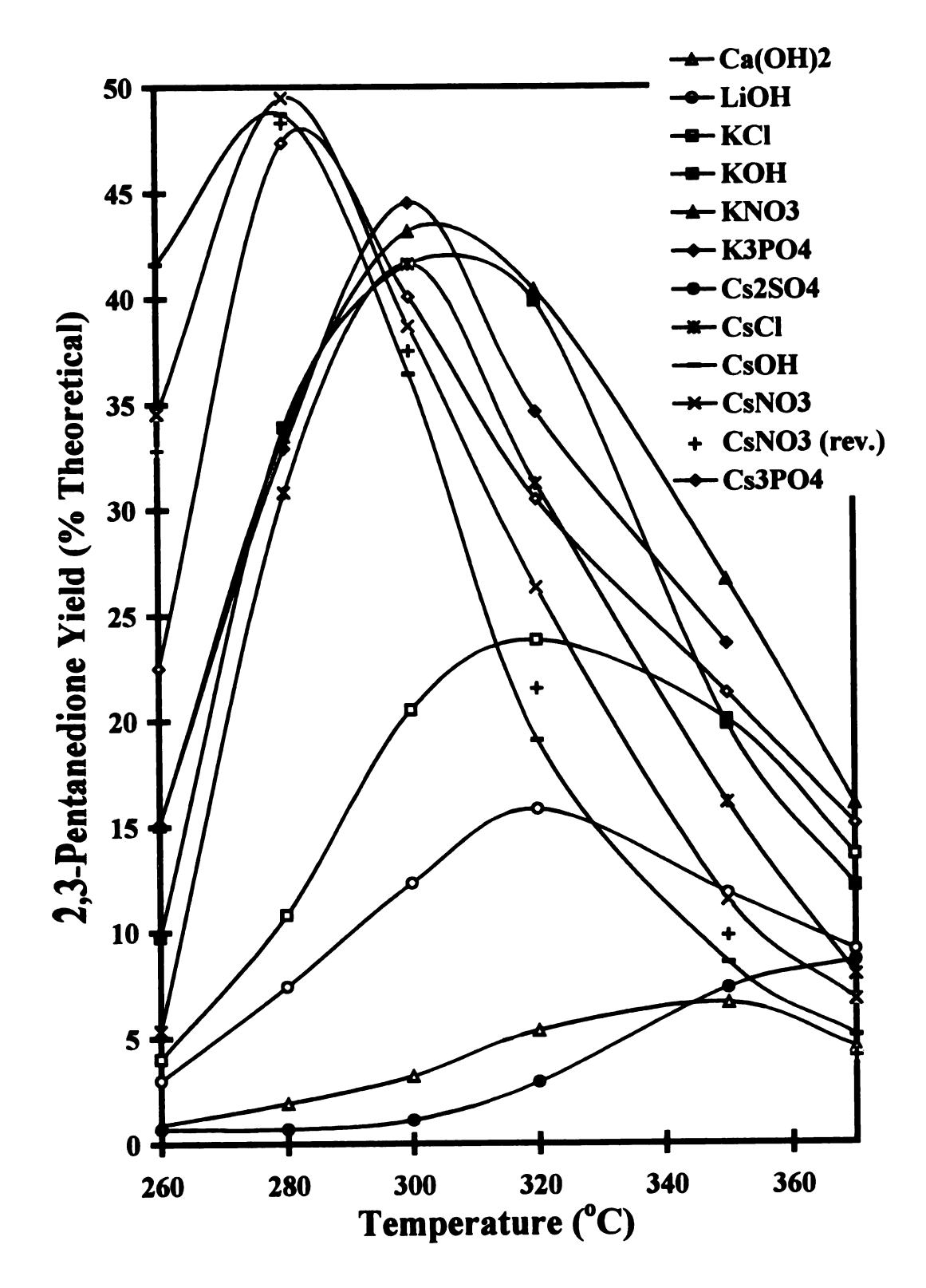


Figure 4.1. 2,3-Pentanedione Yields over Various Alkali Salt Catalysts

Table 4.1. Lactic Acid Conversion over LiOH/CPG and Ca(OH)₂/CPG

Catalyst		1 mm	ol LiOH/	CPG			I mmol	Ca(OH)2	/g CPG	
Temperature (°C)	260	280	, 300 300	320	350	260	280	280 300 3	320	350
Contact Time(s)	3.1	3.0	3.0	2.9	2.8	3.9	3.8	3.7	3.7	3.6
Error (% Carbon)	1.9	7.6	7.8	6.4	-18.3	5.4	3.4	9.2	-10.4	-28.8
Conversion (BOF)	3.0	6.1	20.1	45.0	77.3	-1.9	8 .	2.7	33.8	75.8
Yield (% Theoretical)										
Acrylic acid	9.0	2.0	4.7	8.6	7.2	0.7	6.0	1.9	9.6	9.01
Propionic acid	0.0	0.2	0.4	1.2	3.3	0.5	0.5	0.7	8 .	4.3
2,3-Pentanedione	3.0	7.4	12.3	15.8	11.8	6.0	1.9	3.2	5.3	9.9
Acetaldehyde	2.4	3.6	7.8	17.5	23.4	1:1	1.3	3.0	7.5	16.3
Acetol	0.0	0.0	8 .	4.3	2.9	0.0	0.0	6.0	5.6	3.5
Other	0.0	0.0	0.0	0.2	1.7	0.0	0.0	0.0	0.0	9.0
Unknown	0.0	2.4	4.5	8.9	14.4	0.4	0.5	8.	1.0	6.5
*00	0.4	9.0	1.1	2.2	4.9	0.3	0.7	1.5	3.0	7.8
C02*	0.3	1.0	2.8	5.4	10.9	1.0	8.1	3.9	6.1	9.1
Selectivity (%)										
Acrylic acid	10	15	17	20	14	21	61	20	25	25
Propionic acid	0	7	7	7	7	16	=	7	∞	10
2,3-Pentanedione	20	26	46	32	23	53	42	33	23	91
Acetaldehyde	40	27	29	36	47	34	28	31	33	39
Acetol	0	0	7	6	9	0	0	6	12	∞
Other	0	0	0	0	3	0	0	0	0	2
W.:-141-1-1-1	201	-1-	3 1	-						

*Yields reported as mole per 100 moles of lactic acid fed.

Table 4.2. Lactic Acid Conversion over K₃PO₄/CPG and KCI/CPG

Catalyst		1 mmc	1 mmol K ₃ PO ₄ /	g CPG			I mm	ol KCI / g	CPG	
Temperature (°C)	260	280	300	320	350	260	280	280 300		350
Contact Time(s)	2.9	3.0	2.8	5.6	2.5	3.6	3.4	3.3		3.3
Error (% Carbon)	6.0	-7.4	-14.2	-12.3	-20.0	-2.6	-8.1	-1.0		2.1
Conversion (BOF)	23.7	58.6	6.86	95.9	94.8	14.3	29.9	44.5	56.3	80.0
Yield (% Theoretical)										
Acrylic acid	4.9	11.9	16.5	7.7	1.5	9.0	1.6	4.4	. 9.2	12.8
Propionic acid	0.3	0.3	0.5	6.0	8. 1.8	0.7	9.0	-:	2.7	3.9
2,3-Pentanedione	16.2	35.1	52.6	51.1	35.7	4.0	10.8	20.5	23.8	20.0
Acetaldehyde	3.0	3.2	5.8	7.3	12.1	2.2	2.5	6.5	13.9	9.61
Acetol	0.0	0.0	1.9	1.5	0.0	0.0	0.0	1.3	3.9	4.2
Other	0.7	0.2	0.5	1.3	3.2	0.1	0.0	0.0	0.1	1.2
Unknown	0.5		4 .8	10.8	13.8	5.3	8.1	13.2	8.1	25.4
*00	1.8	1.3	1.6	2.7	6.9	0.1	0.1	0.3	-:	5.6
CO2*	8.2	18.3	38.0	41.7	48.4	0.4	2.4	6.2	10.9	16.0
Selectivity (%)										
Acrylic acid	19	23	21	Ξ	က	∞	01	13	17	21
Propionic acid	-	_	_	_	m	6	4	က	2	9
2,3-Pentanedione	65	69	89	73	99	53	70	9	4	32
Acetaldehyde	12	9	7	10	77	53	91	61	5 6	32
Acetol	0	0	7	7	0	0	0	4	7	7
Other	3	0	_	2	9	_	0	0	0	2
*Yields reported as mole per 10	рег 100 п	ioles of lac	00 moles of lactic acid fed	-ti						

Table 4.3. Lactic Acid Conversion over KOH/CPG and KNO₃/CPG

Catalyst		1 mmol	ol KOH / g	CPG			1 mmo	KNO3/	g CPG	
Temperature (°C)	260	280	300	320	350		280		320	350
Contact Time(s)	3.4	3.8	3.1	3.4	3.6	3.4	3.6		3.1	3.0
Error (% Carbon)	8.9	-15.6	-12.9	-17.1	-28.4		8.5		-15.5	-27.1
Conversion (BOF)	9.4	65.5	84.0	7.96	92.6		42.4		99.1	97.2
Yield (% Theoretical)										
Acrylic acid	2.0	8.9	12.5	13.5	6.1		8.7		9.6	2.7
Propionic acid	0.8	2.0	2.1	3.9	5.4		0.3		1.3	3.1
2,3-Pentanedione	9.7	33.9	41.6	39.8	19.8		33.5		40.4	26.6
Acetaldehyde	2.2	3.9	8.7	11.9	24.7		4.8		16.6	20.0
Acetol	0.4	5.9	6.3	7.6	3.4		2.3		0.9	1.7
Other	0.0	0.4	9.0	1.4	2.2		0.5		1.7	4.1
Unknown	1.3	2.1	2.9	5.1	9.9		6.0		6.9	9.5
*00	1.3	1.5	1.3	2.1	11.5		8 .		3.0	8.2
C02*	5.8	14.1	18.4	20.9	23.0		20.2		40.4	39.3
Selectivity (%)										
Acrylic acid	13	14	17	17	10		17		13	2
Propionic acid	2	4	ю	S	6		_	_	7	ς
2,3-Pentanedione	2	89	28	51	32		<i>L</i> 9		53	46
Acetaldehyde	15	∞	12	15	40		10		22	34
Acetol	7	9	6	01	9		2		∞	3
Other	0	_	-	7	4		_		7	7
Violde remoment of its	100	20130 20100	tio gold for							

Yields reported as mole per 100 moles of lactic acid fed.

Table 4.4. Lactic Acid Conversion over CsCI/CPG and Cs2SO4/CPG

Catalyst		Ē —	mmol CsCl/C	JPG			1 mm	ol Cs2SO4/CPG	/CPG	
Temperature (°C)	260	280	300	320	320		280		320	350
Contact Time(s)	3.2	3.5	3.4	3.5	3.1		3.3	3.0	3.0	3.0
Error (% Carbon)	4.9	4.3	-13.5	-14.5	-12.1		5.5		1.0	5.7
Conversion (BOF)	4.5	34.8	71.8	91.3	84.0		-3.3		9.6	28.1
Yield (% Theoretical)										
Acrylic acid	0.0	1.8	0.0	3.5	2.1	0.0	0.0	0.0	0.5	2.1
Propionic acid	1.2	0.7	9.0	1.1	2.1	1.3	9.0	0.0	0.7	2.1
2,3-Pentanedione	5.3	30.8	41.6	31.2	191	0.7	0.7	-:	2.9	7.3
Acetaldehyde	2.5	3.8	10.0	16.1	20.3	8.	6.0	2.0	6.5	21.0
Acetol	0.0	0.0	3.0	3.0	1.3	0.0	0.0	0.0	0.0	0.3
Other	1.5	0.2	0.0	0.1	0.5	1.4	0.0	0.0	0.0	0.5
Unknown	0.0	8 .	1.7	11.7	16.4	0.0	0.0	0.0	0.1	2.0
*00	0.7	1.2	1.7	4.4	7.8	0.0	0.3	-:	4.0	11.3
C02*	3.4	18.5	33.6	59.2	9.19	0.7	1.0	1.3	3.5	10.4
Selectivity (%)										
Acrylic acid	0	ς	0	9	2	0	0	0	S	9
Propionic acid	12	7	_	7	2	25	27	0	7	9
2,3-Pentanedione	51	83	75	27	38	14	33	36	27	22
Acetaldehyde	24	01	18	53	48	34	40	2	19	4
Acetol	0	0	2	9	8	0	0	0	0	_
Other	14	0	0	0	_	27	0	0	0	-
Viside managed of laive	100	20130 0010	2 1 : : 1							

*Yields reported as mole per 100 moles of lactic acid fed.

Table 4.5. Lactic Acid Conversion over CsOH/CPG and CsNO₃/CPG

Catalyst		1 mmo	CSOH / E	CPG			1 mmo	CsNO,/	g CPG	
Temperature (°C)	260	280		320	350		280		320	350
Contact Time(s)	4.0	3.9		3.7	3.3		3.3		3.2	3.1
Error (% Carbon)	25.7	-13.6	-33.6	-46.3	48.9		-26.7	-28.5	-32.2	-40.8
Conversion (BOF)	27.0	88.0		96.4	94.5	45.3	100.0		296.7	93.8
Yield (% Theoretical)										
Acrylic acid	3.5	6.1	2.4	9.0	0.0	4.6	7.0	4.0	2.2	8.0
Propionic acid	0.0	5.6	4.9	3.6	4.5	0.5	0.5	0:1	1.7	2.5
2,3-Pentanedione	41.6	48.7	36.4	19.1	8.5	34.5	49.5	38.7	26.3	11.5
Acetaldehyde	6.3	8.0	9.1	7.6	10.4	2.9	7.5	10.0	11.1	11.4
Acetol	0.0	4.2	2.5	0.0	0.0	0.0	3.2	2.7	4.	0.0
Other	0.0	6.7	1.3	8 .	2.4	0.5	0.5	1.2	2.1	3.4
Unknown	5.7	4.6	10.3	14.4	14.3	=	3.7	7.8	13.9	14.5
*0D	2.5	1.0	1:1	<u>~</u>	5.1	6.0	1.5	2.3	3.1	9.3
C02*	12.1	19.2	19.0	23.3	30.2	20.5	36.4	41.2	42.0	40.6
Selectivity (%)										
Acrylic acid	7	œ	4	7	0	Ξ	10	7	2	3
Propionic acid	0	m	6	10	<u>8</u>		_	7	4	∞
2,3-Pentanedione	81	2	2	55	33	81	73	<i>L</i> 9	29	39
Acetaldehyde	12	10	91	28	40	7	=	17	25	39
Acetol	0	S	4	0	0	0	2	ς.	3	0
Other	0	6	7	2	6	0	_	7	2	Ξ
olom on Latination of Links	100	201 20 2012	Line Cal							

*Yields reported as mole per 100 moles of lactic acid fed.

Table 4.6. Lactic Acid Conversion over Cs₃PO₄/CPG and CsNO₃/CsOH/CPG

Catalyst		1 mmo	1 Cs ₃ PO ₄ /	g CPG			: I mmol C	CsNO3:CsC	OH/g CPG	
Temperature (°C)		280		320	350	260			320	
Contact Time(s)		3.7		3.5	3.1	3.9	3.7		3.7	
Error (% Carbon)	-2.0	4.8	-33.7	-46.6	-44.7	-15.9	-12.5	-35.9	-47.9	-52.9
Conversion (BOF)		71.4		0.86	97.1	60.5	8.76		95.7	
Yield (% Theoretical)										
Acrylic acid	4.2	7.7	5.5	1.3	0.0	3.6	4.8	=	0.0	0.0
Propionic acid	9.0	0.4	0.5	9.0	1:1	0.5		1.3	1.6	3.5
2,3-Pentanedione	22.5	47.4	40.1	30.5	21.3	35.0	57.0	30.8	10.1	3.5
Acetaldehyde	3.0	4.3	5.5	5.1	6.3	3.8	8.5	10.7	8.9	8.9
Acetol	0.0	4.	1.1	0.0	0.0	0.0	2.7	0.0	0.0	0.0
Other	0.7	9.0	9.0	1.0	3.3	0.5	1.5	1.0	1.3	1.4
Unknown	0.3	1.3	5.2	7.8	8.3	6.0	8.4	12.5	12.9	9.01
*00	5.6	1.5	1.6	1.7	3.6	1.5	1.4	1.5	3.5	5.8
C02*	16.6	38.4	41.6	35.8	55.5	22.1	41.4	38.2	52.2	43.8
Selectivity (%)										
Acrylic acid	14	12	01	33	0	∞	9	7	0	0
Propionic acid	7	_		7	m	_	-	3	7	20
2,3-Pentanedione	72	11	75	79	<i>L</i> 9	8	75	69	46	20
Acetaldehyde	10	7	01	13	70		=	24	41	51
Acetol	0	7	7	0	0	0	4	0	0	0
Other	7	_	_	٣	01	_	7	7	9	∞
4	2	 -								

*Yields reported as mole per 100 moles of lactic acid fed.

compared to their active counterparts. Over Cs₂SO₄, conversion at low temperature was negligible, and at high temperature, acetaldehyde became the dominant product. Since 2 mmol/g was found to be the optimum loading for sodium catalysts (Section 3.1.2), reaction was also conducted with 1:1 mmol CsOH:CsNO₃ / g CPG catalyst (Table 4.6), which is essentially the same as 2 mmol of cesium per gram of support. Results of this experiment showed a higher 2,3-pentanedione yield (57%) at a selectivity of 75%; this is the best yield obtained so far in our effect to optimize the formation of 2,3-pentanedione from lactic acid.

Calcium hydroxide, which contains an alkaline earth metal, was also examined as a potential catalyst for the conversion of lactic acid to 2,3-pentanedione (Table 4.1), but the yield toward 2,3-pentanedione was only 3% of theoretical at 300°C. This is extremely low compared to the alkali metal catalysts. Lactic acid conversion was likewise relatively low and the catalyst was more selective to acetaldehyde and acrylic acid, possibly because of its higher acidity. As mentioned earlier, acetaldehyde formation is favored on acidic catalysts.

A different trend was observed for the acrylic acid formation, for which yield decreases with increasing basicity (Figure 4.2). Again, anions of active cesium and potassium species do not have a significant effect on the yield. Over all, sodium hydroxide was found to be the most promising catalyst for acrylic acid formation, with 23% yield at 350°C (Table 3.2). However, this yield is still too low to be economically competitive with the current petroleum-based production processes for acrylic acid. Further experimental efforts are needed to overcome the formation of acetaldehyde at high temperature and hence increase the selectivity toward acrylic acid.

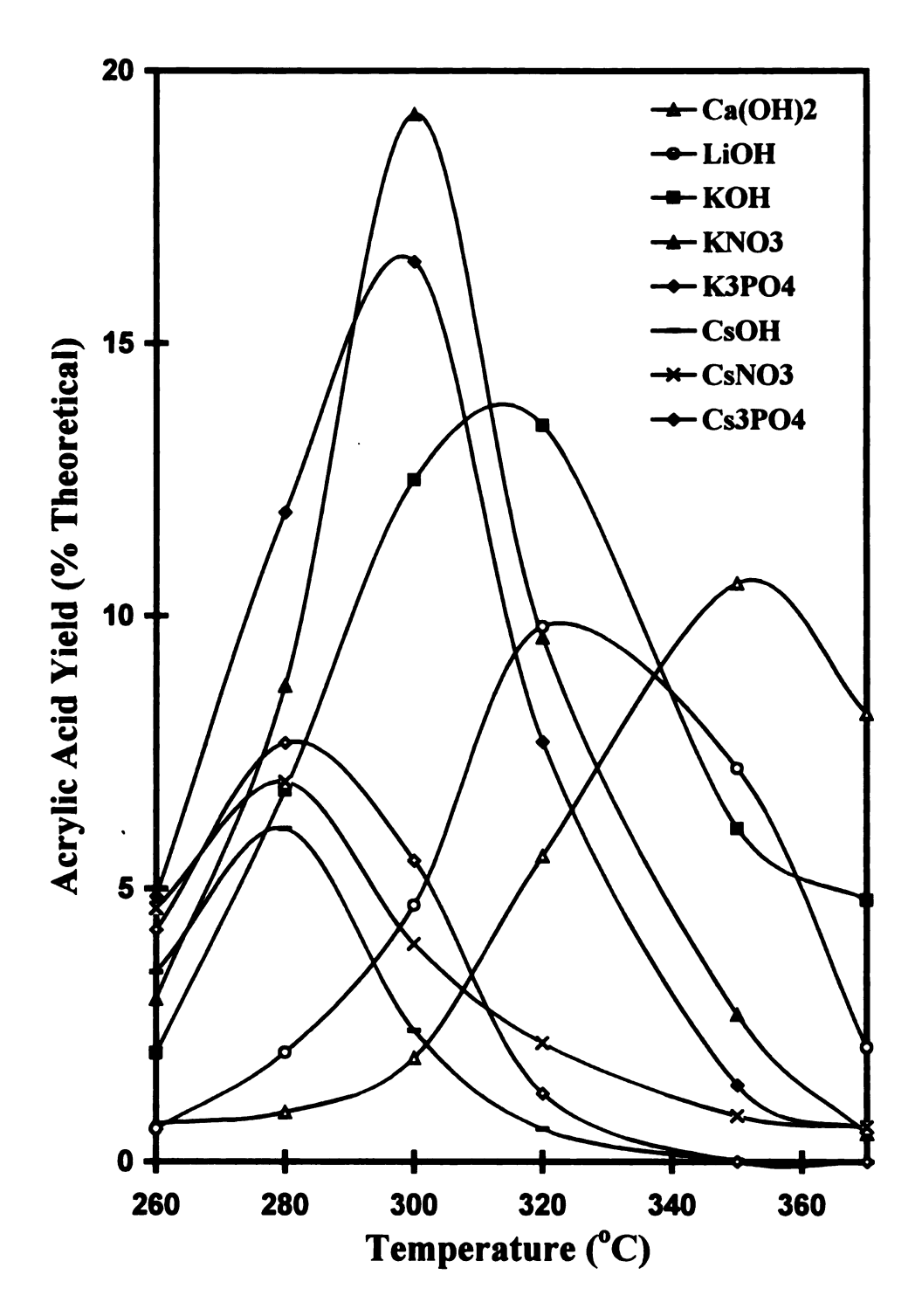


Figure 4.2. Acrylic Acid Yields over Various Alkali Salt Catalysts

4.1.2. Catalyst activity and pathways

Results from the different alkali hydroxides clearly display higher activity and selectivity toward 2,3-pentanedione formation with decreasing Lewis acidity of the alkali metal. At low temperatures, approximately 90% of the carbon was recovered in the products. However, carbon recoveries at 350°C were relatively poor, especially for the cesium catalysts where close to 50% of the carbon was lost due to coking and cracking. This is evident by the large amounts of CO₂ and CO produced (Tables 4.5-4.6).

Product samples were normally collected consecutively from 260°C up to 370°C for each catalyst. To check for hysteresis effects and verify the validity of the yield trends with temperature, an experiment was conducted with reaction temperatures in the reverse order (370°C to 260°C) over 1 mmol CsNO₃ / g CPG. Figure 4.1 contains the product yields of the forward and reverse temperature collection experiments with CsNO₃. The agreement between the results of these two experiments is within experimental error; no catalyst hysteresis with temperature is thus observed. In addition, this result leads to the conclusion that conversion of CsNO₃ to cesium lactate is complete even at the lowest temperature studied. This is supported by the post-reaction FTIR spectra of CsNO₃ (Figure 4.19); we thus conclude that the amount of cesium lactate does not change over the experimental temperature range studied.

The reaction pathway and mechanism for the catalytic condensation of lactic acid to 2,3-pentanedione have been proposed and discussed for sodium salts (Section 3.3.3). In general, the reaction can occur with any alkali salt, but the lower electronegativities of the heavier alkali metals, thus higher negative charges on the carboxylate oxygen, are believed to enhance the deprotonation of the α -hydrogen of another lactic acid molecule

which initiates the condensation toward 2,3-pentanedione. We have also suggested that the formation of alkali lactate via proton transfer from lactic acid to the anion of the salt depends strongly on the vaporization temperature of the corresponding conjugate acid and the melting point of the alkali salt (Section 3.3.2). Clearly, if the conjugate acid formed from proton transfer was continuously vaporized, the reaction would be quickly driven toward complete formation of alkali lactate. Except for H₂SO₄, conjugate acids produced from these salt catalysts with lactic acid vaporize at temperatures much lower than the reaction temperature. Our results also indicate that proton transfer between the alkali salt and lactic acid is much more efficient when the alkali salt has a low melting point. The melting points of the selected alkali salts are listed in Table 4.7. The high melting points of the sulfates and chlorides prevent sufficient conversion of the salt to surface alkali lactate, which is necessary to initiate the formation of 2,3-pentanedione. High conjugate acid boiling point and high salt melting point thus explain the lower 2,3-pentanedione yields obtained from KCl, CsCl, and Cs₂SO₄.

4.1.3. Effect of loading

Lactic acid conversions were conducted with different KOH loadings on CPG (0.05 - 4.0 mmol/g) and on SiGel (0.1 - 3.0 mmol/g) to identify the optimum loading at constant feed composition and residence time. Complete results of lactic acid conversion over SiGel support alone are tabulated in Table 4.8. Because the bulk densities of these two supports were different, the mass of SiGel catalysts used was approximately three-fourths that for CPG to achieve the same residence time (~ 3-4 seconds). Acetaldehyde is the main side-product of the reaction system, especially with SiGel-supported catalysts.

Table 4.7. Melting Points of Alkali Salts and Bases

Melting Point (°C)
450
-H ₂ O, 580
334
360
770
1340
272
414
645
1010

Lactic acid conversion and yields of 2,3-pentanedione and acetaldehyde at 260°C, 280°C, 300°C, 320°C and 350°C over KOH/CPG are plotted on Figures 4.3-4.7, respectively, for each temperature. The corresponding results over KOH/SiGel are given on Figures 4.8-4.12. There appears to be an optimum loading of 2 mmol of KOH per gram of support at 300°C for 2,3-pentanedione formation on both CPG (Figure 4.5) and SiGel (Figure 4.10) catalysts. This was also observed as the optimum loading for sodium salts on CPG catalysts (Section 3.1.2). Further increase in loading to 3 or 4 mmol/g does not significantly change the yield at the optimum temperature; however, both yields and conversions are slightly higher at lower temperature. Yields of 2,3-pentanedione at 2 mmol KOH/g are found to be almost 10% higher over CPG support relative to SiGel support, while the acetaldehyde yields are 10% lower. This is attributed to the lower surface acidic of CPG as compared to SiGel, which reduces acid-site catalyzed

Table 4.8. Lactic Acid Conversion over SiGel Support Alone and KOH/Ba/SiGel

Catalyst		S	SiGel Alone				2 mmol K(KOH / 3% Ba	a/g SiGel	
Temperature (°C)	260	280	300	320	350	260	280	300	320	
Contact Time(s)	3.6	4.1	4.5	3.1	3.8	3.1	3.3	3.6	3.3	2.9
Error (% Carbon)	-22.7	-18.7	-20.8	47.9	-18.7	3	=	-17	-26	-31
Conversion (BOF)	26.4	27.4	41.8	8.9/	79.0	10.3	50.8	74.3	95.7	95.0
Yield (% Theoretical)										
Acrylic acid	0.0	0.0	0.0	0.0	0.0	0.0	1.9	0.0	0.0	0.0
Propionic acid	0.0	0.0	0.0	0.0	1.5	0.0	0.4	0.4	0.7	1.0
2,3-Pentanedione	0.0	0.0	0.0	0.0	0.0	6	31	38	32	91
Acetaldehyde	3.8	11.4	26.9	31.5	59.1	1.7	2.0	13.4	17.2	20.1
Acetol	0.0	0.0	0.0	0.0	0.0	0.0	0.0	3.1	3.0	1.3
Other	1.5	0.7	0.5	5.6	3.2	0.5	0.3	0.1	0.2	0.3
Unknown	0.0	0.0	1.0	0.0	0.0	2.7	8 .	3.0	8.1	11.7
*00	0.7	1.4	4.6	14.5	47.0	8.0	1.2	1.9	2.0	7.3
C02*	0.4	9.0	9.0	6.0	5.6	3.6	16.4	28.9	59.3	65.5
Selectivity (%)										
Acrylic acid	_	0	0	0	0	0	ς.	0	0	0
Propionic acid	0	0	0	0	7	0	_	-	_	က
2,3-Pentanedione	0	0	0	0	0	80	80	69	9	41
Acetaldehyde	71	95	86	85	93	15	13	24	33	53
Acetol	0	0	0	0	0	0	0	9	9	3
Other	28	5	2	15	5	5	-	0	0	-

*Yields reported as mole per 100 moles of lactic acid fed.

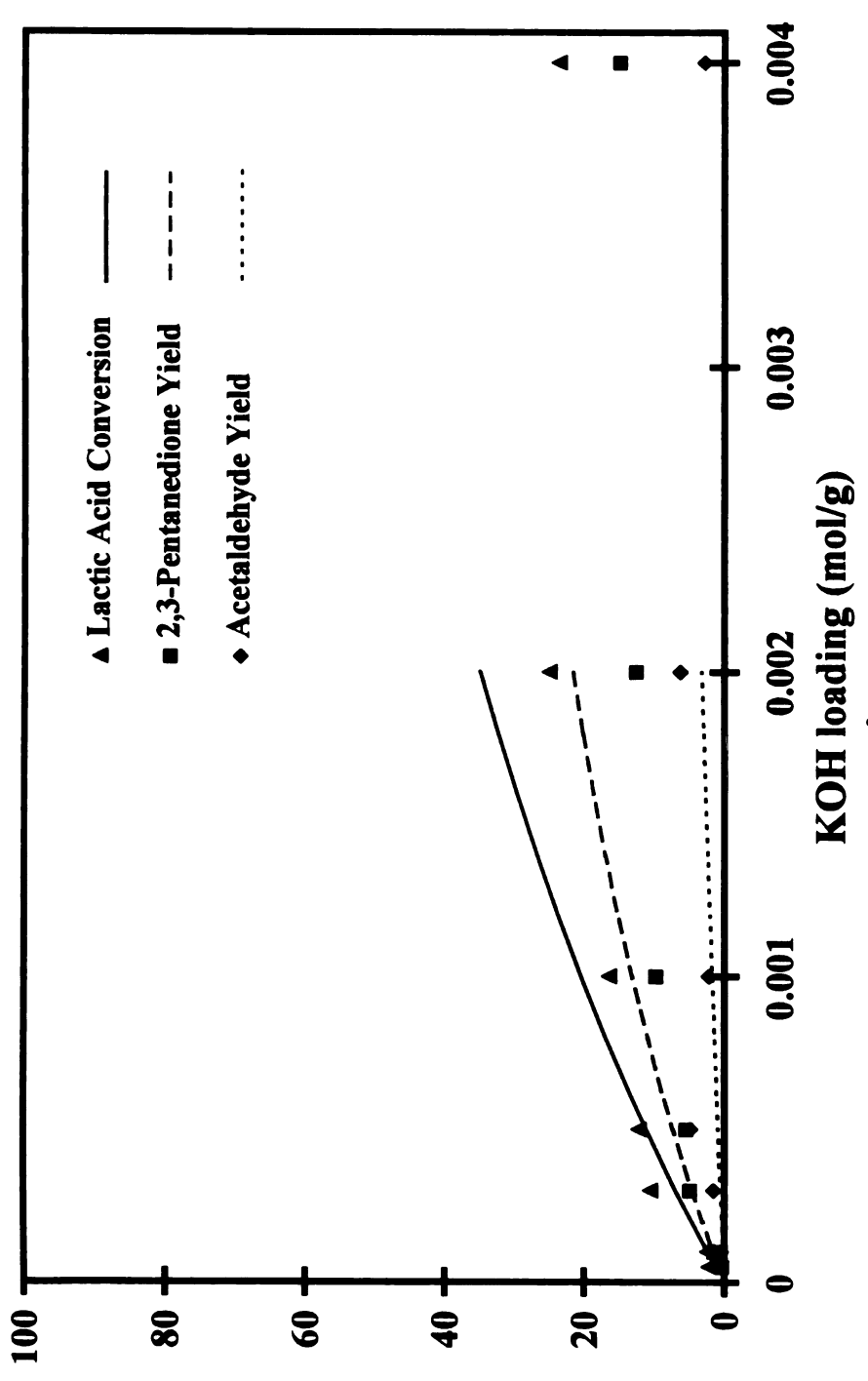


Figure 4.3. Experimental Results over KOH/CPG at T = 260°C [Kinetic Model (lines) conducted at 3.34 s residence time.]

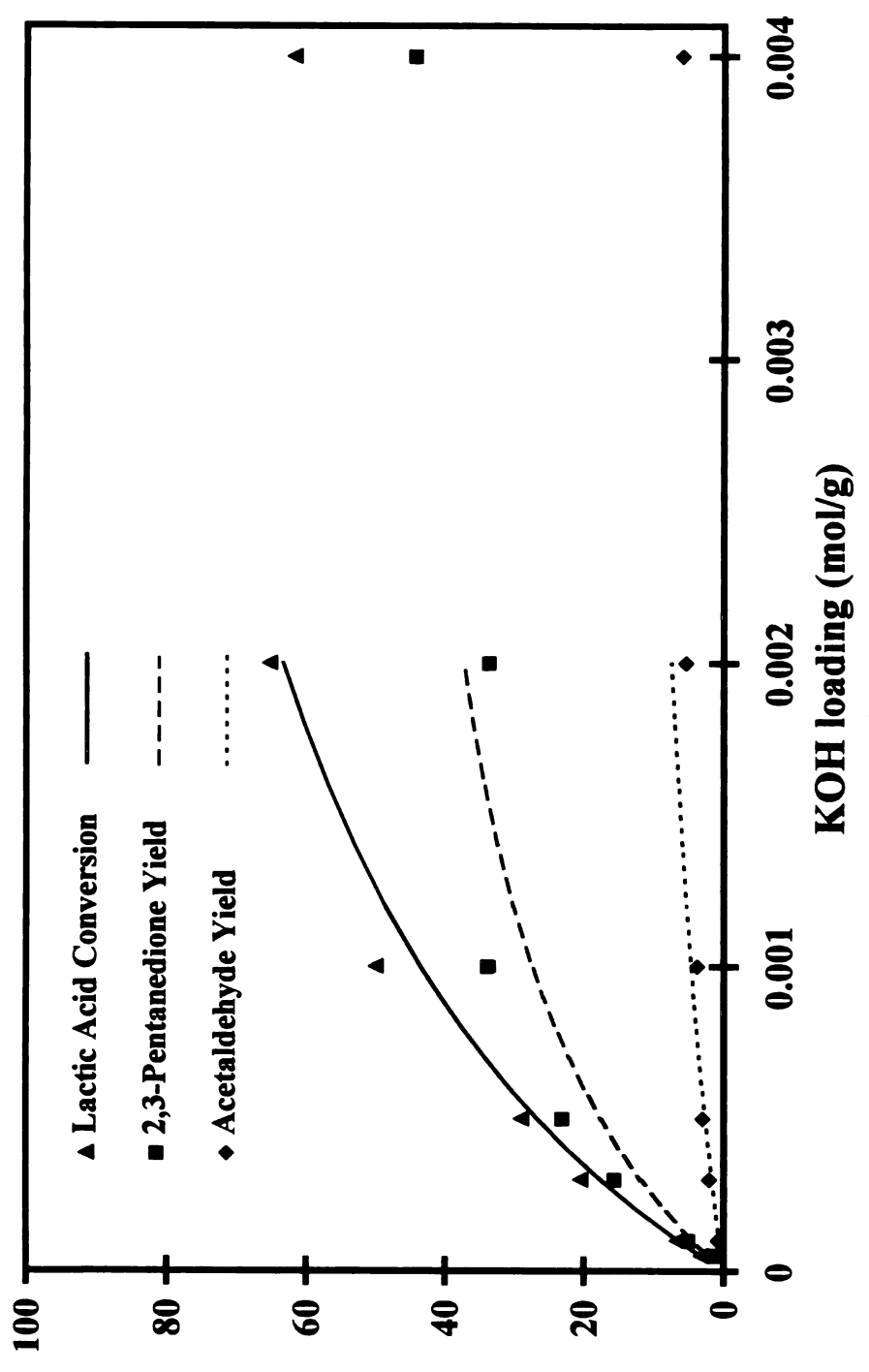


Figure 4.4. Experimental Results over KOH/CPG at $T = 280^{\circ}$ C [Kinetic Model (lines) conducted at 3.34 s residence time.]

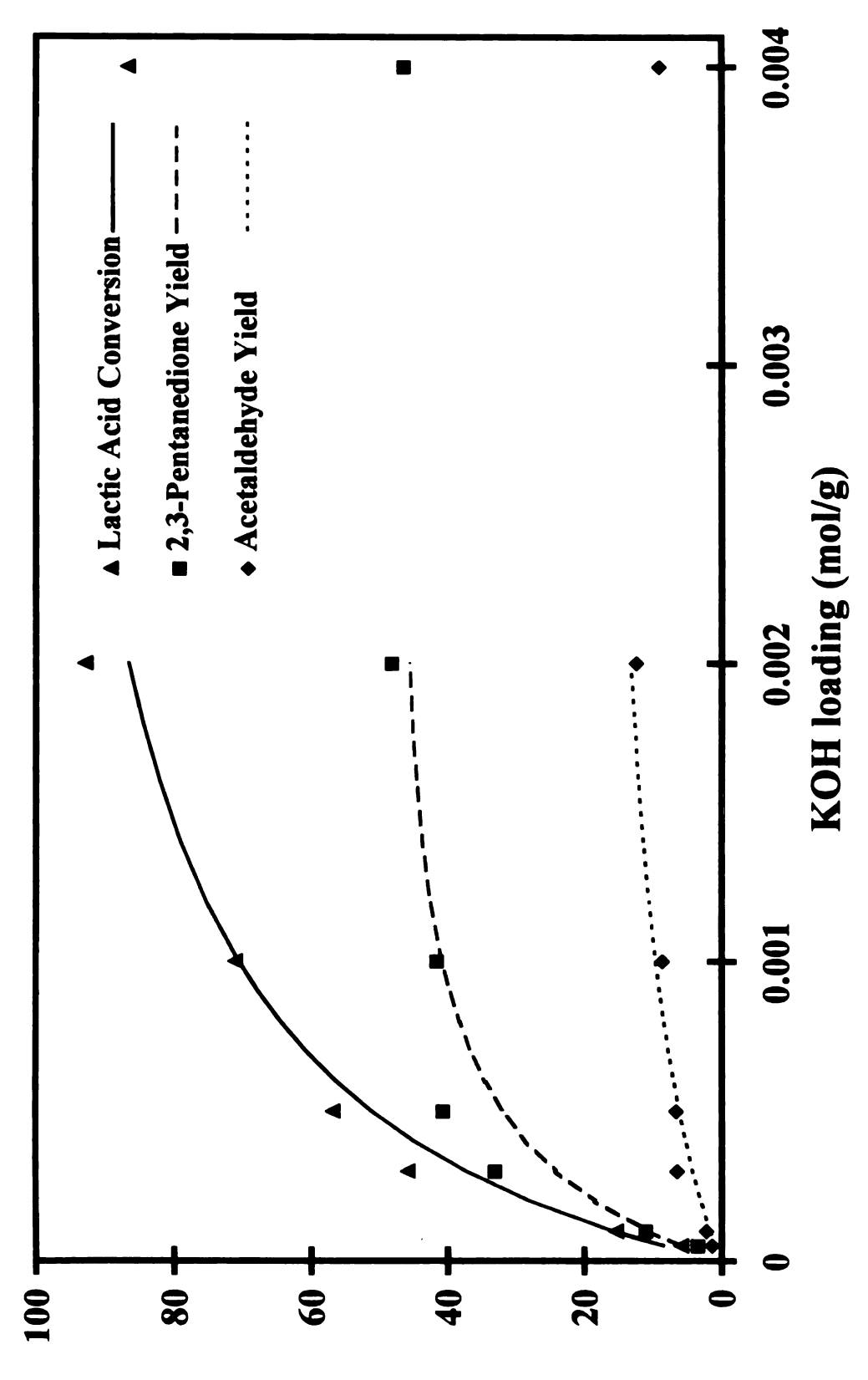


Figure 4.5. Experimental Results over KOH/CPG at T = 300°C [Kinetic Model (lines) conducted at 3.34 s residence time.]

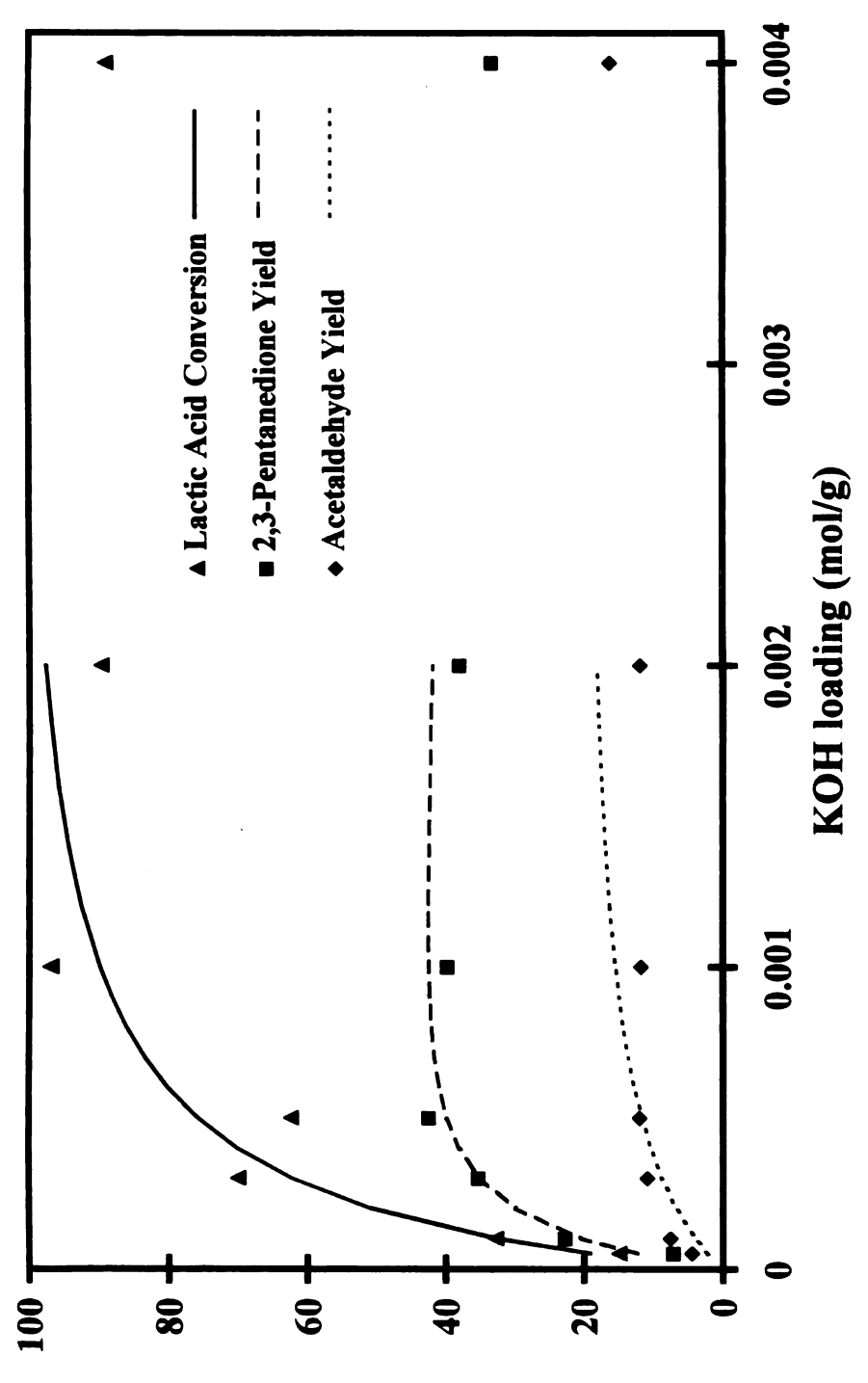


Figure 4.6. Experimental Results over KOH/CPG at T = 320°C [Kinetic Model (lines) conducted at 3.34 s residence time.]

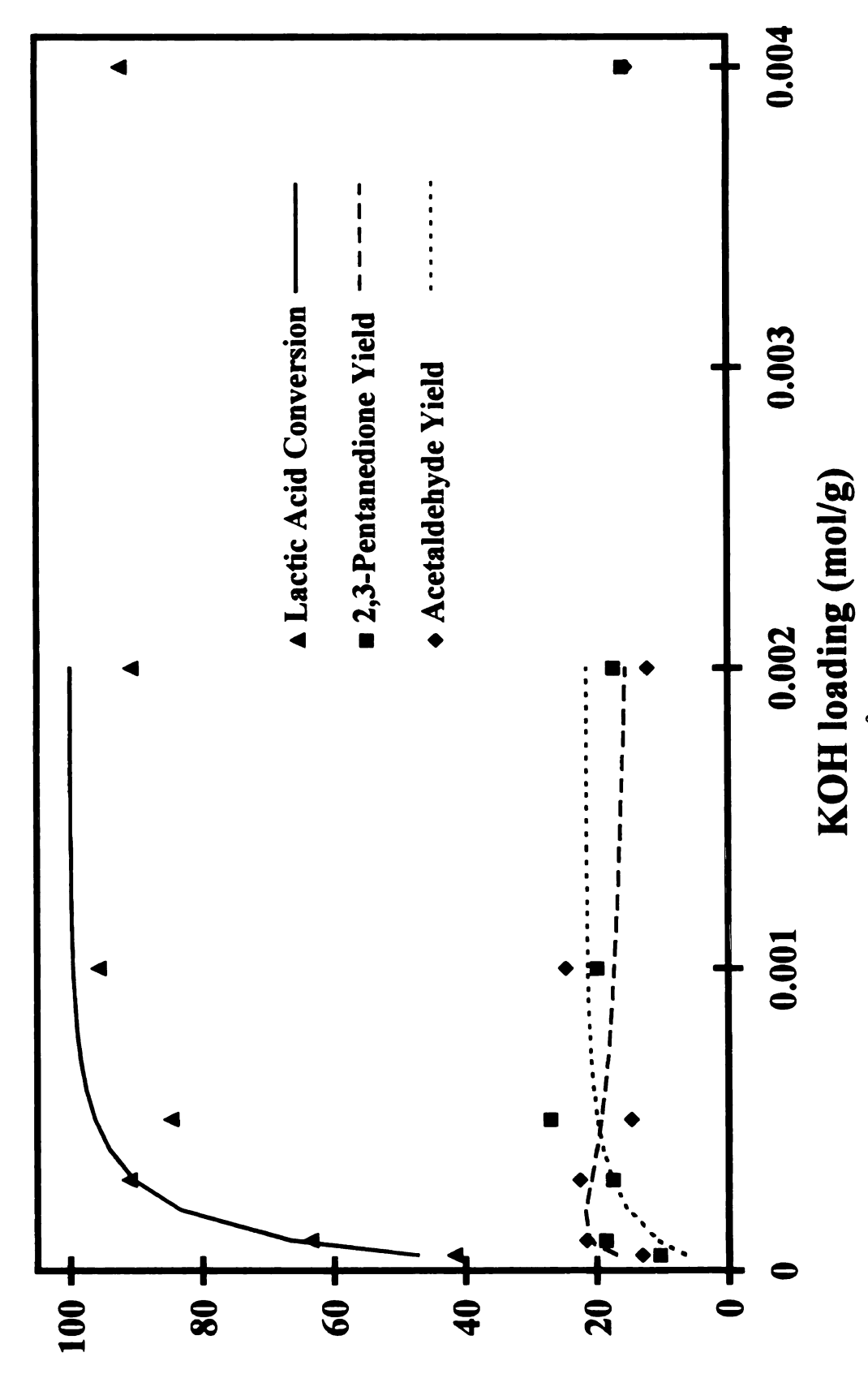


Figure 4.7. Experimental Results over KOH/CPG at T = 350°C [Kinetic Model (lines) conducted at 3.34 s residence time.]

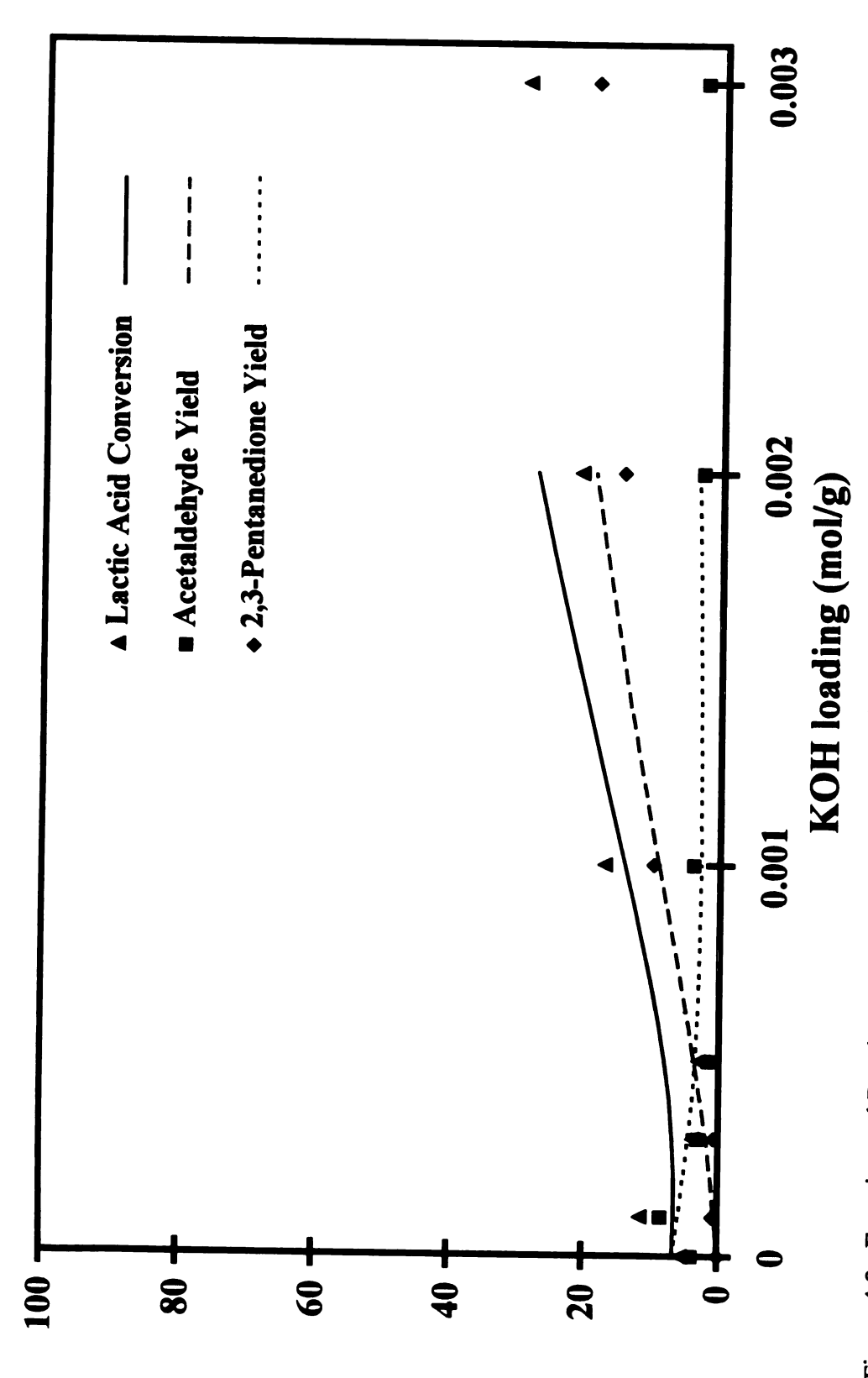


Figure 4.8. Experimental Results over KOH/SiGel at T = 260°C [Kinetic Model (lines) conducted at 3.54 residence time.]

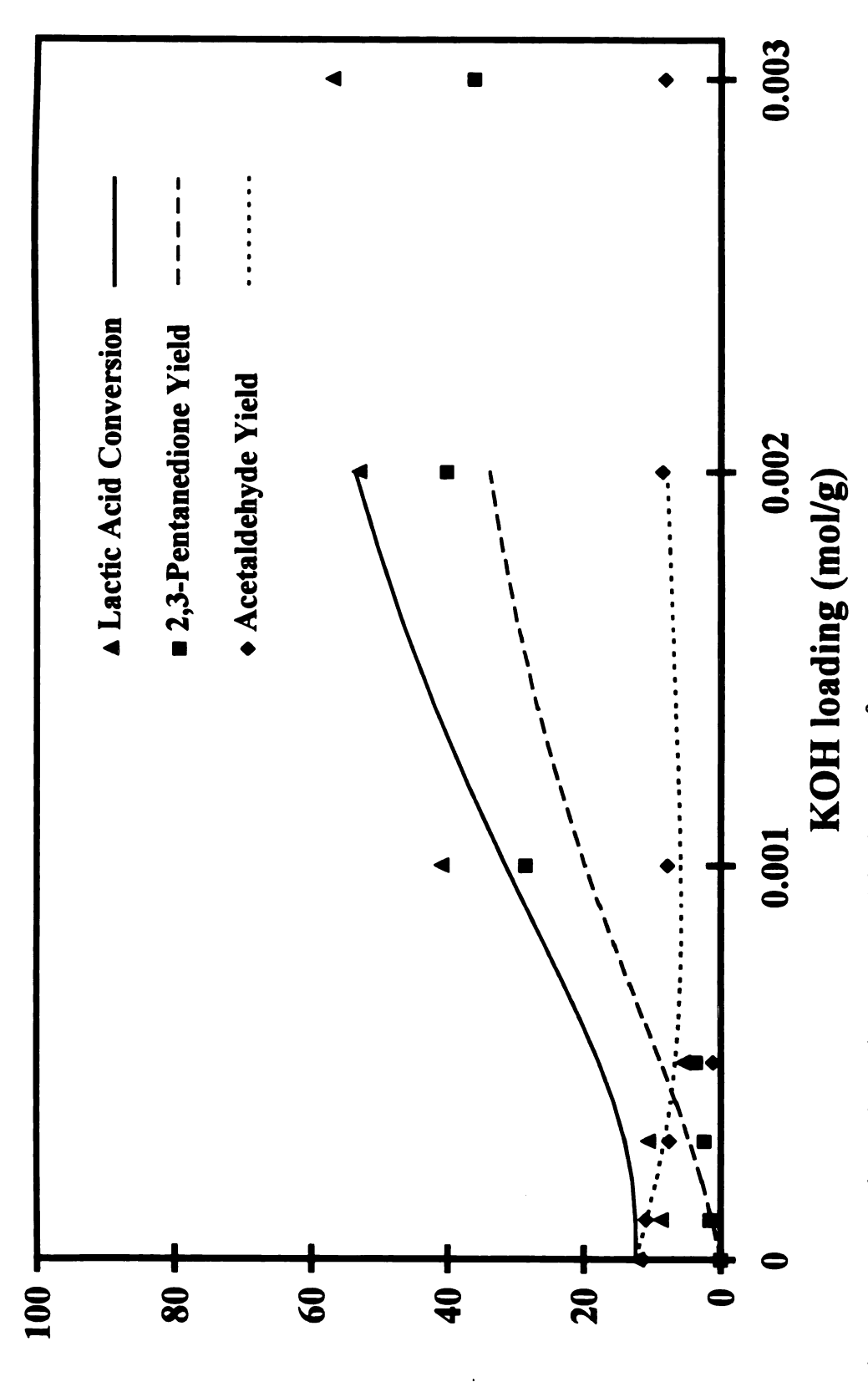


Figure 4.9. Experimental Results over KOH/SiGel at T = 280°C [Kinetic Model (lines) conducted at 3.54 residence time.]

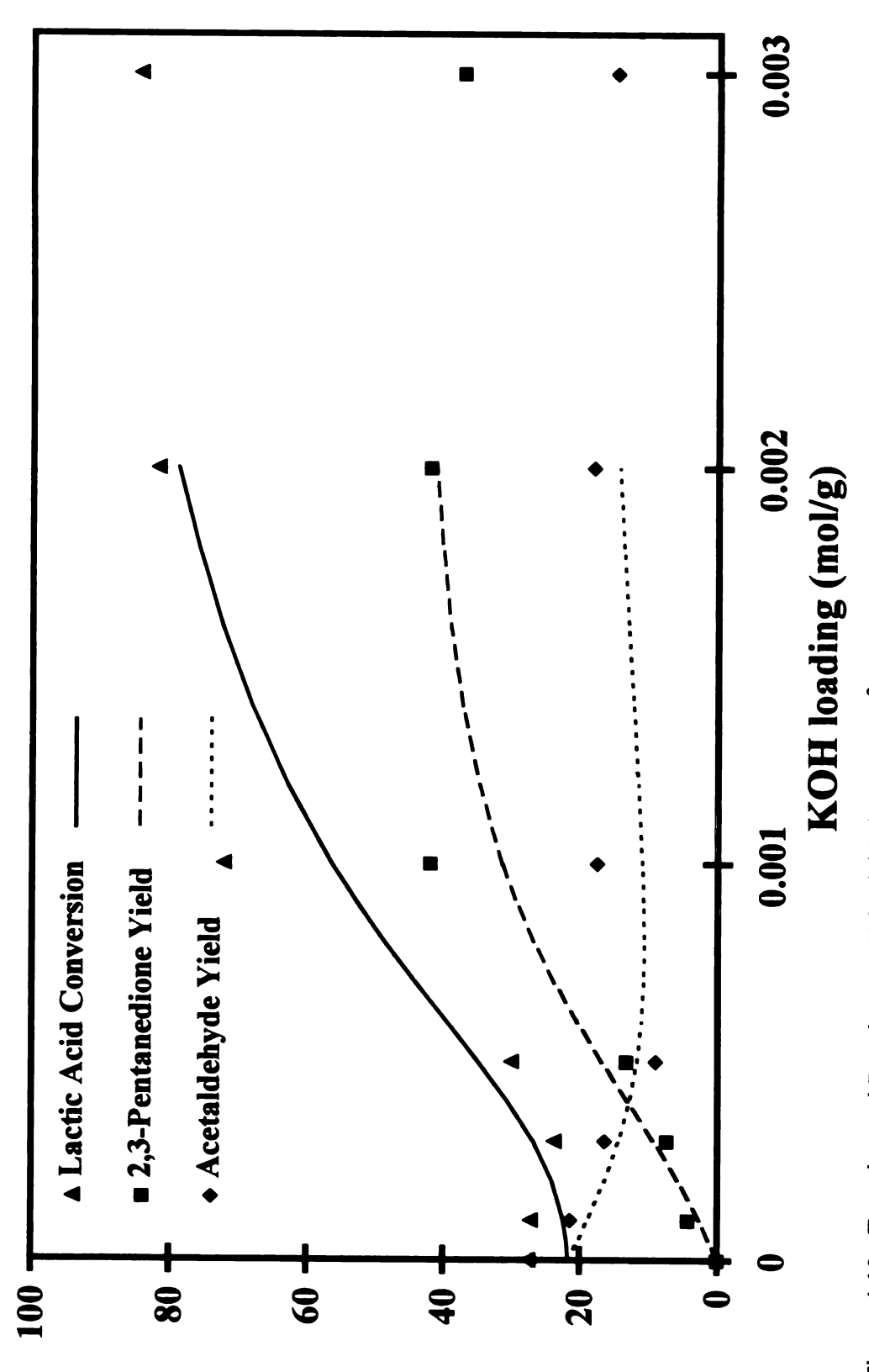


Figure 4.10. Experimental Results over KOH/SiGel at T = 300°C [Kinetic Model (lines) conducted at 3.54 residence time.]

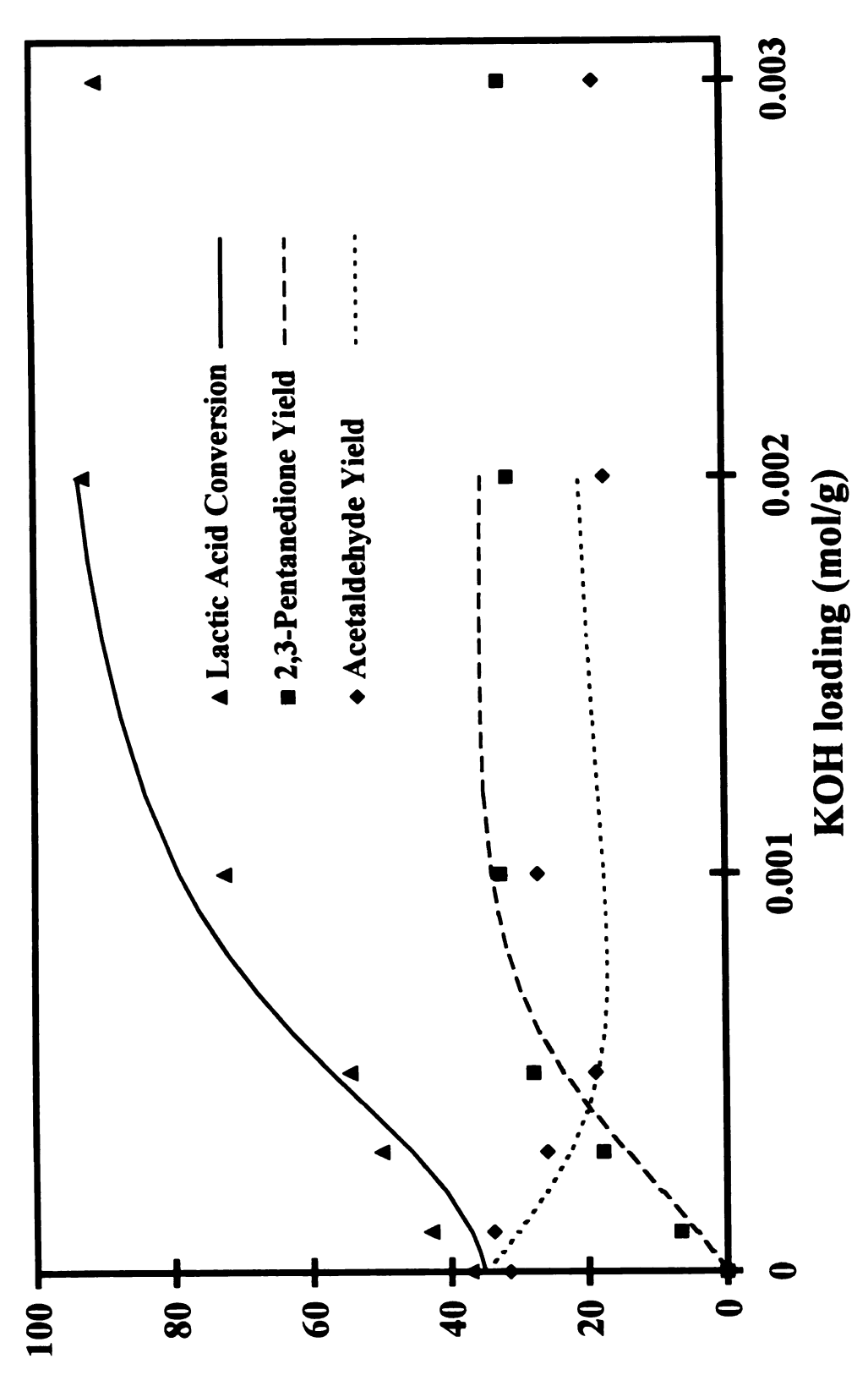


Figure 4.11. Experimental Results over KOH/SiGel at T = 320°C [Kinetic Model (lines) conducted at 3.54 residence time.]

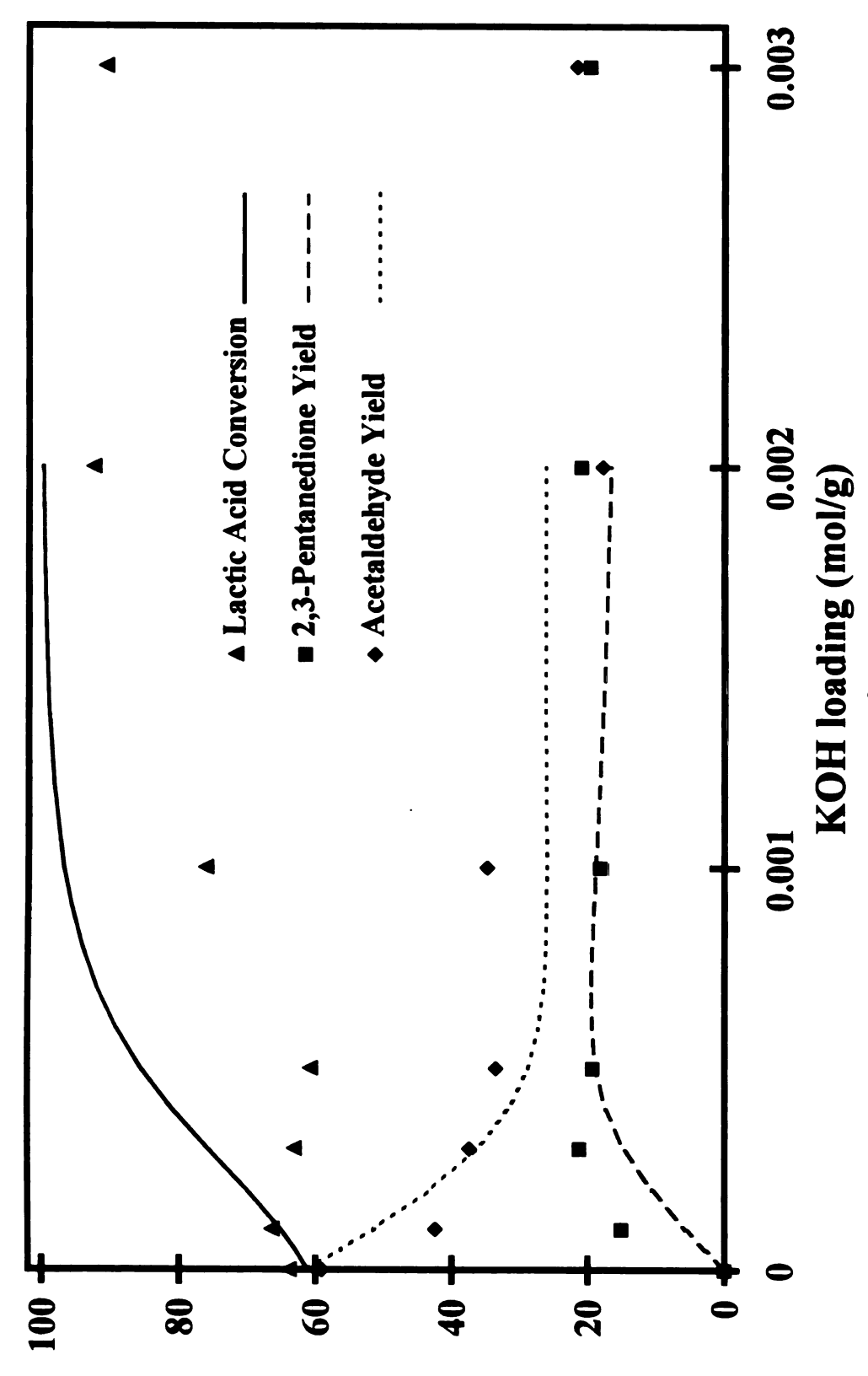


Figure 4.12. Experimental Results over KOH/SiGel at T = 350°C [Kinetic Model (lines) conducted at 3.54 residence time.]

decarbonylation of lactic acid to acetaldehyde and carbon monoxide. Detailed discussion on loading and support effects is presented below in Section 4.3.3.

Sodium and cesium catalyst loadings were also investigated on SiGel with loadings between 0.5-3.0 mmol/g. Lactic acid conversion and yields of 2,3-pentanedione and acetaldehyde are given in Figures 4.13-4.15 for NaOH/SiGel and in Figures 4.16-4.18 for CsOH/SiGel, respectively. Again, the optimum loading for these hydroxides is found to be 2 mmol/g. 2,3-Pentanedione yield on CsOH/SiGel at 2 mmol/g and 280 °C is substantially lower than results obtained from cesium on CPG (Table 4.6), which is also a consequence of the more acidic SiGel support.

4.2. Post-reaction FTIR

Spectra from post-reaction FTIR of CsNO₃ salt are shown in Figure 4.19. Cesium lactate is observed to form upon exposure of CsNO₃ on silicon disk to lactic acid vapor at high temperature. Little CsNO₃ (1763, 1343, 1050, and 834 cm⁻¹) reacted with the lactic acid until above 250°C, where cesium lactate (1598, 1414, 1120, 1042, 854, and 777 cm⁻¹) was observed. It is clear from the IR studies with NaNO₃ (Figure 3.6) that sodium lactate is rapidly formed in the presence of lactic acid vapor at temperatures around 200°C. With CsNO₃, no cesium lactate was observed on the silicon disk until 250°C. This occurred because CsNO₃ melts at a higher temperature than NaNO₃, and thus a slightly higher reaction temperature is needed to form the molten phase which enables fast proton transfer with lactic acid. This reinforces our conclusion (Section 3.3.2) that the melting point of the starting alkali salt is extremely important in the formation of surface alkali lactate and thus catalyst activity. Post-reaction FTIR

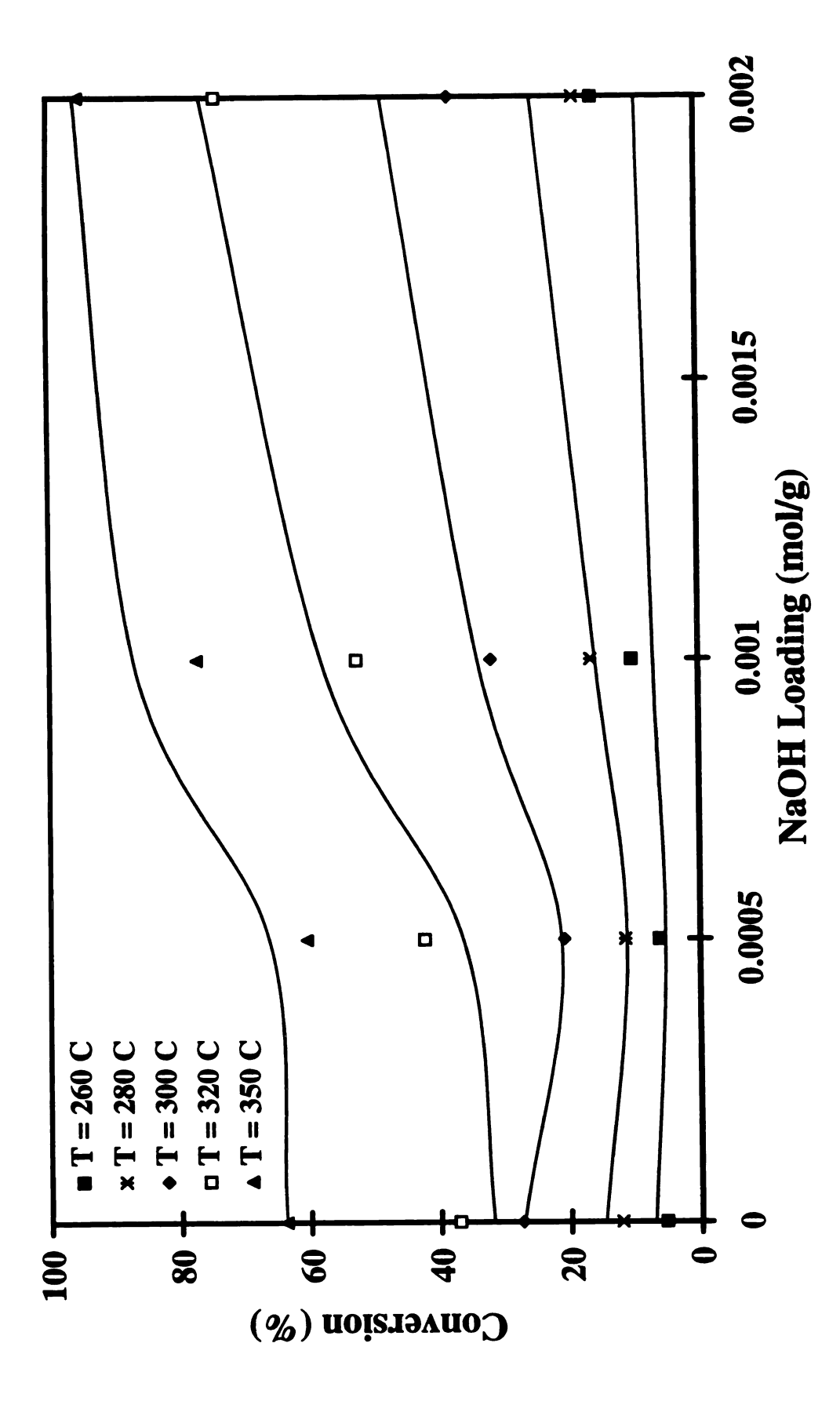


Figure 4.13. Lactic Acid Conversion over NaOH/SiGel

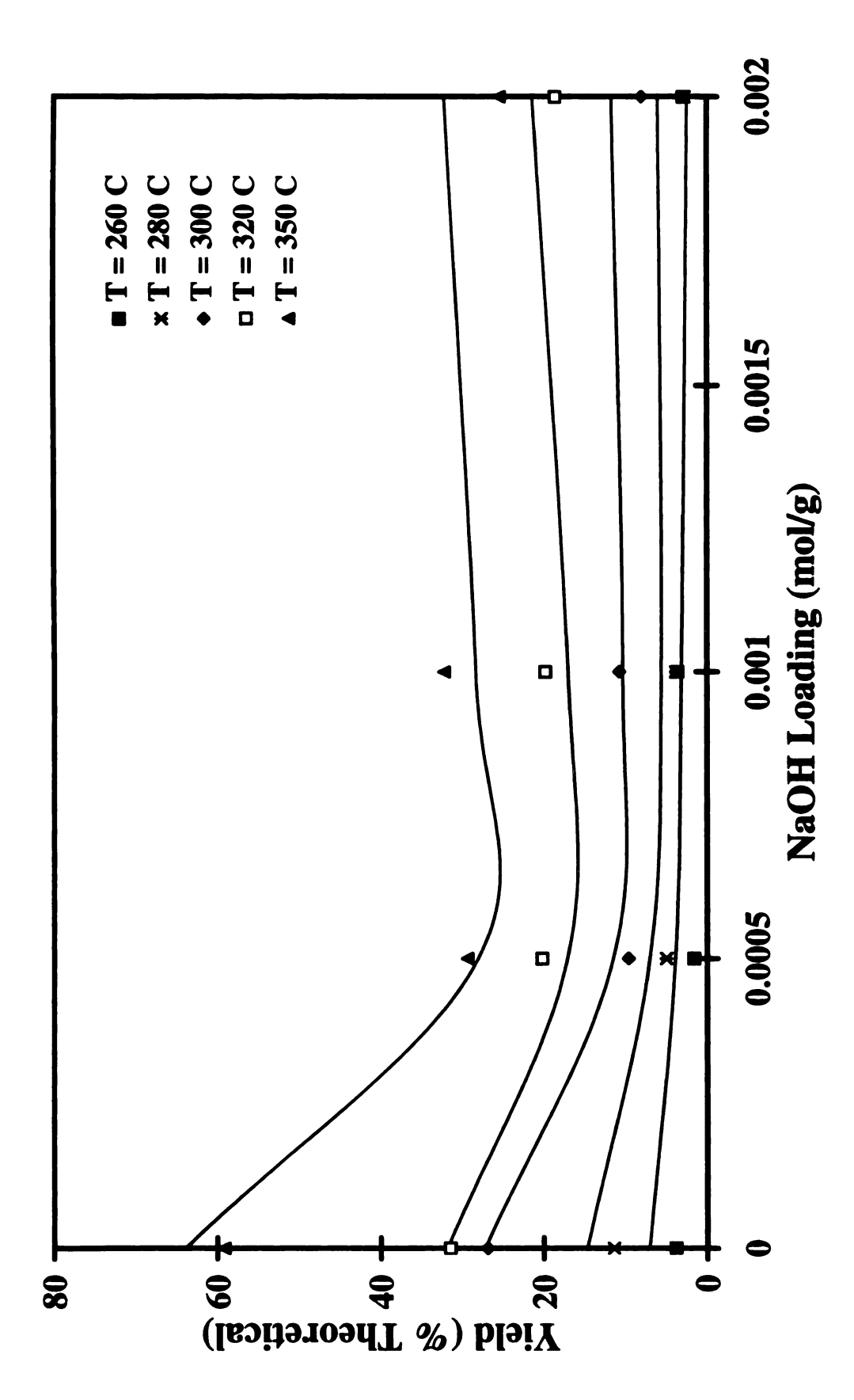


Figure 4.14. Acetaldehyde Yield over NaOH/SiGel

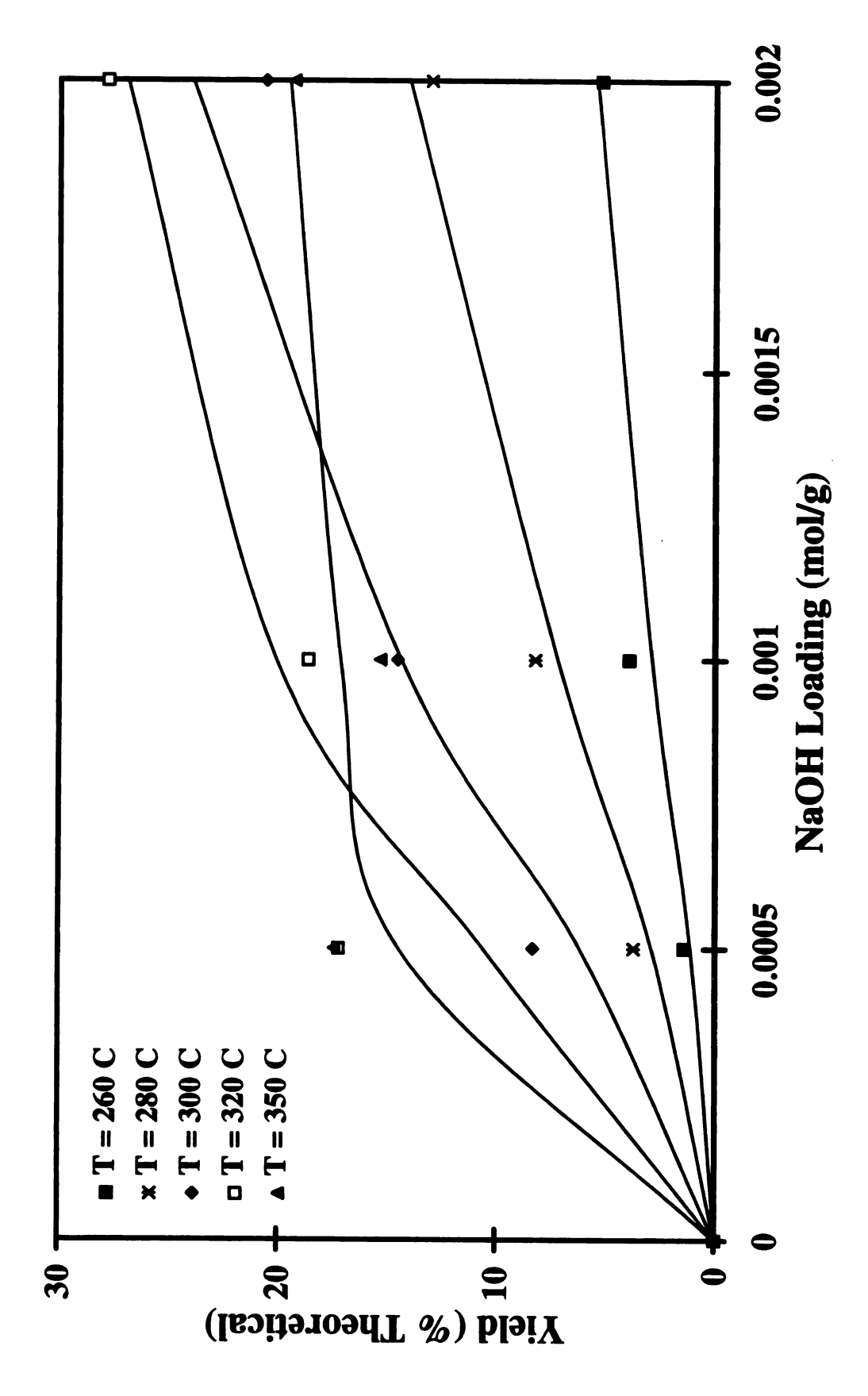


Figure 4.15. 2,3-Pentanedione Yield over NaOH/SiGel

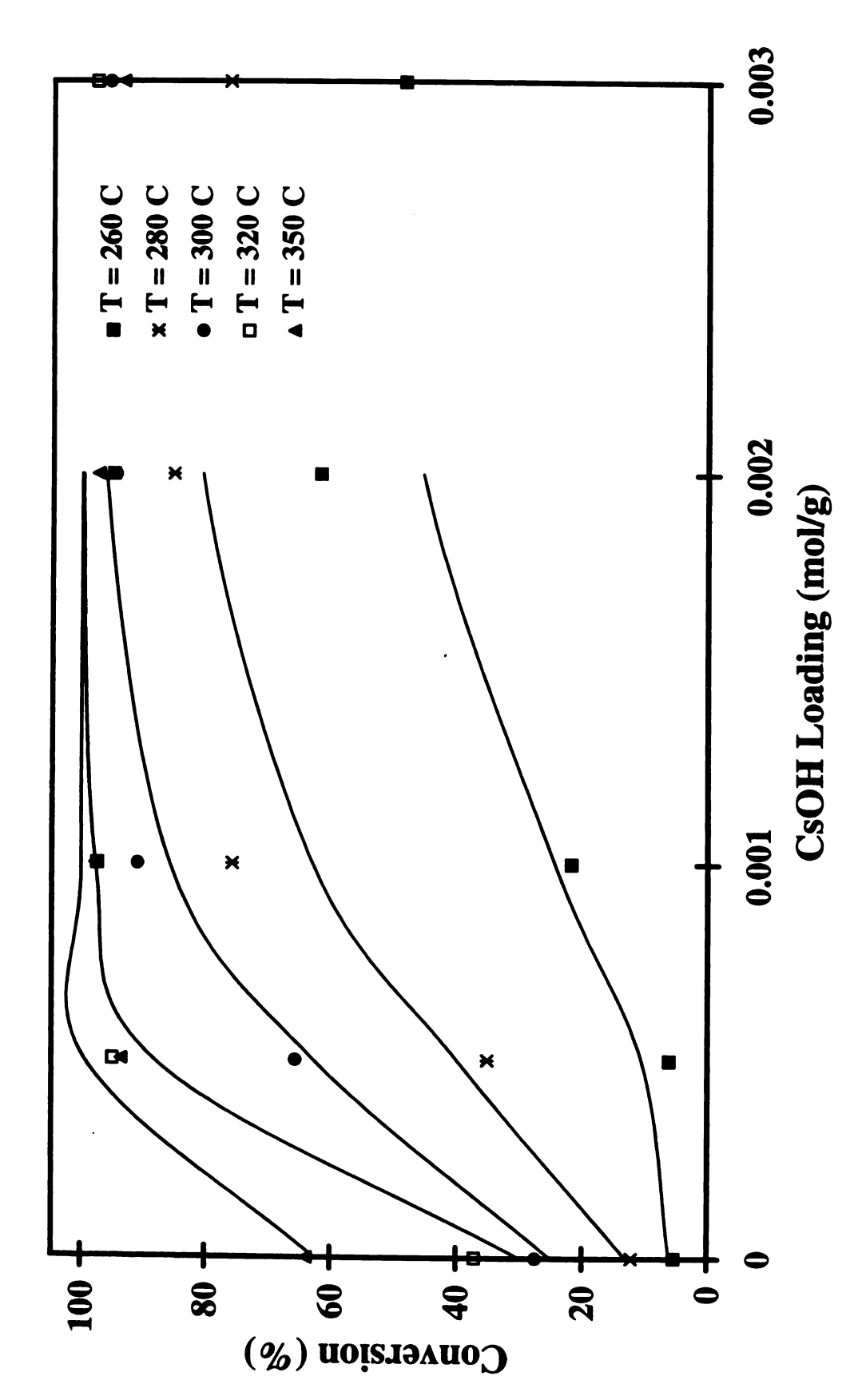


Figure 4.16. Lactic Acid Conversion over CsOH/SiGel

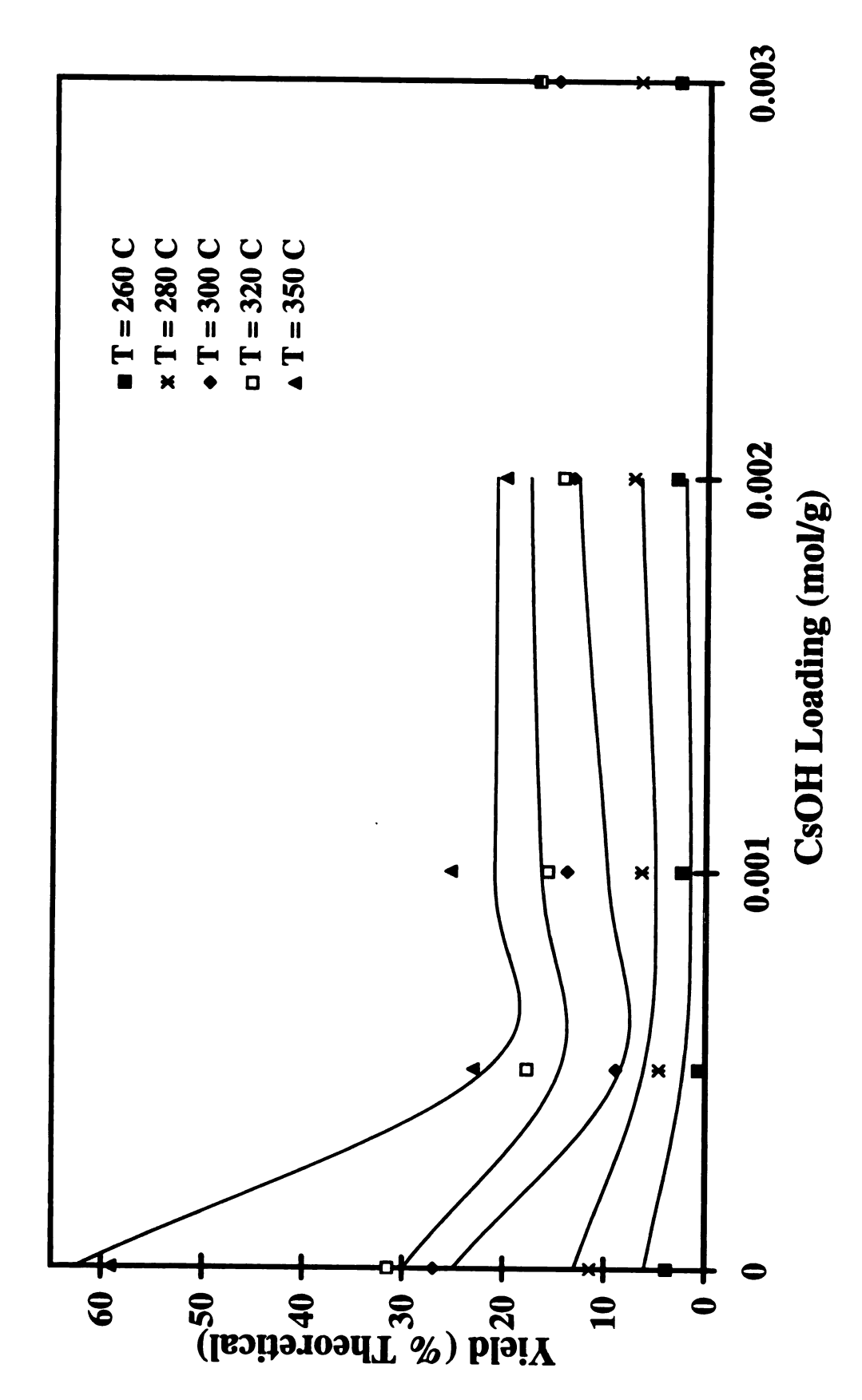


Figure 4.17. Acetaldehyde Yield over CsOH/SiGel

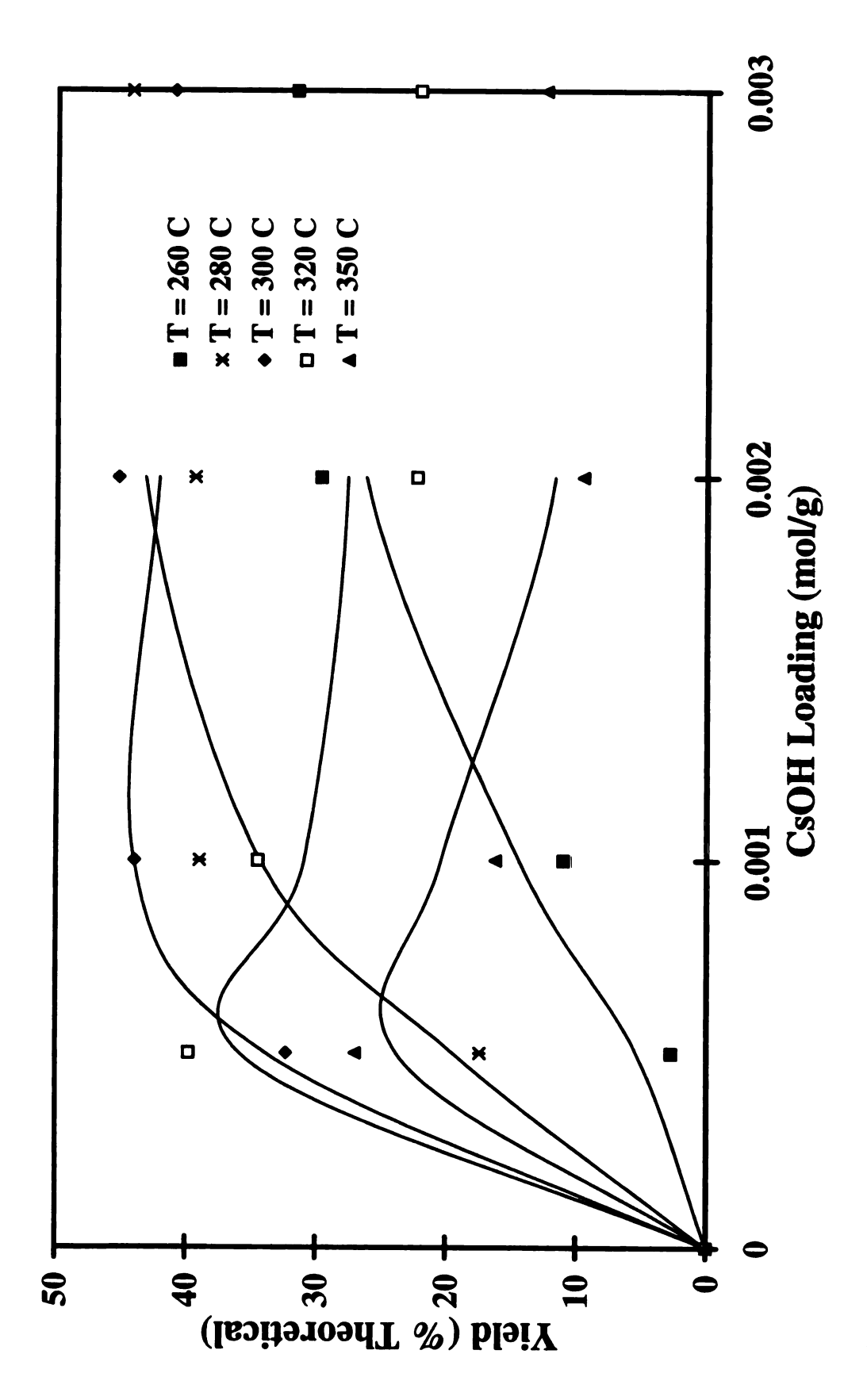


Figure 4.18. 2,3-Pentanedione Yield over CsOH/SiGel

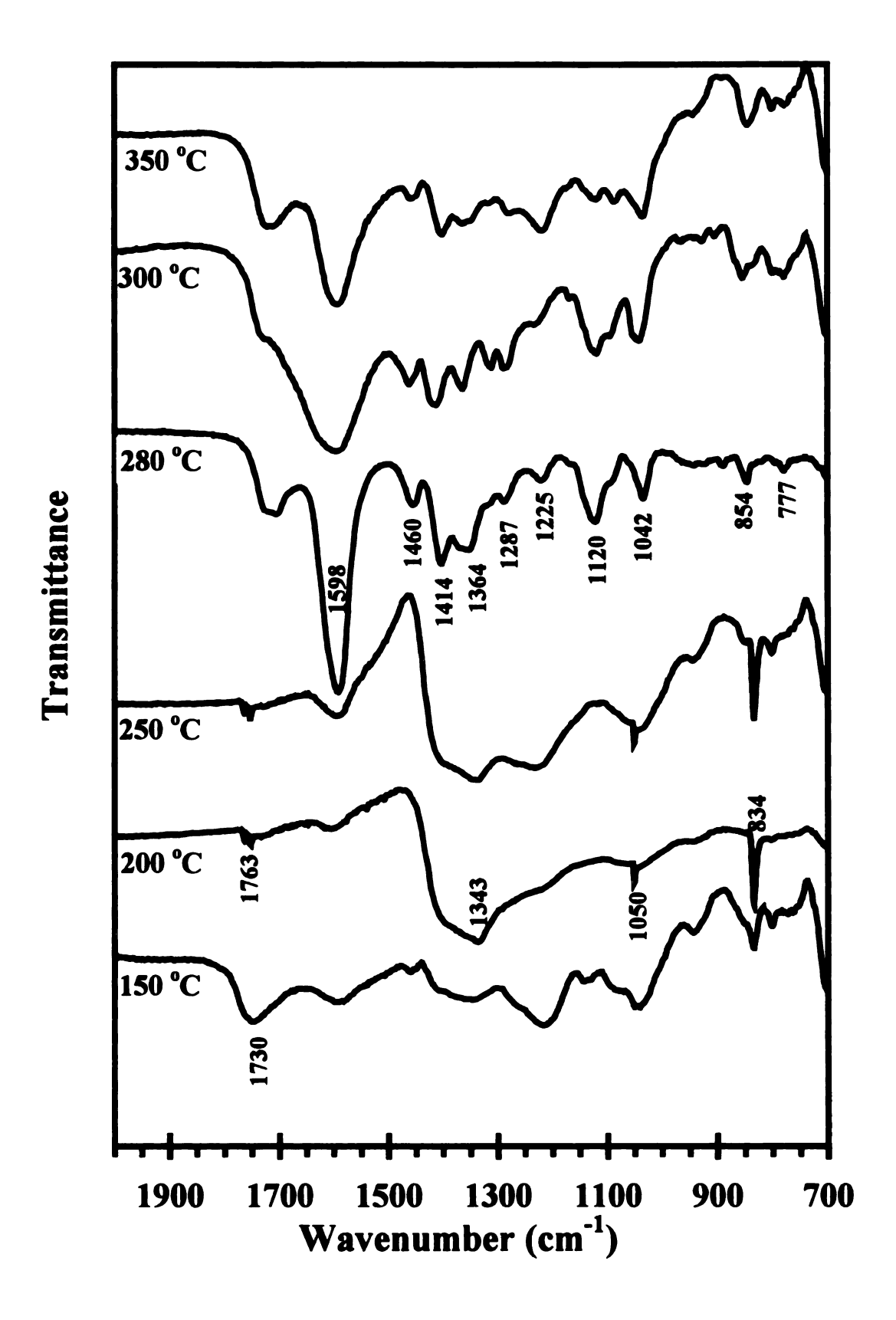


Figure 4.19. Post-Reaction FTIR Spectra of CsNO₃ Exposed to Lactic Acid Vapor

spectroscopy was also done with CsCl (Figures 4.20) and KCl and again, the silicon disk infrared spectrum was not subtracted from these spectra to prevent any misleading distortions. Only a trace amount of lactate was observed at 250°C; this amount of surface lactate was found to increase slightly with temperature in both cases. The ineffectiveness of chlorides in forming lactate is consistent with results observed for NaCl and can be explained by their high melting point (Table 4.7).

4.3. General kinetic model of the reaction system

A detailed kinetic model for the conversion of lactic acid over MOH on silica support has been developed, where M can be any alkali metal. In this model, the rate expression for acetaldehyde formation includes both support acid-site catalyzed decarbonylation (k_{1a}) and base-site catalyzed (k_{1b}) decarboxylation pathways of lactic acid conversion (Figure 1.1).

CH₃CH(OH)COOH
$$\xrightarrow{k_{1a}}$$
 CH₃CHO + CO + H₂O
CH₃CH(OH)COOH $\xrightarrow{k_{1b}}$ CH₃CHO + CO₂ + H₂

Based on our previously proposed pathway for sodium salt catalyst (Section 3.3.2), the formation of 2,3-pentanedione

2 CH₃CH(OH)COOH → CH₃C(O)C(O)C₂H₅ + 2H₂O + CO₂ is expressed in the model as first order with respect to basic site concentration and second order in lactic acid concentration. This is because formation of alkali lactate from lactic acid and MOH is rapid and the condensation reaction between lactic acid and alkali lactate is expected to be the rate-limiting step in 2,3-pentanedione formation. The

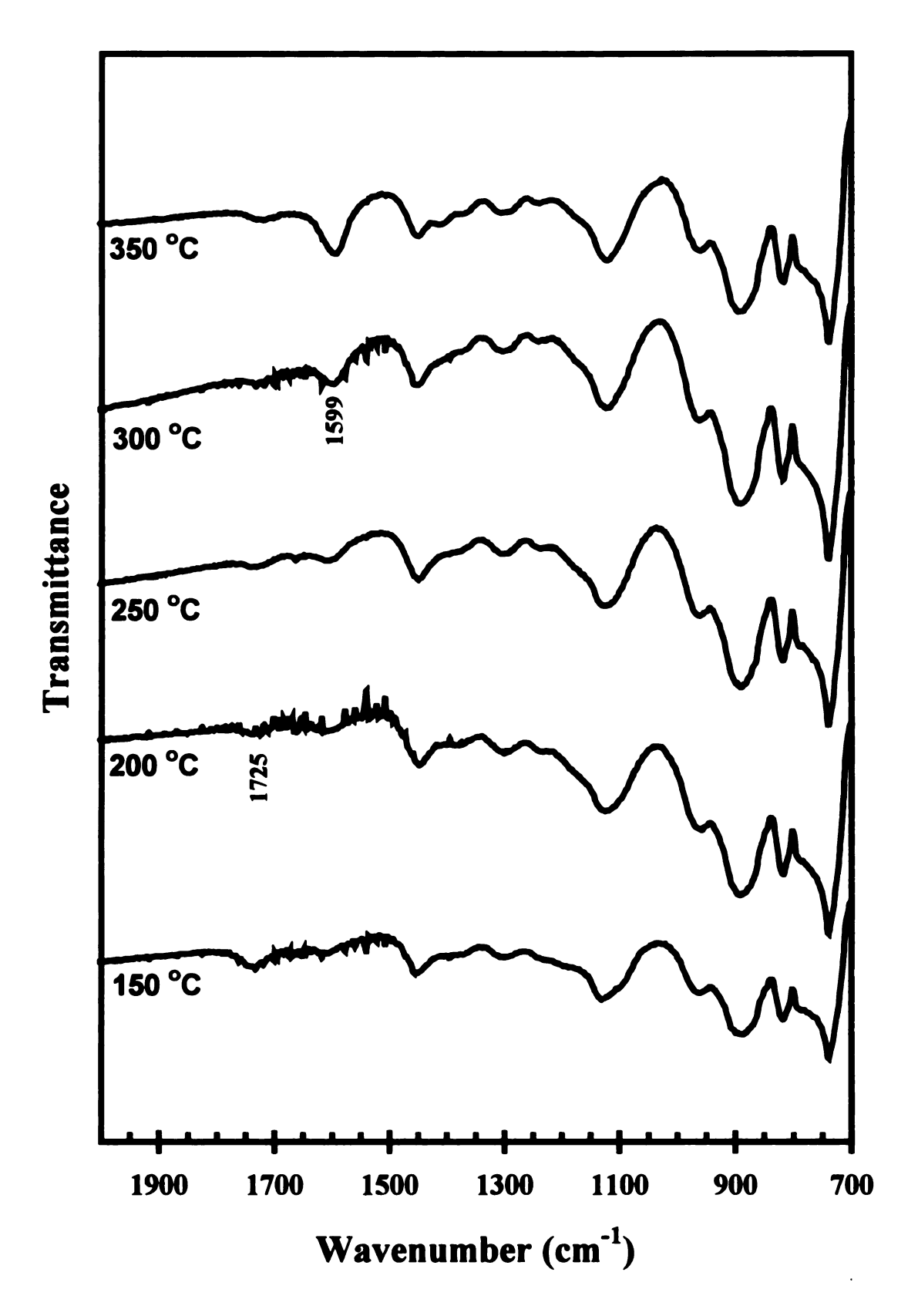


Figure 4.20. Post-Reaction FTIR Spectra of CsCl Exposed to Lactic Acid Vapor

enolization of lactic acid catalyzed by lactate and the subsequent condensation between the enolate lactate and lactic acid are not considered separately in this model.

Two additional reactions are included in the model. The first reaction accounts for minor catalytic conversion of lactic acid to products such as acrylic acid and propionic acid via first order pathways (k₃). The second reaction (k₄) reflects the loss of 2,3-pentanedione via decomposition in the presence of lactic acid vapor (Wadley et al., 1997) and via decomposition of surface alkali lactate at high temperature (Section 3.5).

Finally, the model accounts for neutralization of the acidic support sites (HA), which contribute to lactic acid decarbonylation, by alkali hydroxide via an equilibrium reaction:

$$MOH + HA \stackrel{K_{eq}}{\Longrightarrow} MA + H_{Q}O$$

At steady state,

[MA] = C_n = concentration of neutralized sites = K_e [MOH][HA],

where $K_e = K_{eq}/[H_2O]$.

The one-dimensional molar balances in an integral, tubular reactor are given below for the key species in the reaction system:

Acetaldehyde:
$$\frac{dC_A}{d\tau} = (k_{1a}C_s + k_{1b}C_b) C_L$$
 (1)

2,3-Pentanedione:
$$\frac{dC_p}{dt} = k_2 C_b C_L^2 - k_4 C_p$$
 (2)

Lactic Acid:
$$\frac{dC_L}{dz} = -\frac{dC_A}{dz} - 2k_2C_bC_L^2 - k_3C_bC_L$$
 (3)

where,

C_A, C_p, C_L, are concentrations of acetaldehyde, 2,3-pentanedione, and lactic acid, respectively;

 $C_b = C_{MOH} - C_n = \text{concentration of available MOH on the support after}$ impregnation (mmol/g support);

 $C_s = C_o - C_n = \text{concentration of available acidic sites on the support (mmol/g support);}$

 $C_{MOH} = loading of MOH (mmol/g support);$

 C_o = the initial concentration of acidic support sites on the support (mmol/g support);

and τ = residence time.

An analysis using the Weisz-Prater Criterion gives an observable modulus $\eta \phi^2$ of less than 0.02 for CPG and SiGel at all reaction conditions with an assumed diffusivity of 10^{-6} m²/s, indicating negligible mass transport limitations within the support material. Thus, the intrinsic kinetic rate constants can be obtained from the experimental results.

Equations 1 and 3 can be integrated directly to obtain algebraic expressions for $C_A(\tau)$ and $C_L(\tau)$:

$$C_{A}(\tau) = \frac{a - k_{3}C_{b}}{b} \ln \left(\frac{a + bC_{Lo}}{a + bC_{L}}\right)$$
(4)

$$C_{L}(\tau) = \frac{a}{\left(\frac{a}{C_{Lo}} + b\right)e^{a\tau} - b}$$
 (5)

where,

 C_{Lo} = concentration of lactic acid at t = 0,

$$a = k_{1a}C_s + k_{1b}C_b + k_3C_b$$

$$b = 2 k_2 C_b$$
.

Equation 2 is numerically integrated for the concentration of 2,3-pentanedione with respect to residence time using Euler's method. In this model, acetaldehyde is the dominant product when there is no base added on the support ($C_b = 0$), and hence to a good approximation, lactic acid is entirely converted to acetaldehyde on the support alone and so $C_A(\tau) = C_{Lo} (1-e^{-a\tau})$ and $C_L(\tau) = C_{Lo} e^{-a\tau}$.

A regression scheme is used to obtain the best-fit pre-exponential factors and activation energies of the rate constants in the model to the experimental results. This scheme is essentially a nonlinear least-square error method where the parameters are adjusted simultaneously until the sum of the squares of the residuals between the predicted reactor effluent concentrations and the experimental values is minimized. This is accomplished using the tool "Solver" in Microsoft Excel 7.0 on the above equations.

4.3.1. Kinetic analysis of KOH on CPG

Optimization using the complete kinetic model gave a surface acid site concentration (C_o) of 0.028 mmol/g for CPG. This very low value suggests that support effects can be neglected ($C_o \approx 0$) in the presence of KOH at the loadings that are used. In support of this, a simple calculation shows that even at the lowest KOH loading of 0.05 mmol/g of CPG, there is about one molecular layer of KOH on the support (assuming a molecular area of 26 Å² for KOH). Neglecting support acid site effects simplifies the

model to eight parameters - the pre-exponential factors and activation energies of the remaining four rate constants (k_{1b} , k_2 , k_3 , k_4). Reoptimizing with the simplified model gave essentially the same least square error as with the original model, but with fewer parameters. Optimized parameters for the simplified model, along with calculated turnover frequencies at optimum conditions for 2,3-pentanedione formation (300° C and 0.5 MPa at the reaction inlet) are presented in Table 4.9. Selected results of the model fit to data are presented in Figures 4.3-4.7. The predicted lactic acid conversion and yields of acetaldehyde and 2,3-pentanedione as described by these rate coefficients in the model (Equations 1-3) are plotted as lines along with the experimental values on these figures. An average residence time of 3.34 seconds is used in the simulations, while the experimental values are collected at residence times between 3-4 seconds. Since $C_{KOH} = 2 \text{ mmol/g}$ is experimentally observed to be a saturation limit, simulations are not done beyond a loading of 2 mmol/g where the model does not apply.

4.3.2. Kinetic analysis of KOH on SiGel

The SiGel support has a significant number of surface acidic sites and a high enough surface area such that monolayer coverage of KOH occurs at a loading of about 1 mmol/g. All five rate constants (k_{1a} , k_{1b} , k_2 , k_3 , k_4) and the equilibrium constant (K_e) thus have to be included to adequately represent the experimental results from KOH on this support; values of the optimized rate constants and C_o for the SiGel support, along with turnover frequencies are listed in Table 4.10. Rate constants k_{1b} and k_2 were purposely set to the same values as those obtained for CPG support since they represent the same reactions. We did in some cases allow them to vary (optimized values also given in

Table 4.9. Parameters of Kinetic Model for KOH/CPG

	KOH / CPG	+	
C_{o}	~ 0 (0.028 mmo	l/g CPG)	
	Preexponential Factor	Activation Energy (kJ/mol)	Turnover Frequency* (s ⁻¹)
k _{la}			
k_{1b}	$2.88 \times 10^{14} \text{ g cat. mol}^{-1} \text{ s}^{-1}$	140	4.65×10^{-4}
$\mathbf{k_2}$	$7.95 \times 10^{16} \text{ g cat. liter mol}^{-2} \text{ s}^{-1}$	137	3.43×10^{-3}
k_3	$8.12 \times 10^{11} \text{ g cat. mol}^{-1} \text{ s}^{-1}$	114	8.83 x 10 ⁻⁴
k ₄	$3.16 \times 10^{14} \text{ s}^{-1}$	178	
K_e			

Average Absolute Differences between Predicted and Experimental Values

Lactic Acid Conversion	4.7
Acetaldehyde Yield	2.8
2,3-Pentanedione Yield	3.5

*At 300°C, 0.5 MPa, and reaction inlet concentrations.

Table 4.10), and the least square error was only lowered by 2%. Calculated yields of 2,3-pentanedione and acetaldehyde, and conversion of lactic acid are presented as lines along with the experimental data in Figures 4.8-4.12. The simulations are calculated at an average residence time of 3.54 seconds.

4.3.3. Kinetic model and support effects

Within the range of reaction conditions, the kinetic model predicts 2,3-pentanedione, acetaldehyde, and lactic acid concentrations reasonably well, and supports the formation of 2,3-pentanedione as a condensation between lactic acid and alkali lactate. In general, experimental uncertainty of lactic acid conversion ranges up to $\pm 5\%$,

Table 4.10. Parameters of Kinetic Model for KOH/SiGel

	KOH / SiGel ^a	a		KOH / SiGel	SiGel	
ပ	0.5 mmol / g of	support		0.5 mmol / g of support	of support	
	Preexponential Factor	Activation	Turnover	Preexponential Factor	Activation	Turnover
		Energy (kJ/mol)	Frequency (s-1)		Energy (k.I/mol)	Frequency (s-1)
k _{1a}	3.07×10^9 g cat. mol ⁻¹ s ⁻¹	80	2.51 x 10 ⁻³	3.75 x 10 ⁹ g cat. mol ⁻¹ s ⁻¹	81	2.49 x 10 ⁻³
k _{1b}	$2.88 \times 10^{14} \text{ g cat. mol}^{-1} \text{ s}^{-1}$	140	9.47×10^{-4}	2.58 x 10 ¹³ g cat. mol ⁻¹ s ⁻¹	128	1.08×10^{-3}
k_2	$7.95 \times 10^{16} \text{ g cat. Liter mol}^{-2} \text{ s}^{-1}$	137	6.98×10^{-3}	7.17 x 10 ¹⁶ g cat. liter mol ⁻² s	137	7.37×10^{-3}
				_		
k ₃	$2.40 \times 10^{11} \text{ g cat. mol}^{-1} \text{ s}^{-1}$	107	7.98×10^{-3}	9.13 x 10 ¹⁰ g cat. mol ⁻¹ s ⁻¹	104	1.76×10^{-5}
ķ	$1.31 \times 10^6 s^{-1}$	78	;	$4.43 \times 10^5 s^{-1}$	72	:
ኧ	1.5 x 10 ⁵ g cat. mol ⁻¹	15	1	1.80 x 10 ⁵ g cat. mol ⁻¹	15	;
Aver	Average Absolute Differences between	Predicted and	Predicted and Experimental Values	Values		
T	Lactic Acid Conversion	5.9		Lactic Acid Conversion	5.7	1
	Acetaldehyde Yield	2.6		Acetaldehyde Yield	2.8	~
7	2,3-Pentanedione Yield	2.8		2,3-Pentanedione Yield	2.9	

^aK_{1a} and k_{1b} are taken from optimized values for KOH/CPG (Table 4.9). At 300°C, 0.5 MPa, and reaction inlet concentrations.

largely the result of the relatively difficult GC analysis of lactic acid (Gunter et al., 1994). Duplicate experiments under the same reaction conditions indicate that uncertainties in 2,3-pentanedione and acetaldehyde yields can be as high as ± 3 (e.g. $20\% \pm 3\%$).

From our model fit, the average absolute differences between predicted and experimental values of yield or conversion percent for KOH/CPG (Table 4.9) are 3.5% for 2,3-pentanedione yield, 2.8% for acetaldehyde yield, and 4.7% for lactic acid conversion. For KOH/SiGel, the average differences are 5.9% in lactic acid conversion, 2.8% in 2,3-pentanedione theoretical yield, and 2.6% in acetaldehyde yield. Hence, the predicted yields and conversions are for the most part within experimental errors for catalysts on both supports. The larger differences between the calculated and experimental 2,3-pentanedione yield and lactic acid conversion at 260°C are likely caused by incomplete vaporization of lactic acid in the feed at this low temperature. At 350° C. differences in model and experiment are at least partially caused by thermal decomposition of lactic acid and alkali lactate on the support surface, resulting in higher lactic acid conversion than predicted. Thermal decomposition of alkali lactate to propionate and acetate has been observed in post-reaction FTIR spectroscopy for sodium salts (Section 3.3.4) and, along with less favorable conditions for lactic acid adsorption, explains the sharp reduction in 2,3-pentanedione yield at high temperature.

The sensitivities of these optimized values with respect to the experimental uncertainties were investigated by altering some of the experimental values by the amounts of their respective uncertainties and then re-optimizing to obtain new rate constants. The average changes for some scenarios are reported in Table 4.11. Kinetic constants of major reactions (k_2 and k_{1a}) are found to be relatively insensitive to

Table 4.11. Sensitivity Analysis of Rate Constants (Percentage Change due to Experimental Uncertainties)

		Optimized Consta	Optimized Constants for KOH/CPG		
Rate Constant	Increase 20% of Experimental Values by Uncertainties	Decrease 20% of Experimental Values by Uncertainties	Increase 10% and decrease 10% by Uncertainties	Increase all data by Uncertainties	Decrease all data by Uncertainties
kıb	_	19	5	51	48
k_2	9	4	2	27	18
k_3	4	10	14	6	16
K 4	34	12	42	27	121
		Optimized Constants for KOH/SiGel	nts for KOH/SiGel		
k _{1a}	_	_	-	22	18
kıb	31	18	27	65	23
k_2	. 15	4	6	33	∞
k ₃	49	32	10	=	001
K	29	38	20	12	96
Keq	9	55	27	-	09

experimental uncertainties for both KOH/CPG and KOH/SiGel. As expected, the largest changes occurred when all of the experimental values were either increased or decreased by the uncertainty amounts. Kinetic constants which correspond to minor reactions such as the decomposition of 2,3-pentanedione (k₄) and base-catalyzed decarboxylation of lactic acid (k_{1b}) are found to have the greatest sensitivity to uncertainties.

A simplified kinetic model is sufficient to describe the KOH/CPG system because of the low surface area and low acidity of CPG; even at a loading of 0.05 mmol KOH/g of CPG, monolayer coverage exists and essentially all support acid sites are neutralized. This explains the low carbon monoxide concentrations observed (≤10 moles of CO per 100 moles of lactic acid fed; Table 3.1) from acid-catalyzed decarbonylation with the CPG-supported catalysts at 350°C. At KOH loadings above 0.05 mmol/g, the surface composition stays essentially the same but there are more layers of KOH. It is apparent that multi-layers of KOH are accessible to lactic acid since 2,3-pentanedione yield increases with KOH loading beyond a monolayer. However, results clearly show a limit in catalyst accessibility as KOH loading approaches 2 mmol/g.

The high acidic site concentration and surface area of SiGel support complicates the reaction system, since as the surface composition changes with increasing KOH loading the pathway to acetaldehyde from lactic acid also alters from decarbonylation to decarboxylation. Acidic sites on the SiGel support not only increase the yield of acetaldehyde, they also reduce the activity of the catalyst, resulting in lower 2,3-pentanedione theoretical yield and lactic acid conversion at low loadings of KOH. The shape of the acetaldehyde curve is a direct indication of contributions from both lactic acid decarboxylation and decarbonylation as surface acidic sites are replaced by basic

sites with increased KOH loading. For example, decarbonylation of lactic acid dominates on the support alone at 350°C, resulting in the formation of 47 moles of CO and 1 mole of CO_2 for every 100 moles of lactic acid fed (Table 4.8). At a KOH loading of 3 mmol/g and 350°C, in contrast, the pathway to acetaldehyde is largely through decarboxylation, as evident by the formation of 5 moles of CO from decarbonylation and 17 moles of CO_2 from decarboxylation for every 100 moles of lactic acid fed (some additional CO_2 is liberated in 2,3-pentanedione formation). Since decarbonylation of lactic acid is more favorable than decarboxylation, with a higher rate constant ($k_{1a} > k_{1b}$) and lower activation energy, the minimum in the acetaldehyde formation curve indicates neutralization of the acidic sites.

Our optimized rate constant for the decarbonylation of lactic acid to acetaldehyde is around seventy times greater than that reported by Chuchani et al. (45,46) for thermal decomposition of lactic acid. This is a consequence of the much more rapid heterogeneous acid-catalyzed decarbonylation. As observed by Chuchani et al., a small increase in the surface-to-volume ratio (6 times) resulted in a significant heterogeneous effect which raised the rate constant by 10%. The S/V ratio in our conversion studies is several order of magnitude greater than the studies conducted by Chuchani et al.

4.3.4. Silica support sintering by alkali metal

At loadings below 2 mmol KOH/g, the reaction occurs within the kinetic regime and the rate of 2,3-pentanedione formation is linearly proportional to KOH loading. At higher loadings, the catalytic effect is observed to reach a limit (e.g. not all alkali is accessible to lactic acid), and thus the described kinetic model no longer applies. This

saturation limit is unexpected, since mass transfer calculations indicate negligible pore diffusion or pellet boundary layer resistances. Surface areas of used KOH catalysts were measured by N₂ BET to further understand the observed loading limit.

Used KOH/SiGel catalysts were calcined at 500°C for 5 hours to remove carboneous residues; surface area measurements of selected used catalysts are reported in Table 4.12. Similar surface areas were obtained from used catalysts before the removal of residues. The surface area of these catalysts decreases dramatically with increased KOH loadings. This sintering effect of silicon oxide support upon alkali impregnation is consistent with results observed and reported by Perrichon and others (82-84). At a KOH loading of 3 mmol/g of SiGel support, the resulting catalyst area was similar to that of CPG, which explains the similar observed saturation loading for catalysts on both types of supports. Increasing KOH loading to 9 mmol/g further drops the catalyst surface area to about 1.6 m²/g (Table 4.12), and 2,3-pentanedione yield over this catalyst at 300°C decreases to 18% of theoretical.

As indicated in Table 4.12, support sintering does occur for CPG supported catalysts also. The effect is not as significant as SiGel since CPG already has a very low surface area. Amount of area lost was also found to depend on the basicity of the alkali metal and increases in the order of Cs > K > Na.

The observed saturation loading of KOH is therefore a combination of support sintering, resulting in reduced support surface area, and inaccessibility of lactic acid to alkali lactate on the sintered support. It is clear from a simple calculation that alkali lactate is present in the equivalent of many molecular layers (>50) at KOH loadings

Table 4.12. Surface Areas of Used Catalysts

Catalyst	Loading	Surface Area (m ² /g)
	(mmol/g of support)	
SiGel	0	280
KOH/SiGel	0.3	96.2
KOH/SiGel	1	51.6
KOH/SiGel	3	6.4
KOH/SiGel	9	1.6
KOH/3%Ba/SiGel	3	14.7
CPG	0	7.2
KOH/CPG	1	6.8
CsOH/CPG	2	3.2
NaOH/CPG	4	4.0

above 2 mmol/g, but we cannot say at this time if the inaccessibility results from simple diffusion resistances across this multilayer film, from filling of the sintered support pore volume (thus excluding lactic acid vapor), or from trapping and isolation of a fraction of the catalyst in the support during sintering. In any case, there certainly exists an optimum KOH loading for 2,3-pentanedione formation on silica supports.

In order to decrease silica support sintering from alkali impregnation, barium nitrate was first impregnated onto SiGel before the KOH. Barium is known to strengthen the structures of high surface area aluminum and titanium oxide catalysts and provide good thermal stability on these porous material (85). Crystalline Ba(NO₃)₂ obtained from Mallinckrodt Co. was dissolved in HPLC water and wet impregnated onto SiGel. The mixture was then dried at 100°C to remove most of the water before calcining at 400°C. KOH was further loaded onto the resulting silica support in the same way as described in

Section 2.1.1. Lactic acid conversion is conducted over a 2 mmol KOH/g SiGel containing 3% barium; results are reported on Table 4.8. Yields of 2,3-pentanedione and acetaldehyde and lactic conversion over experimental temperatures are very similar to the ones obtained with 2 mmol KOH/g SiGel (Figures 4.8-4.12). However, as indicated by the N₂ BET measurement of the resulting catalyst surface area (Table 4.12), the use of barium does not significantly decrease support sintering by KOH on SiGel.

4.3.5. Kinetic analysis of NaOH and CsOH on SiGel

The kinetic model was further applied to reaction results from NaOH and CsOH supported on SiGel. Optimization of the rate constants were accomplished with the same method as mentioned for KOH/SiGel in Section 4.2.3 with all of the parameters. The optimized values for these catalysts and turnover frequencies are presented in Table 4.13. Calculated values of lactic acid conversions and yields of acetaldehyde and 2,3-pentanedione using this model are plotted as lines on Figures 4.13-4.18 along with the reported experimental values. Again, simulations were not carried out for metal loadings above 2 mmol/g, where catalyst saturation occurs. Absolute average differences between the predicted and experimental values are also reported in Table 4.13; they are mostly within experimental errors and thus the model describes the system reasonably well.

The turnover frequency of acid-site catalyzed decarbonylation of lactic acid stays essentially constant for all three alkali hydroxides on SiGel, which is expected since this is a support effect. As for base catalyzed decarboxylation and condensation of lactic acid to acetaldehyde and 2,3-pentanedione, the turnover frequencies increase in the order of

Table 4.13. Parameters of Kinetic Model for NaOH/SiGel and CsOH/SiGel

	NaOH / CPG			CsOH / SiGel	SiGel	
ပိ	0.5 mmol / g of support	f support		0.5 mmol / g of support	of support	
	Preexponential Factor	Activation Energy	Turnover Frequency	Preexponential Factor	Activation Energy	Turnover Frequency
kla	2.33 x 10 ⁹ g cat. mol ⁻¹ s ⁻¹	79	2.53×10^{-3}	$4.77 \times 10^9 \text{ g cat. mol}^{-1} \text{ s}^{-1}$	(KJ/IIIOI) 83	2.31×10^{-3}
$\mathbf{k}_{1\mathbf{b}}$	$3.67 \times 10^{14} \text{ g cat. mol}^{-1} \text{ s}^{-1}$	143	6.12 x 10 ⁻⁴	$3.30 \times 10^{21} \text{ g cat. mol}^{-1} \text{ s}^{-1}$	212	2.76×10^{-3}
k_2	$5.95 \times 10^{17} \text{ g cat. liter mol}^{-2} \text{ s}^{-1}$	151	2.93 x 10 ⁻³	1.71×10^{23} g cat. liter mol ⁻² s ⁻²	198	4.63×10^{-2}
				_		
k ₃	$4.66 \times 10^5 \text{ g cat. mol}^{-1} \text{ s}^{-1}$	71	2.94 x 10 ⁻⁶	$1.43 \times 10^8 \text{ g cat. mol}^{-1} \text{ s}^{-1}$	89	1.52×10^{-3}
Ā	$6.94 \times 10^2 s^{-1}$	37	;	$9.23 \times 10^{1} \text{ s}^{-1}$	29	;
ኧ	$1.61 \times 10^7 \text{ g cat. mol}^{-1}$	38	:	$3.62 \times 10^5 \text{ g cat. mol}^{-1}$	15	;
Aver	Average Absolute Differences between Predicted and Experimental Values	Predicted and	Experimental	Values		
7	Lactic Acid Conversion	3.6		Lactic Acid Conversion	4.3	
	Acetaldehyde Yield	3.6		Acetaldehyde Yield	1.7	
2,	2,3-Pentanedione Yield	1.2	:	2,3-Pentanedione Yield	2.5	10

*At 300°C, 0.5 MPa, and reaction inlet concentrations.

Na < K < Cs. These reactions obviously depend significantly on the basicity of the alkali metal, but the ratio between these two turnover frequencies indicate that the increase in 2,3-pentanedione formation from sodium to cesium is greater than that for acetaldehyde formation.

4.4. Methyl lactate vapor-phase reaction studies

4.4.1. Reaction studies

Reaction studies using methyl lactate as feedstock for the formation of 2,3pentanedione and methyl acrylate over sodium, potassium and cesium salts were also
investigated to improve yields to these products. Methyl lactate is easier to vaporize as
compared to lactic acid and thus higher feed concentration (up to 98wt%) can be used,
which should improve condensation toward 2,3-pentanedione yield. Also, methyl lactate
was successfully employed in the formation of methyl acrylate over aluminum phosphate
catalyst with 61% yield (3). All additional chemicals used in this Section are obtained
from Aldrich.

Selected experimental results from these salts at 280°C or 300°C are tabulated in Table 4.14. Sodium lactate is shown as a representative sodium salt and to stress the fact that the alkali lactate is the actual catalyst for the condensation to 2,3-pentanedione from either lactic acid or methyl lactate. As expected, 2,3-pentanedione yield increases from sodium to cesium, but cesium nitrate is clearly much less selective toward the formation of 2,3-pentanedione than cesium hydroxide as a catalyst. This is because the formation of cesium lactate is greatly hindered by the need to form CH₃NO₃ as revealed by post-

reaction FTIR spectra. The CsOH catalyst is also very selective (88%) to the condensation of methyl lactate toward 2,3-pentanedione.

Potassium methoxide is examined as an equivalent to using potassium hydroxide in lactic acid conversion to 2,3-pentanedione; of course, dimethyl ether is formed upon the formation of potassium lactate. It also demonstrates that water is not necessary in the formation of 2,3-pentanedione even though it reduces the activation energy of the pathway by stabilizing the intermediate species formed, as illustrated by molecular modeling (77). In all instances, methyl lactate as a feedstock has proven to be less active than lactic acid in the formation of 2,3-pentanedione, and more prone to coking (decomposition) and the formation of acetaldehyde through base-catalyzed decarboxylation. The yields to acrylate reported in Table 4.14 over these catalysts include both methyl acrylate and acrylic acid. They are also too low to make acrylates from lactate esters economically feasible.

Table 4.14. Partial Conversion Results Using Methyl Lactate as Feedstock

Catalyst on CPG	NaC ₃ H ₅ O ₃	KOCH ₃	CsNO ₃	CsOH
(2 mmol/g)				
Temperature (°C)	300	300	280	280
2,3-Pentanedione	9	16	10	29
Yield (% Theoretical)				
Acrylate	5	9	7	5
Yield (% Theoretical)				
Conversion (%)	55	71	79	33

4.4.2. Post-reaction FTIR

Post-reaction FTIR spectra of CsNO₃ and CsOH after being treated with methyl lactate vapor are given in Figures 4.21 and 4.22, respectively for temperatures of 200°C, 250°C, and 300°C. In the case of CsNO₃, there was only a small peak at 1590 cm⁻¹ even at 300°C, indicating the formation of small quantity of lactate. Most of the CsNO₃ stays unreacted over the reaction temperature in the presence of methyl lactate vapor. On the other hand, CsOH was converted to cesium lactate (1593, 1457, 1309, 1119, 1084, 1035, and 849) at 200°C. Since cesium lactate acts as the actual catalyst for the formation of 2,3-pentanedione, it is understandable that CsOH is more active than CsNO₃. Notice that cesium lactate begins to decompose at 300°C (peak at 1593 cm⁻¹ shifts to 1569 cm⁻¹), which is at a lower temperature than for sodium lactate (decomposition at 350°C) as observed and discussed in Section 3.3.4.

4.5. Summary

In conclusion, it was found that the formation of 2,3-pentanedione from lactic acid vapor over alkali salt improves with decreasing Lewis acidity of the alkali metal. A kinetic model developed from experimental results of different alkali hydroxide loadings on silica further supports the bimolecular scheme proposed for the formation of 2,3-pentanedione. It also illustrates the importance of support surface acidity in the formation of acetaldehyde from decarbonylation of lactic acid, since incorporation of this pathway is needed to sufficiently describe the observed yields. The proposed kinetic model fits best over reaction temperatures from 280-320°C and at alkali metal loadings below 2 mmol/g of support, where desirable product yields are high and mass transport limitations are

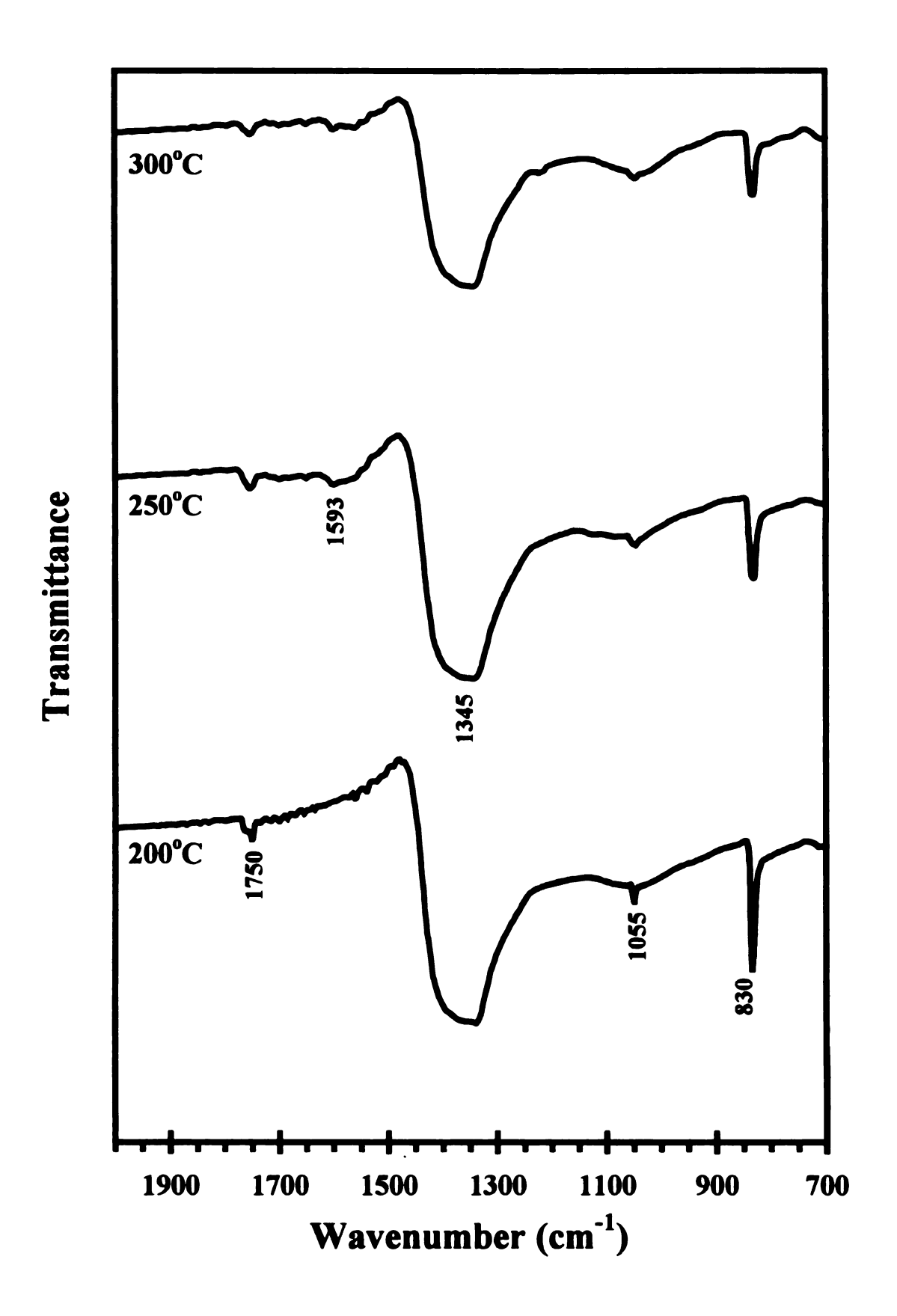


Figure 4.21. Post-Reaction FTIR Spectra of CsNO₃ Exposed to Methyl Lactate Vapor

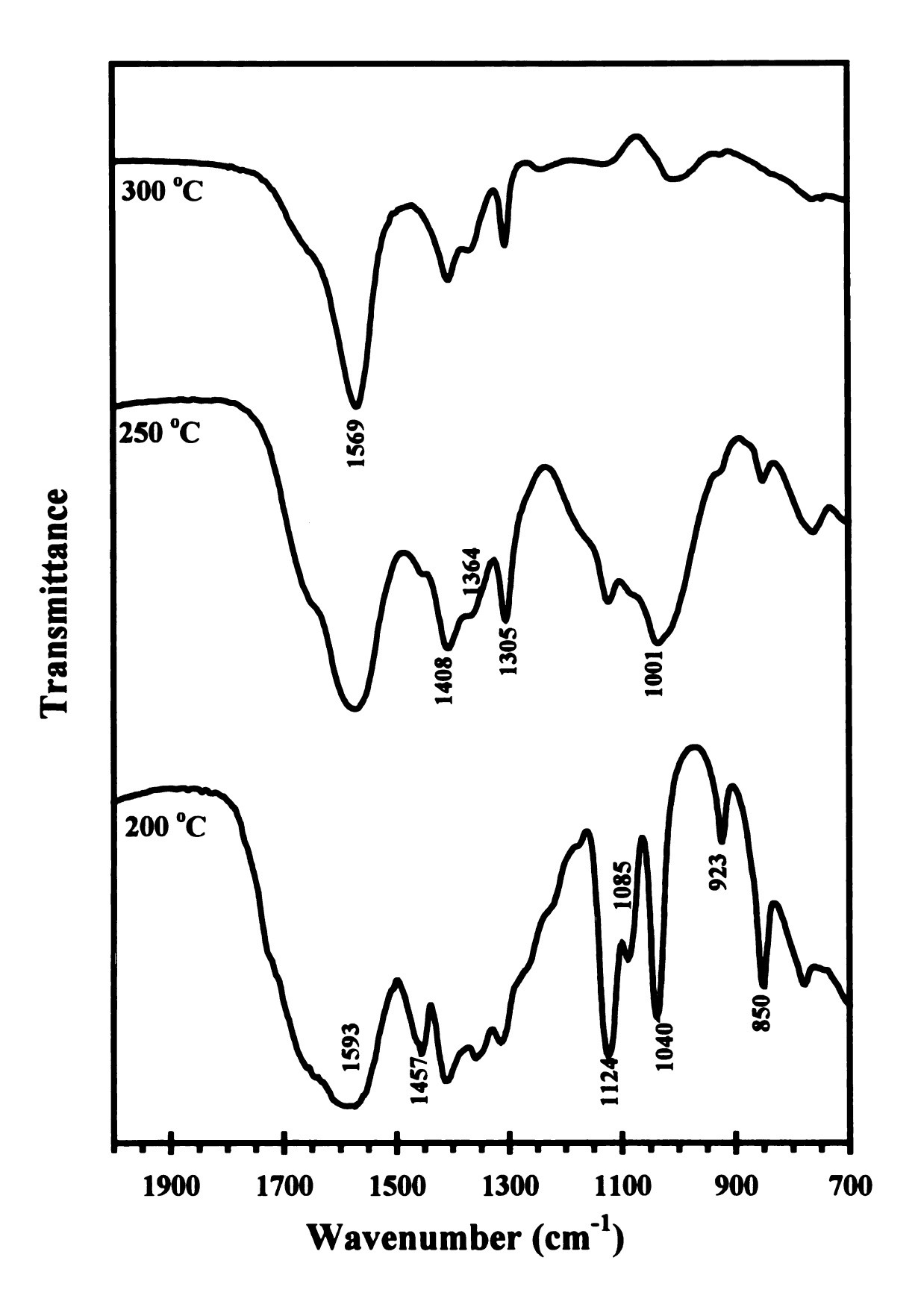


Figure 4.22. Post-Reaction FTIR Spectra of CsOH Exposed to Methyl Lactate Vapor

in .		

negligible. At temperatures below 280°C, complete vaporization of the lactic acid feed is difficult, and at 350°C, other decomposition reactions of lactic acid and alkali lactate complicate the reaction system. Methyl lactate was examined as an alternative feedstock because of its lower boiling point; however, it was found to be less active over all tested catalysts than lactic acid in the formation of 2,3-pentanedione and acrylate.

Chapter 5

CATALYST STABILITY AND THE EFFECT OF FEED IMPURITIES ON THE FORMATION OF 2,3-PENTANEDIONE FROM LACTIC ACID

Investigation of the deactivation of catalysts used in the conversion of fermentation-derived lactic acid to 2,3-pentanedione is reported in this chapter. This chapter also includes catalyst and reaction characterization of lactic acid conversion including support regeneration and the initial reaction transient period before steady state is achieved. Catalyst deactivation with time and by feed impurities have been studied. The feed impurities examined include ammonia, in the form of ammonium lactate, as a pH adjusting agent during lactate fermentation and glucose, representative of residual starting material in the production of lactic acid through fermentation.

5.1. Catalyst support regeneration

The controlled-pore glass (CPG03000D) employed for the preparation of catalysts is an expensive packing used mainly for the purification and separation of biopolymers or synthetic polymers in permeation chromatography. This rigid, high purity silica is chosen as catalyst support to reduce the formation of acetaldehyde because it has a low surface area $(7 \text{ m}^2/\text{g})$ and large pore diameter $(3002 \pm 9.1 \text{ Å})$, and low surface acidity. Regeneration of used CPG is done by washing the used catalysts with concentrated nitric

acid (70%) at 70°C with constant stirring for 10-15 minutes. The acidic phase is then decanted. Nitric acid washing is repeated three times to remove most of the base. After the acid treatment, the CPG is washed with HPLC water five times and then filtered. The slurry is dried in an oven at 100°C for 5 hours and calcined at 500°C for another 5 hours to remove carbonaceous material left on the support.

Lactic acid conversion over regenerated CPG support alone (Table 5.1) indicates that some residual alkali base on the support was not removed or neutralized by the nitric acid treatment. This is apparent by the higher 2,3-pentanedione and acrylic acid yields and lower acetaldehyde yield at 350°C on the regenerated support as compared to fresh CPG (Table 3.1). Potassium hydroxide catalyst prepared on this support with a loading of 1 mmol/g displays similar activity results (Table 5.1) as 1 mmol KOH per gram of fresh CPG (Table 4.2). The lower 2,3-pentanedione yields at 300°C and 320°C on the regenerated CPG catalyst are attributed to the loss of surface area due to sintering of the support as discussed in Section 4.2.4. However, conversion studies with sodium sulfate impregnated on regenerated CPG gave distorted results with higher activities to 2,3-pentanedione due to leftover base on the support. Overall, CPG can be regenerated and used for highly active alkali salts, such as potassium and cesium hydroxides, in the conversion of lactic acid to 2,3-pentanedione.

Catalyst regeneration has also been attempted inside the reactor by passing air into the reactor at 400°C and 0.5 MPa to remove coke formed on the catalyst during reaction.

Air was flowed through the reactor for four hours and lactic acid feed was reinitiated at 280°C with helium carrier. However, very low lactic acid conversion was observed and a DRIFTS spectrum of the resulting catalyst showed only trace amount of lactic acid

Table 5.1. Lactic Acid Conversion over Regenerated CPG and KOH/Regenerated CPG

Catalyst		Reg	Regenerated C	<u>1</u>			mmol KOH	/g Regenerated	nerated CPG	ŋ
Temperature (°C)	760	280	300	320	350	260	280	300	320	350
Contact Time(s)	4.0	3.4	3.3	3.2	3.1	3.8	3.6	3.6	3.5	3.6
Error (% Carbon)	4.4	9.6-	5.1	9.9-	-7.2	18.2	5.8	-12.0	-30.5	-36.8
Conversion (BOF)	-1.3	12.2	-1.0	16.2	61.9	1.0	40.4	81.7	0.96	95.2
Yield (% Theoretical)										
Acrylic acid	0.7	0.4	0.4	0.7	3.0	1.9	5.2	9.4	8.4	4.9
Propionic acid	0.4	0.2	0.3	9.0	1.9	1.0	1.9	3.6	4.9	7.4
2,3-Pentanedione	0.1	0.1	0.3	0.5	1.4	9.5	28.0	36.5	30.1	18.3
Acetaldehyde	<u>8.</u>	1.5	3.1	7.7	55.0	2.8	3.7	9.7	10.0	13.8
Acetol	0.0	0.0	0.0	0.0	0.0	0.0	8 .	5.1	5.5	4.5
Other	0.0	0.0	0.0	0.0	0.5	0.0	0.0	0.5	1.0	2.1
Unknown	0.3	0.7	0.7	9.0	1.7	4.5	7.0	6.6	6.7	8.7
*00	0.5	1.3	8 .1	4.8	26.7	1.3	1.0	1.1	9.1	2.2
C02*	9.0	6.0	6.0	1.5	3.3	5.1	12.8	17.1	22.1	20.4
Selectivity (%)										
Acrylic acid	54	17	6	7	2	12	13	15	14	10
Propionic acid	13	01	∞	9	3	9	ς.	9	∞	4
2,3-Pentanedione	8	7	7	2	7	63	69	28	20	36
Acetaldehyde	9	<i>L</i> 9	92	81	68	18	6	12	11	27
Acetol	0	0	0	0	0	0	4	∞	6	6
Other	0	0	0	0	_	0	0	_	7	4

Yields reported as mole per 100 moles of lactic acid fed.

condensed on the CPG support without any indication of surface lactate. It is believed that while heating to 400°C, the surface alkali lactate melted and carried off the catalyst bed, thus ceasing catalytic activity.

5.2. Initial saturation period before steady state

As mentioned in the procedure for lactic acid conversion studies in Section 2.1.4, lactic acid was fed at a relatively high flow rate (0.5 ml/min) to the reactor at the start of experiment prior to establishing the steady state flow rate for the experiment. This initial lactic acid saturation period is needed to ensure reasonable carbon balances and accurate yields for subsequent product sample collections. As an example, for cesium catalysts at 280°C and 2 mmol/g, the 2,3-pentanedione yield and carbon balance are approximately 55% and -13%.

To investigate the importance of this initial reaction period, the flow rate of lactic acid feed was maintained at 0.1 ml/min right from the beginning without saturating the bed with lactic acid. Table 5.2 shows conversion results over 2 mmol CsOH/g CPG at 280°C of products collected at 30-55, 90-115, and 150-175 minutes after the starting the lactic acid feed into the reactor. As indicated by the first product sample, over 31% of the carbon was not recovered and 2,3-pentanedione yield was lower than the subsequent product samples collected at the same reaction conditions. This is because some of the lactic acid in the feed was consumed initially by conversion of the cesium hydroxide on the catalyst to cesium lactate prior to the formation of 2,3-pentanedione.

More precise experiments show that approximately 6 ml of 34wt% of lactic acid has to be fed over a typical amount of catalyst before product collection in order to obtain

good carbon balance and accurate product yields. Stoichiometrically, about 1.5 ml of feed is consumed in the formation of cesium lactate. Hence, all conversion studies start with a lactic acid saturation period where about 10 ml of feed is passed through the catalyst bed before allowing the reactor to reach steady state at the desired reaction parameters.

Table 5.2. Lactic Acid Conversion - Initial Saturation Period

Catalyst	2 mr	nol CsOH / g	CPG
time (min)	30-55	90-115	150-175
Temperature (°C)	280	280	280
Contact Time(s)	2.8	2.9	2.6
Error (% Carbon)	-30.6	-15.6	-13.7
Conversion (BOF)	94.1	95.0	97.0
Yield (% Theoretical)			
Acrylic acid	0.0	0.0	1.2
Propionic acid	0.7	0.4	0.4
2,3-Pentanedione	36.6	55.1	56.5
Acetaldehyde	9.1	9.2	8.0
Acetol	0.0	1.0	1.8
Other	0.0	0.0	0.0
Unknown	7.4	8.4	6.5
CO*	1.5	1.4	1.5
CO2*	55.6	51.7	61.9
Selectivity (%)			
Acrylic acid	0	0	2
Propionic acid	1	1	1
2,3-Pentanedione	79	84	83
Acetaldehyde	20	14	12
Acetol	0	2	3
Other	0	0	0

5.3. Stability of acrylic acid and 2,3-pentanedione

The stability of acrylic acid and 2,3-pentanedione formed from the catalytic conversion of lactic acid over alkali salts was examined to check for secondary reactions

at 350°C. Conversion results over sodium nitrate at 350°C and different residence time are reported in Table 5.3. These product samples are collected at residence times from 0.6-5.4 seconds at constant feed composition. It is clear that almost complete conversion was achieved at 0.6 second and increase in residence time only affects the conversion slightly. Among the main products, only propionic acid and acetaldehyde seem to increase with residence time. The small increase in acetaldehyde causes the higher conversion of lactic acid. The similar acrylic acid and 2,3-pentanedione yields obtained for higher residence times lead to the conclusion that secondary reactions of these products do not seem to be significant over the catalyst bed even at the highest experimental temperature. Likewise, no reaction is observed when 2,3-pentanedione was fed onto fresh or used sodium nitrate catalysts. However, when 2,3-pentanedione (60g/l) was added into the the standard 34wt% lactic acid feed and fed into the reactor at 350°C, less 2,3-pentanedione was found in the product with increasing residence time (Table 5.3). Thus, secondary reaction of 2,3-pentanedione does take place in the presence of lactic acid and at high temperature, but only to a limited extent.

5.4. Deactivation of catalyst with time

A sixty hour lactic acid conversion experiment was conducted over CsOH/CPG at reaction conditions specified in Table 5.4 to examine catalyst activity over time. These reaction conditions are chosen to optimize 2,3-pentanedione yield and avoid the formation of side-products, especially acetaldehyde. Selectivities of the major products with time are given in Figure 5.1. Yields of 2,3-pentanedione are approximately 45%, with lactic acid conversion around 70%. Clearly, the cesium catalyst is extremely

Table 5.3. Lactic Acid Conversion over NaNO₃/CPG (Studies at Different Residence Times)

Catalyst	1	mmol Na	103 / g CP	U	1	1 mmol NaNO3 / g CPGa	103 / g CPC	Ja
Temperature (°C)		350 350	350	350	350	350	350	350
Contact Time(s)		1.2	2.5	5.4			2.2	4.3
Error (% Carbon)		-19.6	4.4	-11.5		-23.6	-29.2	-7.3
Conversion (BOF)	81.5	9.06	89.1	85.9		89.7	97.5	86.9
Yield (% Theoretical)								
Acrylic acid	12.8	13.9	14.2	12.2	11.8	11.7	12.7	12.8
Propionic acid	2.1	2.8	3.9	5.0	1.8	2.2	3.2	5.7
2,3-Pentanedione	15.2	16.9	15.7	15.1	12.2	12.1	10.9	9.5
Acetaldehyde	15.7	19.5	19.9	20.9	14.1	16.0	21.0	25.9
Acetol	5.2	5.2	3.9	3.1	4.7	4.7	2.0	2.4
Other	0.7	0.4	6.0	9.0	0.0	0.0	0.0	0.0
Unknown	1.9	8.4	21.3	19.3	8.9	16.3	11.5	18.5
*00	3.1	5.2	6.7	3.1	3.0	4.8	7.0	14.4
C02*	22.6	36.4	38.6	21.9	21.8	28.1	32.9	32.5
Selectivity (%)								
Acrylic acid	25	24	24	22	56	25	24	23
Propionic acid	4	2	7	6	4	2	9	01
2,3-Pentanedione	56	53	27	27	27	5 6	21	17
Acetaldehyde	30	33	34	37	32	34	40	46
Acetol	10	6	7	9	10	10	6	4
Other	1	1	1	1	0	0	0	0
"Vielde renorted as mole	ner 100 n	se male ner 100 males of lactic acid fed	tic acid fe	7				

*Yields reported as mole per 100 moles of lactic acid fed.

*Feed contains 60g/l 2,3-Pentanedione.

*Yields exclude 2,3-Pentanedione in feed.

selective toward 2,3-pentanedione formation and very stable throughout the sixty hour experiment.

The catalyst was taken out of the reactor at the end of experiment and found to have gained 3.18g in mass, of which only 10% is weight gained due to the conversion of cesium hydroxide to cesium lactate. The accumulation of coke deposits is responsible for the slow decrease in 2,3-pentanedione selectivity and increase in acetaldehyde selectivity at the end of experiment. Selectivities to acrylic acid and propionic acid remained relatively low and constant throughout the study. Overall, the activity of cesium catalyst is stable in the conversion of lactic acid to 2,3-pentanedione, however, the increase in coke deposit with time does favor the formation of acetaldehyde.

Table 5.4. Reaction conditions of 60 hour run

Temperature (°C)	280
Pressure (MPa)	0.5
Liquid flow rate (ml/min)	0.25
Helium flow rate (ml/min)	30
Vaporized Feed Composition	Lactic acid: 0.08
(mole fraction)	Water: 0.75
	Helium: 0.17
Catalyst weight (g)	4.2
Catalyst bed height (cm)	9.5
Catalyst Loading	1 mmol CsOH / g CPG
Residence time (sec)	2.0-3.0

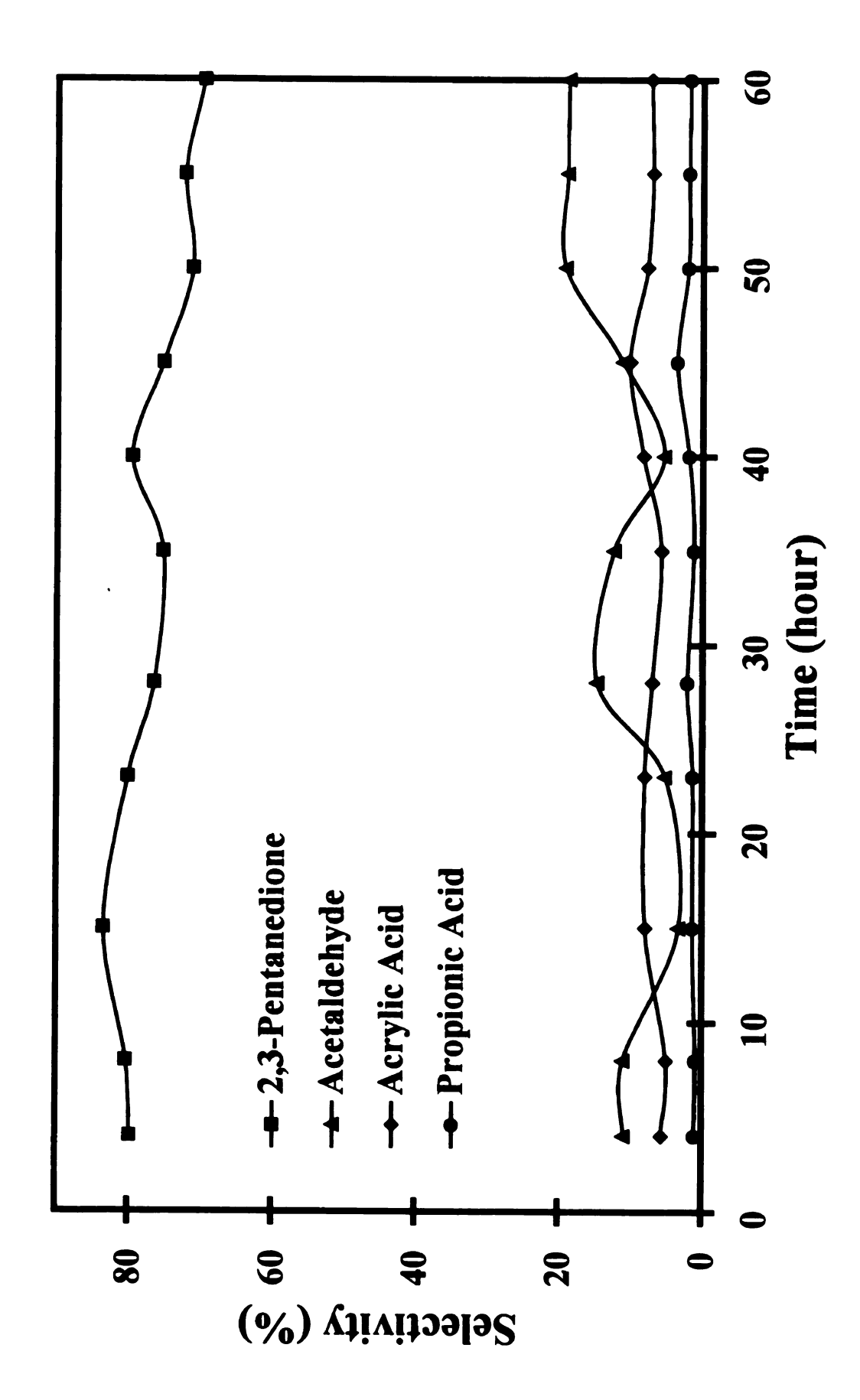


Figure 5.1. Selectivities of Products over Time

5.5. Effect of different lactic acid feedstocks

Lactic acid (88wt%) from Purac, Inc. was employed as feedstock in most studies conducted on the formation of 2,3-pentanedione. This lactic acid is obtained from fermentation and is solely in the l-(+) form. To investigate other feedstocks, a mixture of dl-lactic acid was obtained from Aldrich at 85wt% and diluted to 34wt% before being fed over sodium / CPG catalysts. Results suggest that the condensation to 2,3-pentanedione is not affected by the different stereoisomers of lactic acid. Yields of all major products obtained from the two forms of lactic acid are consistent and no significant difference is observed throughout the range of reaction temperature.

Two other samples of actual lactate fermentation products were also diluted to 34 wt% and used as feedstocks in selected conversion experiments. Feed I, a dark, yellow-brownish liquid obtained from New Energy Company of Indiana, was purified only by membrane nanofiltration and passage over activated carbon. Feed II, provided by Archer Daniels Midland Co., is a semi-refined pilot plant product of light yellow color that was subjected to purification and acidulation to convert lactate largely to free lactic acid. Ammonia is used in both of these lactic acid fermentation processes as the pH adjusting agent because of the advantages discussed in Section 1.2.1.

Analysis of these feedstocks using gas chromatography indicates the presence of lactic acid or lactate in both feeds and a very small amount of ethanol in Feed I. A FTIR spectrum of Feed I (Figure 5.2), however, shows that most of the lactic acid is in the form of lactate. The carbonyl (C=O) of lactic acid stretches at around 1720 cm⁻¹, while the carbonyl band for ammonium lactate appears at around 1580 cm⁻¹. No indication of amide ($v_{as} = 1660 \text{ cm}^{-1}$ for C=O) was observed in this feed. Elemental analysis (CHN) of

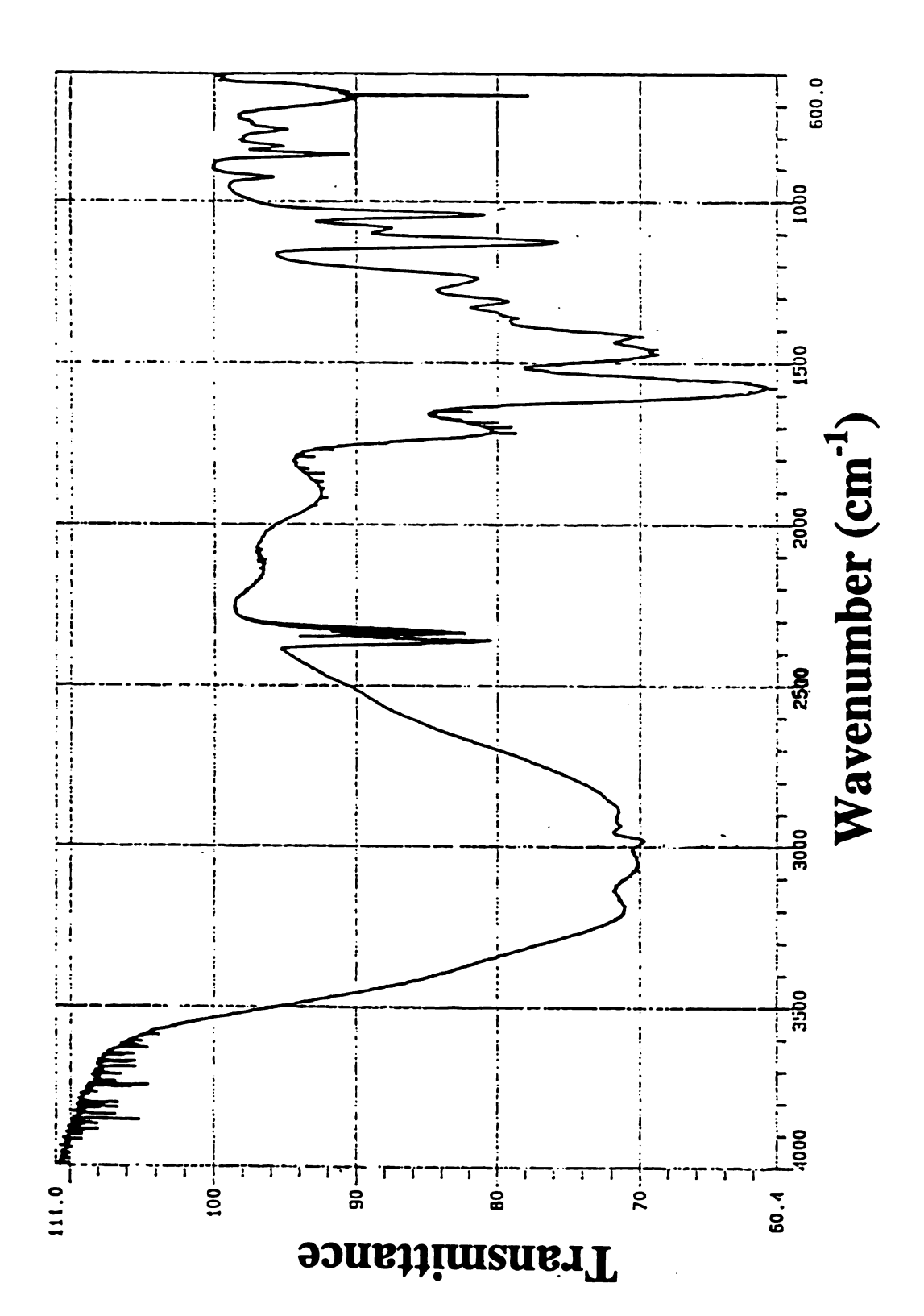


Figure 5.2. FTIR of Feed I

these samples is reported in Table 5.5. Amounts of ammonium lactate present in these samples are calculated based on the assumption that ammonium lactate is the only source of nitrogen. This is a relatively good assumption in light of the fact that most of the protein (enzymes) can easily be removed by membrane nanofiltration.

2,3-Pentanedione yields from these feedstocks, all containing approximately 4.0 M lactate, over 2 mmol CsOH/g CPG at 260-350°C are given in Figure 5.3. It is clear that the product concentration of 2,3-pentanedione decreases dramatically with increased concentration of ammonium lactate in the feed. While high purity lactic acid leads to a 2,3-pentanedione yield of 50-60% with 80% selectivity, Feed I, which is substantially ammonium lactate, gave almost no 2,3-pentanedione. Further, essentially all condensible products from this material have high boiling points and thus were not detected with gas chromatography; only CO and CO₂ formation and coking of the catalyst were observed. Feed II, in which some lactate is present as free acid, gave higher yields but still clearly less than those from high purity lactic acid feed. This surprising result is further investigated and explained in the following sections.

Table 5.5. Elemental Analysis of Feed (CHN)

	Carbon	Nitrogen	Ammonium Lactate
	(wt%)	(wt%)	(molar % of total lactate)
Feed I	13.78	4.05	76
Feed II	13.33	0.94	18

Since ammonium lactate is the cause of low 2,3-pentanedione yield, it was recommended that the fermented lactic acid feedstocks be further purified to convert most

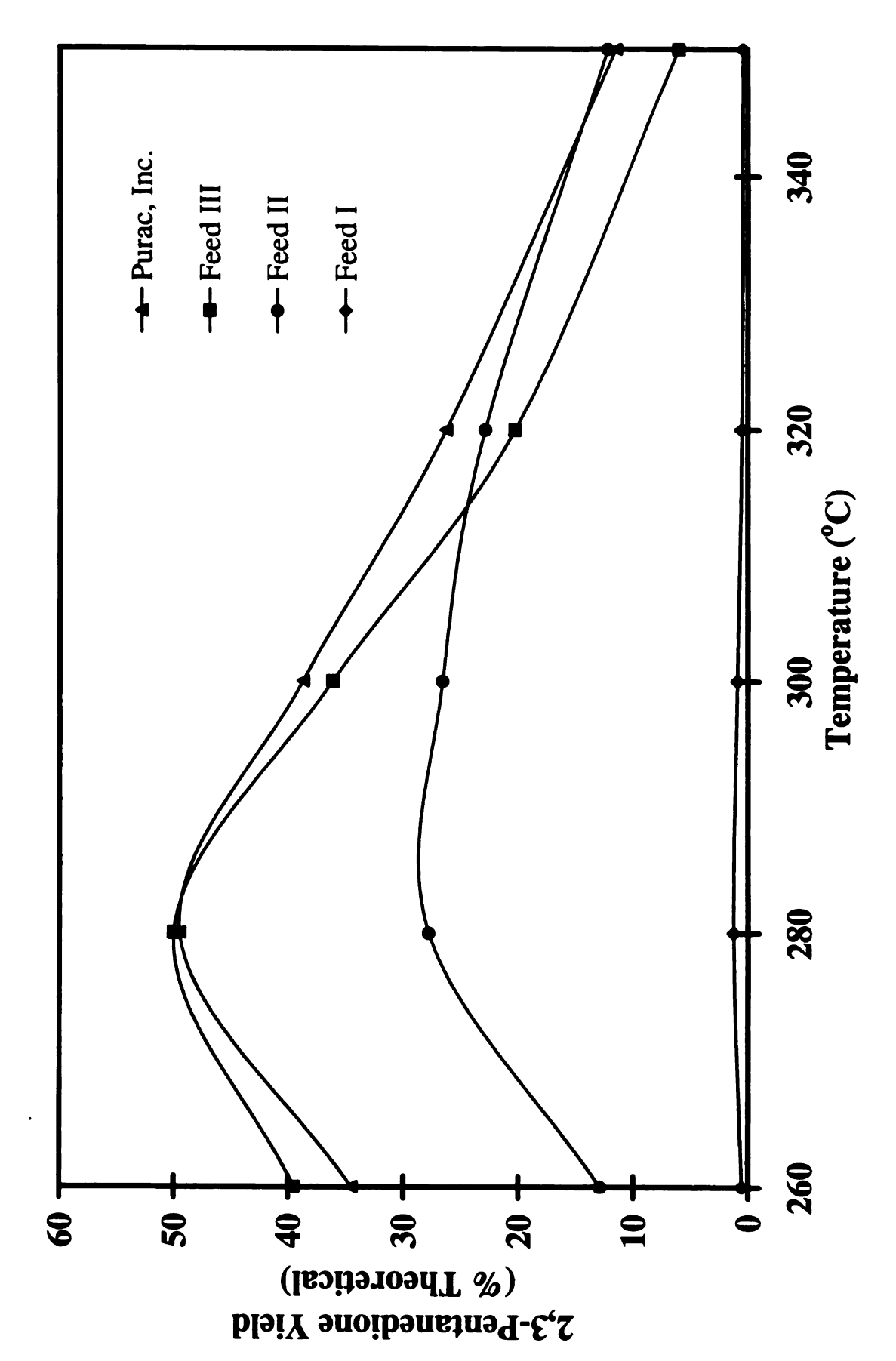


Figure 5.3. 2,3-Pentanedione Yields from Different Feed Stocks

of the lactate to the free acid form, at least below 5% lactate content. The manufacturer of Feed II was able to provide us with a more purified lactic acid feed (Feed III). The 2,3-pentanedione yields from Feed III over the same cesium hydroxide catalyst are shown on Figure 5.3. These results are similar to the ones obtained with lactic acid from Purac, Inc. and hence Feed III is considerably purer than Feed II with essentially no ammonium lactate present.

5.6. Effect of ammonium lactate concentration in feed

5.6.1. Materials and experimental procedure

High-purity fermentation-derived L-(+)-lactic acid (SP-88, 88% from Purac, Inc.) was used as the starting material for all of the experiments presented in previous chapters. Ammonium hydroxide (Aldrich, 30 wt% solution) was added to this material in specified quantities as a model impurity to investigate the effects of ammonia on the conversion of lactic acid to 2,3-pentanedione. The amount of ammonia in the feed is given as the ammonium lactate molar fraction, defined as the fraction of feed lactate present as ammonium lactate. The total feed lactate concentration is maintained at 4.0 M in all experiments described below unless otherwise specified. This molar concentration corresponds to 34 wt% lactic acid solution.

The reactor and reaction procedure are described in Section 2.1.2. All of the following experiments were conducted at 280°C over 2 mmol CsOH/g CPG catalyst. In most situations, multiple points at the same steady state condition were taken; if either feed composition or reaction temperature were changed, the reactor was allowed to reach a new steady state before the collection procedure was repeated.

5.6.2. Reaction results and discussion

Introduction of ammonium lactate into lactic acid feed dramatically reduces the yield of 2,3-pentanedione over silica-supported CsOH catalyst. Figure 5.4 gives 2,3-pentanedione yields from experiments at 280°C where feed composition is switched at "t=0" from high purity lactic acid to "impure" feed containing an ammonium lactate fraction ranging from 0.0 to 0.3. In the experiment with 0.25 fraction of ammonium lactate, the feed was changed back to pure lactic acid at t=6 hr. Stable product yields were achieved around 2 hr exposure to feed; complete, steady state product distributions are given in Table 5.6 (columns A-F) for each concentration of ammonium lactate investigated. An ammonium lactate fraction of 0.05 did not seem to reduce 2,3-pentanedione yield significantly below the typical range obtained with pure lactic acid feed (set of first points on left side of Figure 5.4). Interestingly, it was observed that the stable 2,3-pentanedione yields varied linearly with the concentration of ammonium lactate in the feed as shown on Figure 5.5, in which the final 2,3-pentandione yields are plotted against ammonium lactate fraction in feed.

The results in Table 5.6 show that the carbon balance was not satisfactorily closed during experiments with ammonium in the feed. However, the total mass balance (including H_2O) around the reactor system over the entire experiment was found to be within the acceptable range of ± 1 -2%, gas evolution as CO and CO₂ were within the normal ranges, and the weight gain of the catalyst bed was around 1 g, which is typical. The quantity of organic material detectable by gas chromatography in the product solution was much less than typically observed with pure lactic acid feed. Further analysis of the product solution with HPLC showed large quantities of organic species (UV detector at

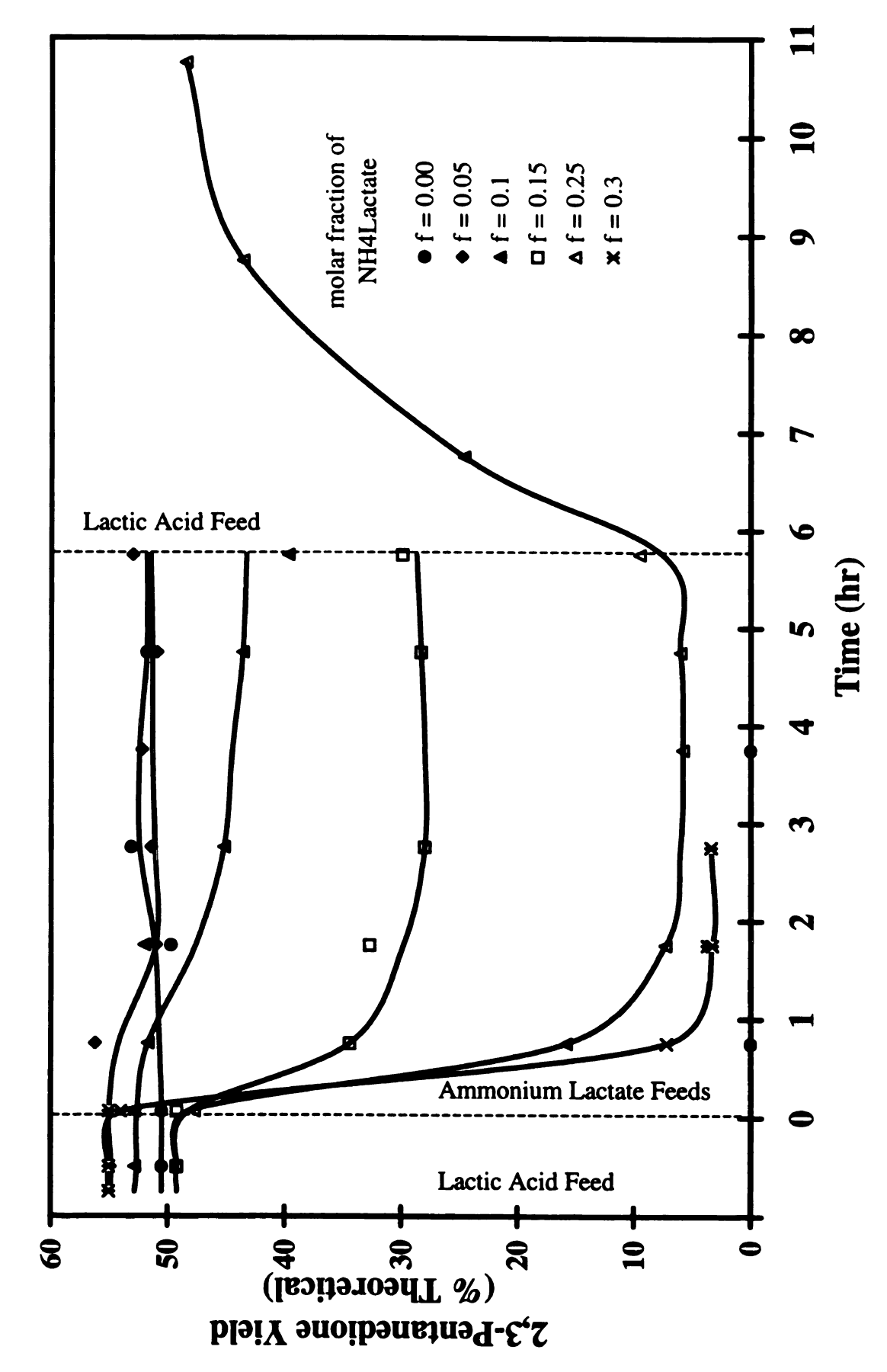


Figure 5.4. Deactivation of 2,3-Pentanedione by Ammonium Lactate ($T = 280^{\circ}$ C and P = 0.5 MPa)

Table 5.6. Product Yields^a (Selectivities^b) from Different Feeds over CsOH/CPG Catalyst

Column	А	В	C	D	E
Liquid Feed Composition					
Lactic Acid	4.0 M	3.8 M	3.6 M	3.4 M	3.0 M
NH ₄ Lactate		0.2 M	0.4 M	0.6 M	1.0 M
Other					
Molar fraction NH ₄ Lactate	0.0	0.05	0.10	0.15	0.25
Product					
2,3-Pentanedione	54.9 (70)	53.0 (71)	43.6 (69)	28.3 (61)	6.0 (25)
Acrylic Acid	1.0(1)	0.0 (0)	0.3(1)	0.4(1)	0.4(2)
Acetaldehyde	9.5 (12)	10.8 (14)	11.2 (18)	13.2 (29)	8.1 (34)
Propionic Acid	1.4 (2)	0.5(1)	0.6(1)	0.7(2)	0.2(1)
Hydroxyacetone (Acetol)	2.2 (3)	1.3 (2)	0.8(1)	0.9 (2)	0.0 (0)
Others	9.4 (12)	9.3 (12)	7.1 (11)	2.8 (6)	9.4 (39)
00	2.5	1.3	1.0	1.0	1.1
CO ₂	48.0	45.0	37.6	33.4	30.8
Lactic Conversion (based on					
lactic acid recovered)	74.3	82.8	96.2	91.1	0.98
Carbon Recovery (%)	108.1	95	69.1	57.4	44.8

^aProduct yields are defined as percentage of theoretical based on amount of lactic acid in feed.

bSelectivities are defined as percentage of lactic acid converted to the specified product among reported products.

Table 5.6. Product Yields^a (Selectivities^b) from Different Feeds over CsOH/CPG Catalyst (continued)

Column	ᅜ	Ð	Н	pI	J
Liquid Feed Composition					
Lactic Acid	2.8 M	3.15 M	3.0 M	3.0 M	4.0 M
NH ₄ Lactate	1.2 M		1.0 M	1.0 M	
Other			$0.21 \mathrm{M}^{\mathrm{c}}$		$0.056\mathrm{M}^{\mathrm{c}}$
Molar fraction NH ₄ Lactate	0.30	0.00	0.25	0.25	0.00
Product					
2,3-Pentanedione	3.4 (15)	49.7 (67)	2.6* (15)	2.9 (12)	48.6 (67)
Acrylic Acid	0.0 (0)	0.0 (0)	0.3 (2)	0.0 (0)	0.0 (0)
Acetaldehyde	7.7 (34)	11.2 (15)	8.9 (53)	4.1 (17)	7.7 (11)
Propionic Acid	0.6(3)	0.4(1)	0.0 (0)	0.5(2)	0.7(1)
Hydroxyacetone (Acetol)	0.0 (0)	2.3 (3)	0.0 (0)	0.0 (0)	1.4 (2)
Others	10.9 (48)	10.7 (14)	5.1 (30)	17.0 (69)	14.5 (20)
00	1:1	1.5	0.7	0.3	1.6
CO ₂	41.9	54.9	36.4	6.4	44.5
Lactic Conversion (based on					
lactic acid recovered)	95.9	93.0	61.7	24.8	88.2
Carbon Recovery (%)	36.5	88.0	33.6f	83.3	89.2f
Co 2 Dontonodione					

c2,3-Pentanedione

dReaction conducted on silica support (CPG) alone.

eD-Glucose

fCarbon recovery based only on the lactate fed.

*Yield excludes 2,3-pentanedione fed.

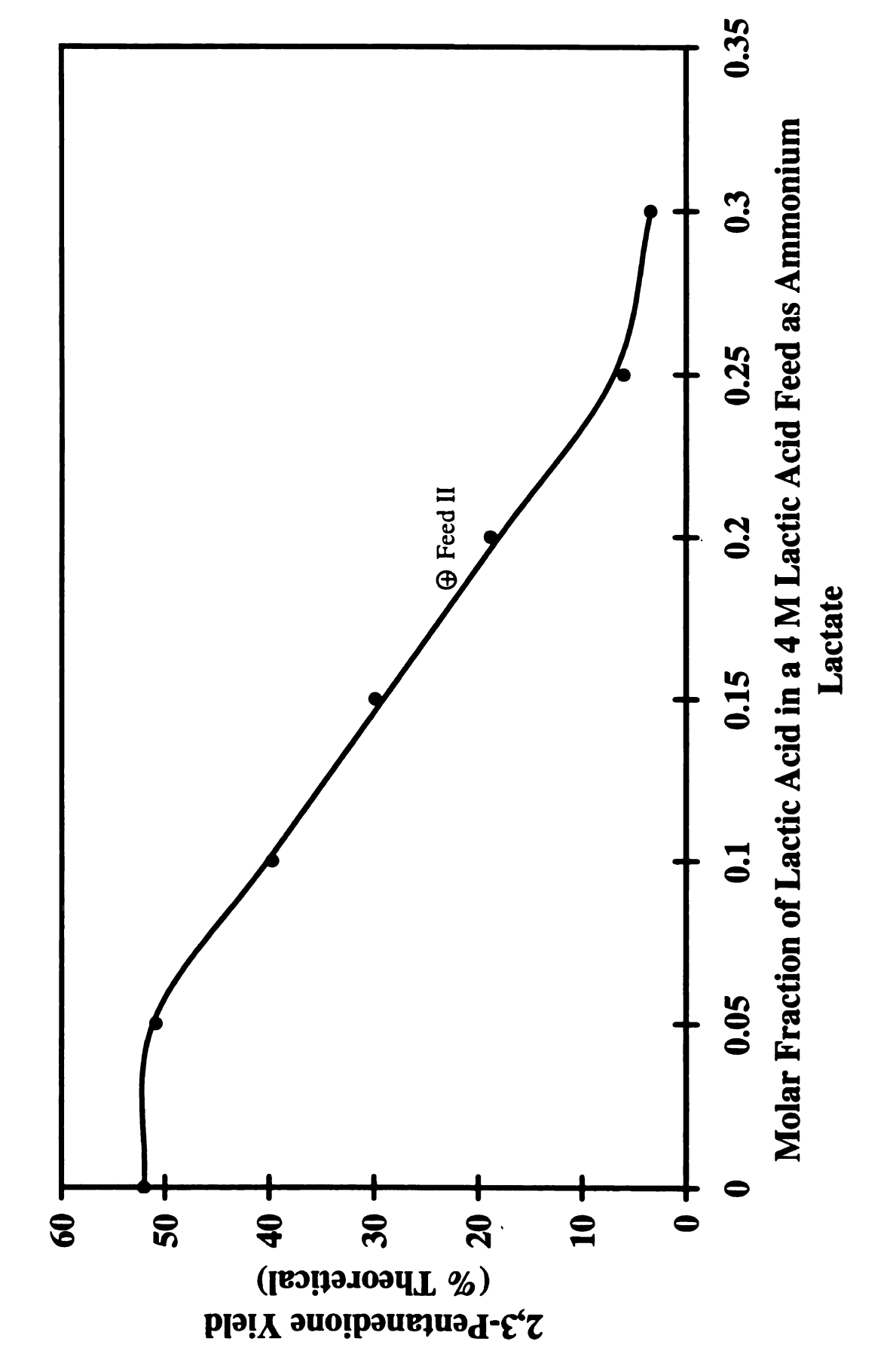


Figure 5.5. 2,3-Pentanedione Yield vs. Ammonium Lactate Molar Fraction in Feed

260 nm) that were not observed in gas chromatographic analyses. This indicates that species of low volatility are formed in the presence of ammonia and are present in the product solution; these species are not eluted during our usual gas chromatographic analysis at 200°C and are thus not recovered for inclusion in the carbon balance.

Results in Figure 5.4 illustrate several key points regarding the disappearance of 2,3-pentanedione with ammonia. First, 2,3-pentanedione yield is strongly affected by the amount of ammonium lactate in the feed as clearly demonstrated on Figure 5.5. Second, the deactivation is reversible in that yield of 2,3-pentanedione returns to its original value when ammonium lactate is removed from the feed. Third, acetaldehyde yield is not greatly affected by the addition of ammonium lactate, indicating that ammonia does not affect the decarboxylation pathway. Thus, ammonia seems to affect product distribution after lactic acid has been converted to 2,3-pentanedione.

Several other experiments with different feeds and catalysts were conducted to explain the deactivating effects of ammonia. Key results of these experiments are also given in Table 5.6. Most obviously, it is necessary to determine if ammonia addition simply lowers the effective concentration of free lactic acid and thus lowers the yield of 2,3-pentanedione. To do this, a series of pure lactic acid feeds of lower lactic acid concentration (down to 3.1 M, or about 80% of the original concentration) was examined and only a slight decrease in 2,3-pentanedione yield over this range (Table 5.6, column G) was found. It was also observed that lactic acid elutes from our gas chromatograph upon injection of ammonium lactate, suggesting that the salt fully decomposes to lactic acid and ammonia upon injection at 200°C. From these observations, it was concluded that

the deactivating effect of ammonium lactate is much greater than would be expected by the simple reduction in free lactic acid concentration.

Next, an experiment (column H in Table 5.6) with feed enriched in 2,3pentanedione was conducted to investigate secondary degradation of 2,3-pentanedione by
ammonia as the deactivation pathway. The feed contained 3.27 wt% (0.21 M) 2,3pentanedione and an ammonium lactate fraction of 0.25; this 2,3-pentanedione
concentration is around half of that obtained in a typical condensed reactor effluent over
CsOH catalyst. All 2,3-pentanedione fed, plus a small additional quantity formed from
lactic acid, was recovered in the reactor effluent, illustrating that secondary 2,3pentanedione degradation does not seem responsible for reduced 2,3-pentanedione yields.
The carbon balance for this experiment (excluding 2,3-pentanedione fed) was comparable
with results (column E) using the 0.25 fraction ammonium lactate feed alone, with the
difference mostly accounted for by the difference in observed lactic acid conversion, a
value for which uncertainty typically approaches 15%.

A set of feeds with different ammonium lactate fractions from 0.0 to 0.25 were used in an experiment over the silica support (CPG) alone; the result for the ammonium lactate fraction of 0.25 is given in Table 5.6 (column I). As expected, conversion was low and the predominant product was acetaldehyde. Over the range of ammonium lactate fraction up to 0.25, the carbon recovery was on the order of 80-90%, much better than the 40-50% obtained with the same feed, at the same conditions, when CsOH catalyst was present (column E). Acetaldehyde yields were only slightly lower over the support alone; the only clear differences with and without CsOH present are the larger CO₂ evolution and much higher lactic acid conversion in the presence of catalyst. Clearly, CsOH

contributes to cracking or condensation of lactate in the reactor in the presence of ammonia, leading to products that exit the reactor (no excessive coke buildup is observed) but are not detected by gas chromatographic analyses (hence the poor carbon recovery).

5.6.3. Post-reaction FTIR results

Further insight into the possible influence of ammonia on lactate conversion is given via post-reaction FTIR spectroscopic analyses. It has been clearly demonstrated from previous chapters that lactic acid reacts with a variety of alkali metal salt catalysts to form alkali metal lactate, which is the dominant species on the catalyst surface at conditions favorable to 2,3-pentanedione formation (260-320°C). These alkali lactate salts are characterized by a strong IR absorption band (C=O stretch) at 1590-1600 cm⁻¹, whereas free lactic acid exhibits a band for the same vibrational mode at 1720-1730 cm⁻¹.

A post-reaction DRIFTS spectrum, collected on a Perkin-Elmer System 2000 IR with DTGS detector, is given as Figure 5.6 a) for a catalyst exposed to ammonium lactate in the reactor. The bands at 1105 and 1400 cm⁻¹ are attributed to the CPG support. The presence of a band at 1650 cm⁻¹ in the C=O stretch region in addition to that for cesium lactate (1591 cm⁻¹) is clearly visible, suggesting that ammonium lactate is forming an additional compound on the surface. The location of the band is consistent with the C=O stretch of an amide. This the band at around 1650 cm⁻¹ arises as a result of ammonium lactate decomposition is supported by the spectrum in Figure 5.6 b), which is a DRIFTS spectrum of the solid residue from ammonium lactate pyrolyzed at 280°C for 1 hr. The band at about 1650 cm⁻¹ is clearly present. Ammonium lactate is expected to decompose

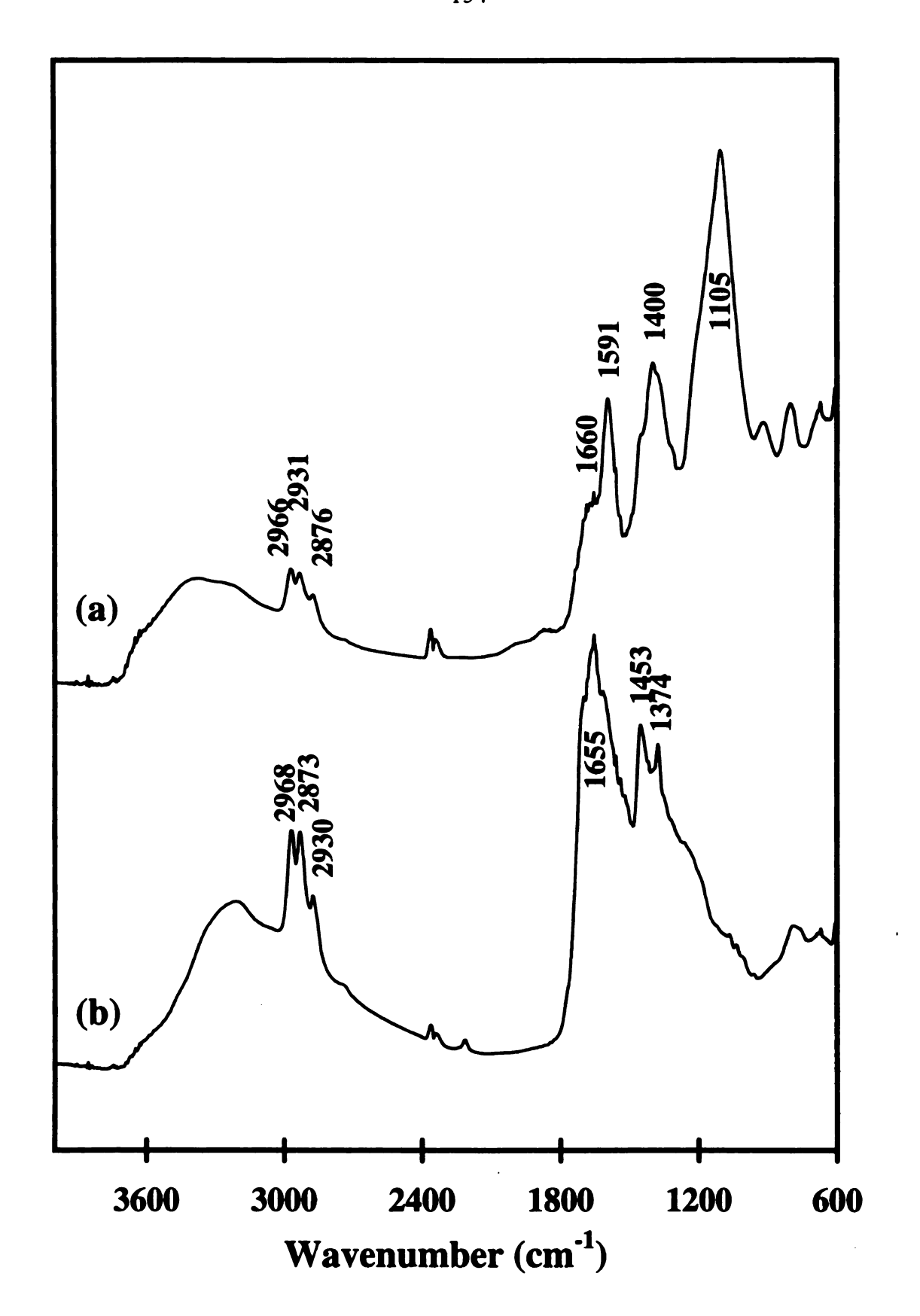


Figure 5.6. DRIFTS Spectra of Catalyst after Exposure to Ammonium Lactate

to ammonia and lactic acid upon heating, and since the weight gain on the catalyst is relatively small, the thermal decomposition of ammonium lactate to amide is not substantial. Yet, it may account for the 10% error in carbon balance when feeds containing ammonium lactate are fed over the support alone.

5.6.4. Reactions of 2,3-pentanedione in presence of ammonium hydroxide

Since it is known that ammonium lactate converts to ammonia and lactic acid upon heating to reaction temperature (86), the reactions between 2,3-pentanedione and ammonium hydroxide at room and higher temperatures were examined. Studies were conducted with the addition of various amount of ammonium hydroxide to saturated aqueous solutions of 2,3-pentanedione. It was found that the concentration of 2,3-pentanedione decreased rapidly in the presence of ammonium hydroxide even at room temperature. Almost half of the 2,3-pentanedione was consumed when 1.5 x 10⁻³ moles of NH₄OH was added to 60 g/l 2,3-pentanedione solution. When the mixture was left alone for 24 hours, needle-like crystals were formed. These crystals were extracted with d-toluene and subsequently identified as duroquinone using ¹H and ¹³C NMR. A detailed discussion of the condensation of 2,3-pentanedione to duroquinone in the presence of base can be found in Section 1.2.2. The yield of duroquinone formed from this mixture has been calculated to be around 13%, which is close to the results obtained using triethylamine (38).

When a similar mixture of 2,3-pentanedione and ammonium hydroxide was heated to around 100°C directly after mixing, a polymeric material was formed. This product resembles our reaction products obtained from feeds with ammonium lactate, and

was also obtained during our investigation in the formation of duroquinone from 2,3pentanedione. We are still in the process of identifying the material; the pathways by
which this product and duroquinone are formed are indicated in Figure 1.4. Neither
product vaporizes below 200°C and is thus not eluted during GC analyses of the products.

As a result, it is concluded that the ammonium lactate does not truly deactivate the alkali metal catalysts toward the formation of 2,3-pentanedione from lactic acid, although a small amount of amide is formed. Instead, the ammonium hydroxide that is formed from aqueous ammonium lactate decomposition reacts with 2,3-pentanedione formed in the catalytic process to produce a nonvolatile substance. Because the reaction between 2,3-pentanedione and ammonium hydroxide occurs mostly after passing through the catalyst bed at reaction temperature, the material is carried into the product samples.

5.7. Effects of glucose in feed

Results of an experiment in which 1 wt% glucose was added to lactic acid feedstock over CsOH catalyst are given in Figure 5.7 and in Table 5.6 (column J).

Glucose was fed with lactic acid over a six-hour period, and only a slight decline in 2,3-pentanedione yield was observed over the course of reaction. The effect was clearly reversible, as the yield returned to its initial value once glucose was removed from the feed solution. Upon disassembly of the reactor, significant carbon deposits were observed both on the walls of the quartz tube above the catalyst bed and on the top of the catalyst bed itself. It is clear that long-term use of a feed containing substantial amounts of glucose would eventually plug the reactor with carbonaceous residue from the glucose decomposition. The carbonaceous material can also facilitate the formation of

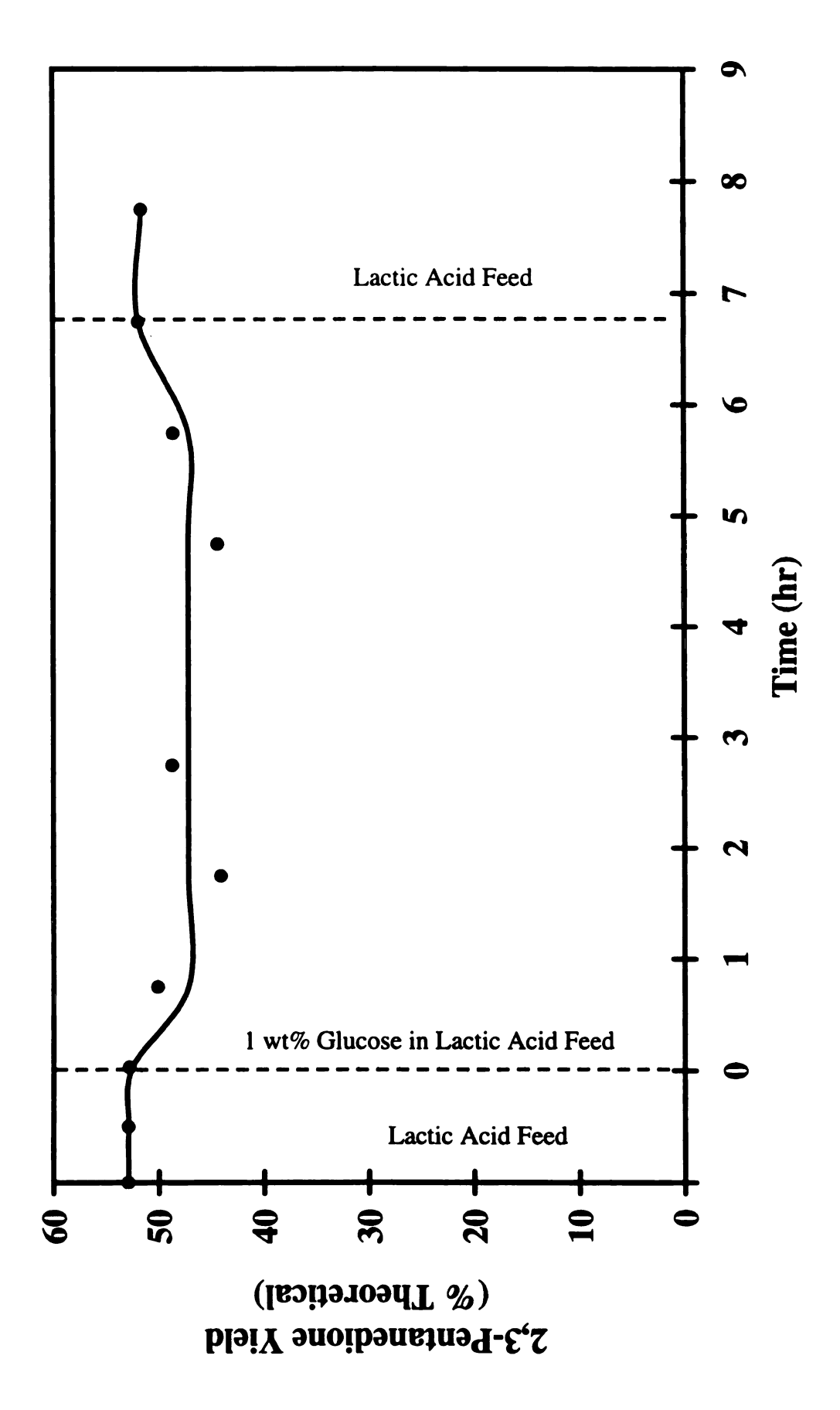


Figure 5.7. Effect of Glucose on 2,3-Pentanedione Formation ($T = 280^{\circ}$ C and P = 0.5 MPa)

acetaldehyde and propionic acid from lactic acid, as it was found that catalysts with carbon supports are extremely selective to these side-products. Nevertheless, the current experiment shows that glucose in small quantities does not poison the reaction, and that as long as exposure of the catalyst to such feeds is kept to a minimum, there will be little effect on desired product yields.

5.8. Summary

Deactivation of the alkali metal catalyst toward the formation of 2,3-pentanedione from lactic acid is negligible for the first forty hours of the reaction. 2,3-Pentanedione yield beyond this point decreases slightly due to coking of the catalyst. Ammonia used in pH adjustment during lactate fermentation does not directly effect the catalyst activity toward the formation of 2,3-pentanedione. However, 2,3-pentanedione formed during the catalytic reaction is consumed in the presence of ammonium hydroxide and at high temperature to form nonvolatile species which exit the reactor with products. The effect is noticeable when greater than 5% of the feed lactate is in the form of ammonium lactate, and at 25% ammonium lactate essentially all of the 2,3-pentanedione formed is reacted and leading to a very low 2,3-pentanedione yield. Fortunately, this effect of ammonium hydroxide does not deactivate the catalyst. Glucose has little effect on catalyst activity other than acting as a source for coke formation, which will eventually plug the reactor at the top of the catalyst bed.

Chapter 6

PRODUCTION OF PROPIONIC ACID FROM LACTIC ACID

This chapter documents our preliminary conversion studies of lactic acid to propionic acid over transition metal catalysts. Currently, synthetic propionic acid is priced below lactic acid and it is not economically feasible to investigate this pathway unless the propionic acid produced by this route is categorized as natural. Since propionic acid has found its use primarily as a preservative, environmentally benign and low-toxicity metals are used as catalysts. Molybdenum catalysts are found to have high selectivity toward propionic acid, while other selected metals favor the formation of acetaldehyde. Although the reaction conditions for the formation of propionic acid from lactic acid have not been optimized, the relatively low yields from our initial studies do not indicate an economically promising pathway.

6.1. Catalyst preparation and reaction conditions

The transition metal salts (Na₂MoO₄, Cu(NO₃)₂•xH₂O, SnO, and Fe(NO₃)₃•9H₂O) used in the reduction of lactic acid to propionic acid were obtained in solid form from Aldrich. Purity and concentration of these compounds are reported in Table 2.1. These metal salts and oxide were dissolved in HPLC water and wet impregnated onto a 16 mesh silica alumina (7% Al) support with a surface area of about 5

m²/g. The mixture was dried on a hot plate to remove most of the water and then calcined in air at 400°C for 4 hours.

The catalyst pellets are loaded into the reactor described in Section 2.1.1, where lactic acid conversion was studied at 300-400°C under atmospheric pressure with helium as carrier gas. Residence time of these experiments is around 5 seconds; other experimental conditions are reported in Table 2.1. Pellets of 16 mesh were employed because it was found that catalysts with smaller size tend to harden upon heating and plug the reactor. Also, conversion over these fine particle catalysts show predominantly acetaldehyde formation.

6.2. Lactic acid conversion over molybdenum and iron catalysts

The study of the reduction of lactic acid to propionic acid was prompted by the observed high selectivity toward propionic acid over sodium molybdate (VI) while screening for potential catalysts for 2,3-pentanedione formation. Detailed conversion results between 280-350°C are given in Table 6.1. Yields of propionic acid were as high as 20% with lactic acid conversion over 90%, however, over 40% of the carbon was usually not recovered. Acetaldehyde and carbon dioxide were also formed in high yields, especially at high temperatures. Even though propionic acid yields were relatively high, molybdenum was found to leach into the products as indicated by the dark violet color of the liquid samples collected.

As mentioned in Section 1.3.4, Velenyi and Dolhyj were able to obtain a propionic acid yield of 64% from lactic acid by using a combination of molybdenum, copper, and tin oxides on silica-alumina catalyst conducted at 350°C and 1 atmosphere

Table 6.1. Lactic Acid Conversion over Na₂MoO₄/Si-Al and MoCuSn/Si-Al

Catalyst	I m	mol Na ₂ M	004/gS	-Al	1.0.7.0	17 mmol 1	:0.7:0.17 mmol MoCuSn / g	g Si-Al
Temperature (°C)	280	300	300 320 35	350	300	320	350	370
Contact Time(s)	3.3	3.1	2.5	2.5	5.7	8.9	5.7	5.5
Error (% Carbon)	-48.3	45.3	-38.7	-34.3	-42.3	-34.9	-34.5	44.5
Conversion (BOF)	97.6	92.1	87.0	94.5	86.7	79.9	87.4	90.4
Yield (% Theoretical)								
Acrylic acid	0.0	0.0	0.0	0.0	0.0	0.0	0.0	0.0
Propionic acid	13.8	17.7	19.4	19.2	20.1	24.7	27.0	20.1
2,3-Pentanedione	9.0	8.0	6.0	2.4	1.3	1.2	1.5	2.0
Acetaldehyde	0.9	8.1	8.2	17.4	5.0	5.0	5.8	8.4
Acetol	0.0	0.0	0.0	0.0	0.0	0.0	0.0	0.0
Other	0.3	0.4	0.5	1.2	2.2	0.1	0.0	0.1
Unknown	17.4	16.0	14.0	17.4	2.0	3.9	5.5	8.9
*00	1.1	1.7	1.4	2.2	1.9	2.0	2.8	4.2
C02*	24.4	18.8	23.7	25.1	39.2	34.6	43.3	25.2
Selectivity (%)								
Acrylic acid	0	0	0	0	0	0	0	0
Propionic acid	<i>L</i> 9	9	<i>L</i> 9	48	20	80	79	99
2,3-Pentanedione	က	က	8	9	4	4	2	7
Acetaldehyde	53	30	78	43	<u>&</u>	16	17	27
Acetol	0	0	0	0	0	0	0	0
Other	_	7	7	က	∞	0	0	0
Vields managed of mole	100 :	ماعو موامه	biog pito	6.4				

*Yields reported as mole per 100 moles of lactic acid fed.

with nitrogen as the carrier gas (62). These metals are in a ratio of Mo₅Cu₄SnO_x and comprised about 30 wt% of the total catalyst. A similar catalyst was prepared in our laboratory and lactic acid conversion studies were performed under similar conditions. Conversion and yields over 300-370°C are listed in Table 6.1. Propionic acid yields are only slightly higher than using Na₂MoO₄ alone; however, leaching of molybdenum into the products was not observed. Thus, the copper and tin metal oxides act as promoters for the formation of propionic acid, and stabilize the molybdenum oxides on the catalyst. Acetaldehyde yields were also lower in the presence of this combination of oxides, but 20% of the carbon was still unaccounted for in the products.

Studies of lactic acid conversion to propionic acid were also conducted over iron catalysts either alone or in place of molybdenum with copper and tin metal oxides. The yields to propionic acid were very similar in both catalysts (Table 6.2) at values less than 10%; it was observed that acetaldehyde formation was dominant within the experimental temperature range. When hydrogen was used as the carrier gas over the iron catalyst, it was found that the yield of propionic acid increased to 16% at 350°C. However, acetaldehyde yield was still relatively high at 30%.

The absence of acrylic acid formed through the reduction of lactic acid to propionic acid suggests that the pathway to propionic acid does not involve the dehydration of lactic acid to acrylic acid first and then further hydrogenation to propionic acid. The reduction of these oxides on the catalyst is not fully understood, although the large amount of carbon dioxide emitted seems to indicate that lactic acid was involved. If this is the case, then theoretical yield to propionic acid would be much lower than 100% since lactic acid is consumed in the reduction of the metals. Further studies of the

Table 6.2. Lactic Acid Conversion over FeCuSn/Si-Al

Catalyst	-	0.7:0.17 n	mol FeCu	1:0.7:0.17 mmol FeCuSn / g Si-Al	7
Temperature (°C)	300	320	350	370	400
Contact Time(s)	2.3	2.3	2.4	2.4	2.5
Error (% Carbon)	-34.7	-18.9	-7.8	-14.2	-24.6
Conversion (BOF)	84.1	82.8	79.0	83.2	89.2
Yield (% Theoretical)					
Acrylic acid	0.0	0.0	0.0	0.0	0.0
Propionic acid	4.1	9.9	8.0	8.5	6.7
2,3-Pentanedione	1.9	3.2	3.7	3.5	3.0
Acetaldehyde	17.9	24.3	26.1	27.0	30.7
Acetol	1.9	1.5	0.0	0.0	0.0
Other	2.8	4.9	1.8	5.5	3.5
Unknown	6.7	12.1	17.5	13.9	18.1
*00	8.1	9.2	11.8	13.4	35.0
C02*	48.1	57.4	61.2	55.6	2.7
Selectivity (%)					
Acrylic acid	0	0	0	0	0
Propionic acid	14	16	70	19	21
2,3-Pentanedione	7	00	6	∞	9
Acetaldehyde	63	09	99	19	65
Acetol	7	4	0	0	0
Other	10	12	4	12	1

*Yields reported as mole per 100 moles of lactic acid fed.

oxidation states of the metals before and after the reaction are necessary to understand this direct pathway to propionic acid from lactic acid.

Chapter 7

SUMMARY AND RECOMMENDATIONS

7.1. Summary

Lactic acid obtained from fermentation can be converted to 2,3-pentanedione, acetaldehyde, acrylic acid, and propionic acid in a fixed-bed, down-flow reactor.

Formation of acrylic acid from lactic acid is relatively low at 23% yield over NaOH at 350°C because of the competing decarboxylation reaction to acetaldehyde at high temperature. However, 2,3-pentanedione can be produced in high yield over alkali metal catalysts at temperatures between 280-300°C with yield increasing in the order of Na < K < Cs. 2,3-Pentanedione yield as high as 60% theoretical with a 80% selectivity is obtained over a 2 mmol CsOH/g silica catalyst at 280°C. Catalyst loading also increases the yield to 2,3-pentanedione proportionally up to a saturation limit of 2 mmol of metal per gram of support.

Post-reaction FTIR spectra of these alkali metal catalysts after exposure to lactic acid vapor indicate the formation of alkali lactate as the dominant species on the surface at 260-320°C. Along with the fact that similar yields can be obtained with sodium lactate as the catalyst, it is thus concluded that the anions of initial sodium salts used do not participate in the condensation to 2,3-pentanedione. Thus, the proposed mechanism for the formation of 2,3-pentanedione involves presence of both lactic acid and alkali lactate.

Conversion of the alkali salt to lactate is found to be greatest when a low melting point salt with a volatile conjugate acid is used.

The decarbonylation of lactic acid to acetaldehyde can be greatly reduced by using a silica support with low surface acidity. A kinetic model of the reaction system is developed and the agreement between the predicted values and experimental data supports the reaction between lactic acid and lactate in the formation of 2,3-pentanedione. The alkali metal catalyst was found to be relatively stable toward the formation of 2,3-pentanedione with time and glucose impurity. However, 2,3-pentanedione selectivity decreases slowly with coking which enhances the formation of acetaldehyde. The presence of ammonium lactate in feed does not significantly deactivate the pathway to 2,3-pentanedione, but the formation of ammonium hydroxide in the product causes secondary reactions of 2,3-pentanedione and thus very little 2,3-pentanedione is observed in product at high levels of ammonium lactate in feed.

Our preliminary studies in the formation of propionic acid from lactic acid over molybdenum and other mixed transition metal catalysts show a 28% yield at 350°C and 5 second residence time. However, further investigations on reducing side-reactions of lactic acid at these reaction conditions are needed to make this pathway valuable.

7.2. Recommendations

The optimization of the conversion of lactic acid to 2,3-pentanedione in the vapor phase is mostly complete and the best catalysts for the reaction have been found. The sintering effect on high surface area silica support by alkali hydroxide has limited our studies to only low surface area silica at optimum conditions. Since there is a direct

2,3-pentanedione yield slightly further by loading the alkali lactate directly onto a high surface area support. The alkali lactates are only weak bases and should not cause significant support sintering. However, higher surface area corresponds to higher surface acidity and higher selectivity toward the formation of acetaldehyde.

Since ammonium lactate does not deactivate the catalytic pathway to 2,3-pentanedione from lactic acid, 2,3-pentanedione from lactic acid feed containing ammonium lactate can be obtained by eliminating the ammonium hydroxide produced from the decomposition of ammonium lactate. The slow reactions between 2,3-pentanedione and ammonium hydroxide at room temperature indicate that most of the 2,3-pentandione is consumed inside the reactor once it is formed. It is possible to eliminate the formation of ammonium hydroxide by the addition of nitric acid to the feed hence converting the ammonium lactate to lactic acid and ammonium nitrate. Since ammonium nitrate is soluble in water and known to decompose to H₂O and N₂O at 210°C (80,87), it does not seem to pose any problem to the catalytic conversion of lactic acid. However, because the decarbonylation of lactic acid to acetaldehyde increases with in acid medium, the addition of nitric acid to the feed must not be in excess. The addition of acid at the product stream can also prevent secondary reaction of 2,3-pentanedione with ammonium hydroxide.

The yield of propionic acid from lactic acid conversion over transition metals can still be increased by the use of higher surface area support, especially activated carbon supports. Carbon support was observed to increase the selectivity for propionic acid in

our studies with sodium phosphates. Using hydrogen as the carrier gas should also favor the formation of propionic acid although higher reaction pressure may be needed.



LIST OF REFERENCES

- 1. McCoy, M., Ed., Chem. Mktg. Rep., 5 (July 14, 1997).
- 2. Holmen, R. E., U. S. Patent # 2,859,240 (1956).
- 3. Paparizos, C., S. R. Dolkyj, W. G. Shaw, U. S. Patent # 4,786,756 (1988).
- 4. Odell, B., G. Earlam, D. J. Cole-Hamilton, J. Organometallic Chem., 290, 241 (1985).
- 5. Sugiyama, S. N. Shigemoto, N. Masaoka, S. Suetoh, H. Kawami, K. Miyaura, H. Hayashi, *Bull. Chem. Soc. Jpn*, 66, 1542 (1993).
- 6. Tsujino, T., S. Ohigashi, S. Sugiyama, K. Kawashiro, H. Hayashi, J. Mol. Catal., 71, 25 (1992).
- 7. Ghose, T. K., Ed., Bioprocess Engineering The First Generation, 367, Ellis Horwood Limited (1989).
- 8. Kroschwitz, J. I., M. Howe-Grant, Eds., Kirk-Othmer Encyclopedia of Chemical Technology 4th ed., 13, 1043, John Wiley and Sons, New York (1992).
- 9. Kirk, R. E., D. F. Othmer, Eds., Kirk-Othmer Encyclopedia of Chemical Technology 2nd ed., 8, 167, Interscience Encyclopedia, Inc., New York (1952).
- 10. Monteaguo, J. M., L. Rodriguez, J. Rincon, J. Fuertes, J. Chem. Tech. and Biotech., 68, 271 (1997).
- 11. Silva, E. M., S. T. Yang, J. Biotech., 41, 59 (1995).
- 12. Davison, B. H., C. D. Scott, Biotechnology and Bioengineering, 39, 365 (1992).
- 13. Urbas, B., U. S. Patent # 4,444,881 (1984).
- 14. Jeantet, R., J. L. Maubois, P. Boyaval, Enzyme and Microbial Tech., 19, 614 (1996).

- 15. Moueddeb, H., J. Sanchez, C. Bardot, M. Fick, *J. Membrane Sci.*, **114**, 59 (1996).
- 16. Ye, K., S. Jin, K. Shimizu, J. Chem. Tech. and Biotech., 66, 223 (1996).
- 17. Giorno, L., P. Spicka, E. Drioli, Separation Sci. Tech., 31, 2159 (1996).
- 18. Rincon, J., J. Fuertes, J. F. Rodriguez, L. Rodriguez, J. M. Monteagudo, Solvent Extraction and Ion Exchange, 15, 329 (1997).
- 19. Srivastava, S., P. K. Roychoudhury, v. Sahai, *Biotechnology and Bioengineering*, **39**, 607 (1992).
- 20. Miller, R. W., M. C. Cockrem, J. J. de Pablo, E. N. Lightfoot, *Ind. Eng. Chem. Res.*, **35**, 1156 (1996).
- 21. San-Martin, M., C. Pazos, J. Coca, J. Chem. Tech. and Biotech., 65, 281 (1996).
- 22. Boniardi, N., R. Rota, G. Nano, B. Mazza, J. Appl. Electrochemistry, 27, 125 (1997).
- 23. Boniardi, N., R. Rota, G. Nano, B. Mazza, J. Appl. Electrochemistry, 27, 135 (1997).
- 24. Chemical Week, 32 (June 26, 1991).
- 25. Filachione, E. M., J. Am. Chem. Soc., 73, 5265 (1951).
- 26. Filachione, E. M., Ind. Eng. Chem., 44, 2189 (1952).
- 27. Walkup, P. C., C. A. Rohrmann, R. T. Hallen, D. E. Eakin, U. S. Patent # 5,071,754 (1991).
- 28. McCoy, M., Ed., Chem. Mktg. Rep., (November 10, 1997).
- 29. Simpson, F. J., Ed, McGraw Hill Encyclopedia of Science and Technology 5th ed., 7, 513, McGraw Hill Pub. Co., New York (1982).
- 30. McCarthy, S. L., J. Am. Soc. Brew Chem., 53, 178 (1995).
- 31. Semmelroch, P., W. Grosch, Food Sci. Technol.- LEB, 28, 310 (1995).
- 32. Furia, T. E., N. Bellanca, Fenaroli's Handbook of Flavor Ingredients 2nd ed., 2, 454, CRC Press, Inc. (1975).
- 33. von Pechmann, H., Ber. Der Deut. Chem. Ges., 21, 1411 (1888).

- 34. Akiyama, T., Y. enomoto, T. Shibamoto, J. Agric. Food Chem., 26, 1176 (1978).
- 35. Barlin, G. B., Chemistry of Heterocyclic compounds The Pyrzines, 41, 11, John Wiley and Sons, New York (1982).
- 36. Nakel, G. M., B. M. Dirks, U.S. Patent #3,579,353 (1971).
- 37. Maresca, L. M., U.S. Patent #4,611,033 (1986).
- 38. Thiel, M. A., Masters Thesis, Michigan State University (1996).
- 39. Kroschwitz, J. I., M. Howe-Grant, Eds., Kirk-Othmer Encyclopedia of Chemical Technology 4th ed., 1, 287, John Wiley and Sons, New York (1992).
- 40. Mark, H. F., D. F. Othmer, Eds., Encyclopedia of Chemical Technology 3rd ed., 16, 637, John Wiley and Sons, New York (1978).
- 41. Hsu, S. T., Yang, S. T., Biotechnology and Bioengineering, 38, 571 (1991).
- 42. Colomban, A., L. Roger, P. Boyaval, *Biotechnology and Bioengineering*, 42, 1091 (1993).
- 43. Lewis, V. P., S. T. Yang, Biotechnology and Bioengineering, 40, 465 (1992).
- 44. McCoy, M., Ed., Chem. Mktg. Rep., 49 (February 24, 1997).
- Chuchani, G., I. Martin, A. Rotinov, R. M. Dominguez, J. Phys. Org. Chem., 6, 54 (1993).
- 46. Chuchani, G., I. Martin, A. Rotinov, Int. J. Chem. Kinet., 27, 849 (1995).
- 47. Langford, R. H., Masters Thesis, Michigan State University (1993).
- 48. Hiltunen, K. J. V. Seppala, M. Harkonen, *Macromolecules*, 30, 373 (1997).
- 49. Lipinsky, E. S., R. G. Sinclair, *Chem. Engr. Prog.*, **82**, 26 (1986).
- 50. Hiltunen, K., J. V., Seppala, M. Harkonen, J. Appl. Poly. Sci., 63, 1091 (1997).
- 51. Hiljanen-Vainio, M., J. Kylma, K. Hiltunen, J. V., Seppala, J. Appl. Poly. Sci., 63, 1335 (1997).
- 52. Linko, Y. Y., J. Seppala, CHEMTECH, 26, 25 (1996).

- Van der Meer, S. A., J. R. De Wijn, J. G. Wolke, *Journal Materials Science:* materials in Medicine, 7, 359 (1996).
- 54. Fisher, C. H., C. E. Rehberg, L. T. Smith, J. Am. Chem. Soc., 65, 763 (1943).
- 55. Fein, M. L., W. P. Ratchford, C. H. Fisher, J. Am. Chem. Soc., 66, 1201 (1944).
- 56. Filachione, E. M., J. H. Lengel, C. H. Fisher, J. Am. Chem. Soc., 66, 494 (1944).
- 57. Ratchfor, W. P., C. H. Fisher, *Ind. Engr. Chem.*, 37, 382 (1945).
- 58. Filachione, E. M., M. L. Fein, J. H. Lengel, C. H. Fisher, *J. Am., Chem. Soc.*, 70, 526 (1948).
- 59. Sawicki, R. A., U. S. Patent # 4,729,978 (1988).
- 60. Mok, W. S., M. J. Antal, Jr., M. Jones, Jr., J. Org. Chem., 54, 4597 (1989).
- 61. Lira, C. T., P. J. McCrackin, Ind. Eng. Chem. Res., 32, 2608 (1993).
- 62. Gunter, G. C., Ph.D. Dissertation, Michigan State University (1994).
- 63. Kida, K., S. Morimura, Y. Sonoda, *Journal Fermentation and Bioengineering*, 75, 213 (1993).
- 64. Velenyi, L. J., S. R. Dolhyj, U. S. Patent # 4,663,479 (1987).
- 65. Gunter, G. C., J. E. Jackson, D. J. Miller, J. Catal., 148, 252 (1994).
- 66. Gunter, G. C., R. H. Langford, J. E. Jackson, D. J. Miller, *Ind. Eng. Chem. Res.*, 34, 974 (1995).
- 67. Gunter, G. C., R. Craciun, M. S. Tam, J. E. Jackson, D. J. Miller, *J. Catal.*, 164, 207 (1996).
- 68. Wadley, D. C., M. S. Tam, P. B. Kokitkar, J. E. Jackson, D. J. Miller, J. Catal., 165, 162 (1997).
- 69. Nagai, M., L. L. Lucietto, Y. E. Li, R. D. Gonzalez, J. Catal., 101, 522 (1986).
- 70. Philipp, R., K. Fujimoto, J. Phys. Chem., 96, 9035 (1992).
- 71. Sullivan, D. H., W. C. Conner, M. P. Harold, *Appl. Spect.*, **46**, 811 (1992).
- 72. Mirth, G., F. Eder, J. A. Lercher, Appl. Spect., 48, 194 (1994).

- 73. Datka, J., Z. Sarbak, R. P. Eischens, J. Catal., 145, 544 (1994).
- 74. Blitz, J. P., S. M. Augustine, Appl. Spect. 45, 1746 (1991).
- 75. Holmes, P. D., G. S. Mcdougall, L. C. Wilcock, Catalysis Today, 9, 15 (1991).
- 76. Henderson, D. O., E. Silberman, N. Chen, F. W. Snyder, *Appl. Spect.*, **47**, 528 (1993).
- 77. Christy, A. A., E. Nodland, A. K. Burnham, O. M. Kvalheim, B. Dahl, *Appl. Spect.*, **48**, 561 (1994).
- 78. Stenhagen, E., S. Abrahamsson, F. W. McLafferty, Registry of Mass Spectral Data, Interscience Publishers, John Wiley and Sons, New York (1974).
- 79. Pouchert, C. J., *The Aldrich Library of FT-IR Spectra*, Aldrich Chemical Company, Inc. (1985).
- 80. Lide, D. R. Ed., CRC Handbook of Chemistry and Physics 75th ed., CRC Press, Inc. (1994).
- 81. Craciun, R., Ph.D. Dissertation, Michigan State University (1997).
- 82. Perrichon, V., M. C. Durupty, Appl. Catal., 42, 217 (1988).
- 83. Jeon, G. S., J. S. Chung, *Appl. Catal. A: General*, 115, 29 (1994).
- 84. Pereira, E. B., G. Martin, Appl. Catal. A: General, 115, 135 (1994).
- 85. Groppi, G., M. Belloto, C. Cristiani, P. Forzatti, P. L. Villa, Appl. Catal., 104, 101 (1993).
- 86. Holten, C. H., A. Muller, D. Rehbinder, Lactic Acid Properties and Chemistry of Lactic Acid and Derivatives, Verlag Chemie (1971).
- 87. Budavari, S., M. J. O'Neil, A. Smith, P. E. Heckelman, J. F. Kinneary, Eds., *The Merck Index 12th ed.*, Merck & Co., Inc. (1996).

